THERMAL ANALYSIS OF COMPACT SEALED COMPUTERS

THERMAL ANALYSIS OF COMPACT SEALED COMPUTERS

By

CHARLES YOUNG, B. ENG.

A Thesis

Submitted to the School of Graduate Studies

in Partial Fulfillment of the Requirements

for the Degree

Master of Applied Science

McMaster University

Hamilton, Ontario, Canada

MASTER OF APPLIED SCIENCE (2009)
(Mechanical Engineering)

McMASTER UNIVERSITY
Hamilton, Ontario, Canada

TITLE: Thermal Analysis of Compact Sealed Computers

AUTHOR: Charles H. Young, B. Eng.

SUPERVISOR: Dr. J. S. Cotton

NUMBER OF PAGES: xviii, 146

ABSTRACT

Thermal performance of a cooling system for a small sealed computer is investigated. The cooling system consisted of a heat pipe unit which transfers heat from the CPU and *northbridge* chip to the case wall which had vertical fin channels mounted on the outside. Natural convection and radiation moved the heat from the fin plate to the surroundings. An initial benchmarking experiment determined the temperature drop across each component in the system and identified the areas of focus for further research.

The heat pipe unit was selected for initial analysis based on the benchmarking experiment. Heat pipes with sintered wick and grooved wick structures were tested at different orientations with respect to gravity. Gravity was found to cause failure of the groove wick heat pipe in certain orientations while the sintered wick was able to function adequately in any orientation.

Carbon foam is a new material with the potential for very high thermal conductivity, 2-3 times that of copper. Based on the variable performance of heat pipes, carbon foam was investigated as a possible solution. Investigations determined carbon foam had thermal conductivity in the range 30-130 W/mK, but it had high specific thermal conductivity, over four times that of copper which means it could be useful in applications that are weight sensitive.

Literature research was conducted on the topic of rectangular channel fin performance and an analytical model was found to estimate performance for different fin

geometries. A radiation shape factor equation for rectangular channel fins was also found. Together the models were used to estimate the best fin geometry to maximize natural convection and radiation heat transfer. Heat spreading in the fin plate was investigated using numerical simulation validated by the analytical models and previous studies of similar geometries.

A system model is developed to combine the temperature drops of all components of the system to quickly determine the affect of changing one parameter on the temperature of the CPU. Notable results include the highest power CPU that can be used in the current system, the highest surrounding temperature that a 35 W CPU can run in and the size of fin plate needed to run a 65 W CPU in a 40°C environment.

ACKNOWLEDGEMENTS

The author would like to acknowledge the superb supervision of Dr. J. Cotton throughout the project. Additional thanks to Dr. C. Y. Ching for his guidance and suggestions over the course of the project.

I am grateful for the study provided by Dr. Robinson and Roger Kempers to accurately measure the conductivity of carbon foam and to supply scanning electron microscope images of the carbon foam.

I would like to thank M. Kamrul Islam Russel for his work testing the heat pipes in the controlled heat pipe test facility. Without his hours of hard work the detailed experimental results would not be available.

The technicians in the Mechanical Engineering department shop, Joe Verhaeghe, Ron Lodewyks, Jim McLaren, Mark Mackenzie and J. P. Talon provided valuable help at many points during the project.

Ontario Centres of Excellence, the Natural Sciences and Engineering Research Council of Canada and SmallPC all contributed funding to make this project possible. SmallPC and ThermalCentric each contributed in-kind supplies to the project.

Finally, I would like to thank my family, friends and colleagues in the Thermal Management Research Laboratory for the help and support throughout this project.

TABLE OF CONTENTS

List of Tables

List of Figures

Nomenclature

Symbols	
A	Area, m^2
A_w	Wick Area, m^2
D_g	Groove Depth, m
D_h	Hydraulic Diameter, m
F	Shape Factor
g	Gravitational constant
H	Fin Height, m
h_c	Heat Transfer Coefficient, W/m^2K
k	Thermal Conductivity, W/mK
K_w	Permeability
L	Distance, m
Nu	Nusselt Number
Pr	Prandtl Number
q	Heat Transport, W
R	Thermal Resistance, K/W
r_c	Radius of Curvature, m
Re	Reynolds Number
s	spacing distance, m
t	Fin Thickness, m
t_b	Fin Base Plate Thickness, m
U_∞	Free Stream Velocity, m/s
W	Width, m
x	Characteristic Dimension, m
Greek	
α	Thermal Diffusivity, m^2/s
ε	Emissivity
ν	Kinematic Viscosity, m^2/s
ρ	Density, kg/m^3
σ	Stefan-Boltzmann constant
σ	Surface Tension, N/m
φ	Inclination angle, rad
ΔT	Temperature Drop, K
Δp	Pressure Drop, Pa
Δh	Change of Height, m

Subscripts	
amb	Ambient
c	Condenser
cap	Capillary
e	Evaporator
eff	Effective
f	Fluid
g	Gravity
max	Maximum
v	Vapour
l	Liquid
1	Surface 1
2	Surface 2
1-2	Between 1 and 2

Glossary

CPU	Central Processing Unit – Computer chip responsible for the main processing in a computer.
DTS	Digital Thermal Sensor – Temperature sensor embedded in CPU to monitor temperature and prevent overheating.
TDP	Thermal Design Power – Heat load required to be dissipated by the processor cooling system.
northbridge	Processing chip that handles memory access, graphics and communication with other system components

Chapter 1 Introduction

1.1 Background

Personal computers have become increasingly integrated into most aspects of daily life, for both personal uses as well as in commercial and industrial applications (Chu et al., 2004). Electronic components inside computer casings generate heat due to the electrical current flowing through them. Although many components generate heat, the most critical are silicon chips due to high heat fluxes and low maximum operating temperature limits. Typical computer designs use fans to force air past a heat sink to remove heat from the processor and other fans to move cool air into and hot air out of the computer case (Saimi and Webb, 2003). This design works well in typical environments where computers operate in clean, cool air. However, there are many locations where this type of design is not feasible. For example, a computer used in a medical facility, such as an operating room, needs to have ambient air kept out of the case so it can be easily sanitized. Factory and industrial environments with high levels of particulate matter in the air also cause problems for typical computers when contaminates accumulate in the sensitive electronic components. In specialty vehicles, including coast guard ships and police cars, computers can be exposed to many different environmental conditions, including particulate in the air, splashing water and elevated ambient temperatures. In these demanding conditions, particulate matter or dust can cause many problems inside traditional forced convection cooled computers. Particulate matter can accumulate on fin surfaces and act as a thermal insulator and it can build up on the entrances to fins and

block flow from entering fin channels (Nabi et al., 2006). Additionally it can penetrate into fan motors and bearings and cause mechanical failure.

A simple solution for many special environments is to use a sealed computer case that does not allow airflow in or out of the case. By sealing the case, dust and biological contaminants, as well as splashing water, are prevented from entering the case. An example of this is a custom casing developed by Small PC that only has one removable side panel and one opening for all the cables and connections. A gasket seals the single opening and a special grommet plate is used to seal around each individual cable.

In order for the computer to function properly in a sealed case without airflow and at elevated ambient temperatures, the cooling system needs to be rigorously designed. Since most computer cooling systems rely on ambient air, common cooling methodologies cannot be used and new strategies must be developed.

1.2 Sealed Computer System under Study

Two systems are studied as part of this project. One of the systems consists of a flat panel, liquid crystal display (LCD) monitor and computer integrated into a sealed case (Figure 1-1) and the other system consists of only a computer system mounted in a sealed case (Figure 1-2). Both computer systems have a similar hardware configuration (Table 1-1) and cooling system, consisting of a heat pipe unit made from of two U-shaped heat pipes connected between two heat spreaders (Figure 1-3) which moves the heat from the computer components to the finned case wall. During testing of the LCD computer system power to the LCD screen was removed and an external monitor was used, making both computers functionally the same. The operation of heat pipes is

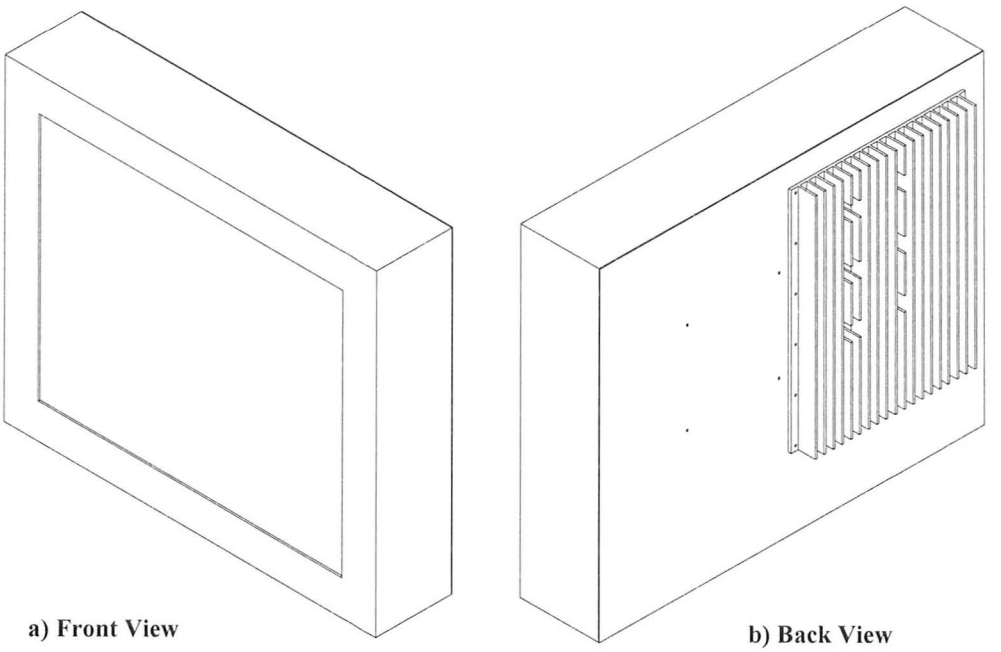

Figure 1-1: Sealed LCD Computer

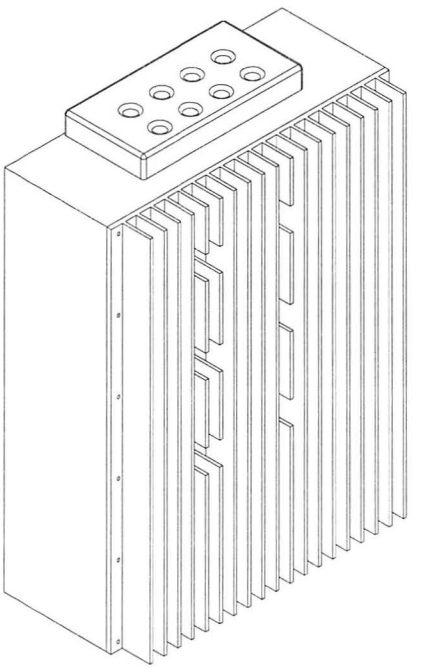

Figure 1-2: Sealed Computer

the central processing unit (CPU) and the graphics and memory controller hub (GMCH); which is also known by the term "northbridge". The CPU is responsible for executing the software instructions and doing the arithmetic calculations for the system. The *northbridge* handles the memory access required by the CPU, the graphics processing and communication to the other system components (Figure 1-4). The power that must be dissipated from each chip is specified by the manufacturer and is known as the Thermal Design Power (TDP). For the systems studied, an Intel Core 2 Duo T8300 processor was used with a TDP of 35 W (Intel, 2008). The *northbridge* used was an Intel 945GME and had a TDP of 7 W (Intel, 2007). The term "chip" will be used to refer to any heat generating electronic component including the CPU and *northbridge*.

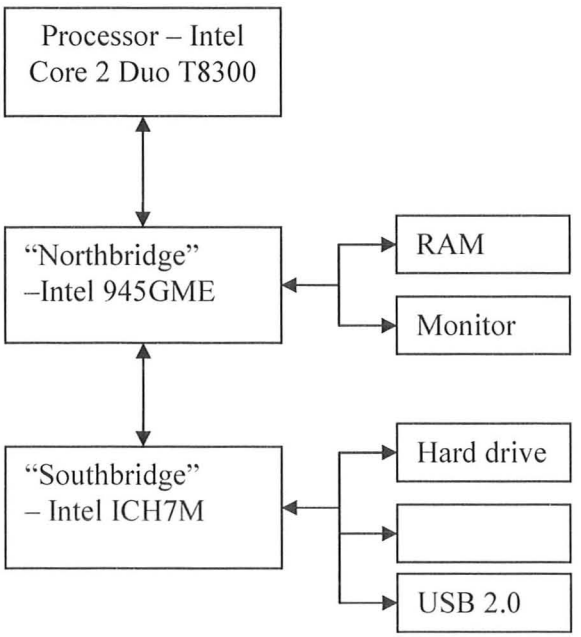

Figure 1-4: Computer System Schematic

1.3 Problem

This project focuses on understanding and developing cooling systems for small sealed personal computers. Current top-of-the-line mobile computer processors require dissipation of 45 W of thermal energy (Intel Corporation, 2009a) while desktop processors require dissipation of 130 W of thermal energy (Intel Corporation, 2009b). The CPUs used in this investigation have a maximum temperature of 100°C (Intel Corporation, 2009a). The system specifications include operation in environments with an ambient temperature of up to 40°C. The heat dissipation required and specified operating conditions preclude the operation of these systems without an advanced thermal management solution. This project consists of first evaluating the current thermal solution used in sealed computers and then using this information to create a road map to guide testing and development of cooling system components. Based on the results of the initial testing presented in Chapter 4, the thermal resistance of each part of the system was determined (Figure 1-5). The key areas of thermal resistance were identified as being the heat pipe unit, which moves heat to the fin plate from the chip surface and the fin, which releases heat to the surroundings. The heat pipes investigated were found to have performance that varied with changes in orientation and this prompted consideration of new solutions for moving heat from the chip to the fins. The use of carbon foam was proposed to directly conduct heat to the case wall. Current carbon foam has thermal conductivity in the range 150-250 W/mK (POCO, 2002 and Klett, 2000) and porosities of

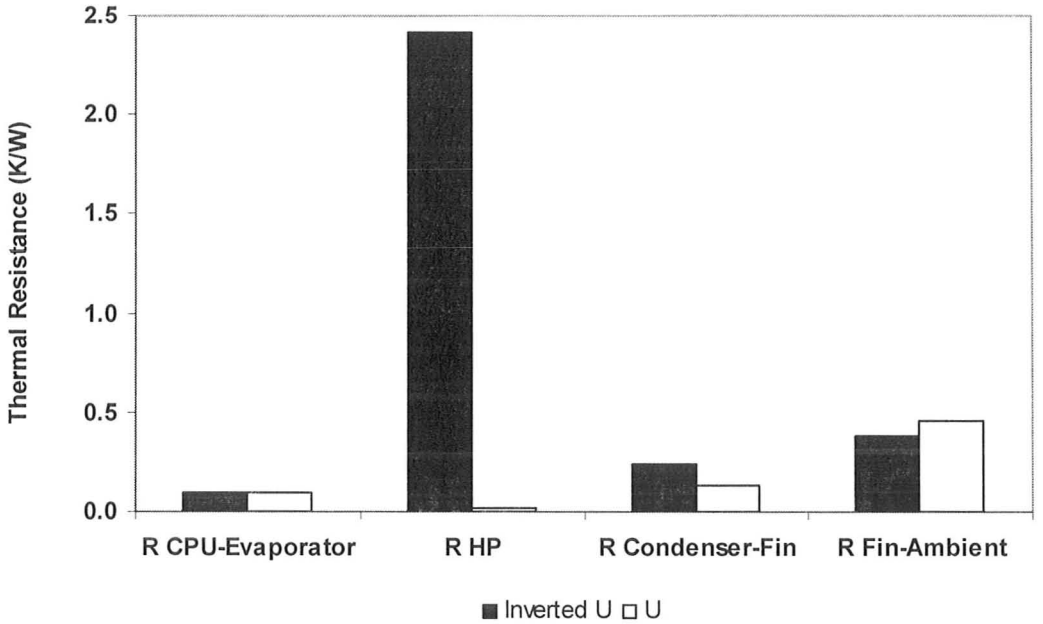

Figure 1-5: Thermal Resistances of System Determined in Benchmarking Experiment

between 61%-78% (POCO, 2002 and Koppers Inc., 2006). With the conductivity scaling as the porosity is reduced to the order of 20% with new manufacturing techniques, it was hypothesized that carbon foam could provide similar performance to heat pipes regardless of orientation.

Natural convection from the fin plate to the surroundings was found to contribute second highest thermal resistance after the heat pipe and because of this was the second area of focus. The final part of the project involved compiling all aspects of the analysis together and making a one-dimensional model for the entire system. The goal of the system model is to analyse the result of all parts of the system working together and to allow for rapid parametric analysis of the whole system.

1.4 Scope of Work

Based on the guidelines set out by the manufacturer of the sealed computers, the problem under consideration is limited to moving the heat from the surface of the chip package to the surroundings. Although design of the chip package itself is important for the overall thermal design, it is well beyond the scope of this project and is already included in the commercially available processors used. Design of the motherboard which influences the geometric constraints is also fixed by using commercially available components. Changes to the physical configuration of the board and components are well beyond the scope of the project. Liquid cooling or refrigerant based cooling solutions are not applicable due to the power requirements and the complexity and cost required for a reliable system. Since the systems must run in a specified range of ambient conditions, control of the local environment is also beyond the scope of this project.

This thesis is divided into six chapters. Chapter 2 provides background on heat transfer required to understand the work done, and on research done in the areas of computer cooling, and natural convection. Chapter 3 outlines the experimental set up and method used for the experiments. Chapter 4 discusses the results of the experimental program backed up with numerical analysis and validation. Chapter 5 introduces a system model and provides examples of cases considered. Chapter 6 summarizes the work and provides recommendations going forward. The appendix of the thesis contains information on thermal properties of carbon foam including testing details and results of testing.

Chapter 2 Background

2.1 Heat Transfer

Analysing heat transfer occurring in the many parts of a computer cooling system requires a basic understanding of heat transfer science. Many terms are used throughout this thesis and are defined in this section.

Heat transfer occurs via, conduction, convection, radiation, evaporation and condensation. Evaporation and condensation are discussed in section 2.2. Conduction takes place inside solid materials when there is a temperature gradient between two points. The rate of heat flow, q, is dependent on the temperature gradient, dT/dx, the cross sectional area, A, and the thermal conductivity of the material, k. For a given temperature difference the rate of heat flow is given by the Fourier Conduction equation

$$q = -kA\frac{dT}{dx}. \tag{2.1}$$

Although k, being a material property varies with T, for many situations and materials it can assumed to be constant, and if one-dimensional, steady state conduction is assumed, (2.1) can be rearranged to yield

$$q = \frac{\Delta T}{L/kA} \tag{2.2}$$

where ΔT, is the temperature difference between two points in the direction of heat flow and L, is the distance between those two points. Alternately the material can be considered to provide a resistance to the flow of heat, limited by thermal conductivity.

The resistance can be written for steady state conduction in a material with isotropic thermal properties as

$$R = \frac{L}{kA} \tag{2.3}$$

where L, is the distance between which the resistance is acting. This thermal resistance allows an analogy between electrical circuits and thermal pathways where the temperature difference, ΔT, provides the potential, analogous to voltage difference, and the rate of heat flow, q, is analogous to the current. Non-homogeneous materials have an effective thermal conductivity, which is a combination of the thermal conductivities of the constituent materials and their interaction. Effective conductivity can be used to simplify analysis of more complex systems such as modeling the temperature drop across a heat pipe by calculating an effective thermal conductivity for the heat pipe.

No solid surface is perfectly smooth and when two surfaces are in contact voids are present between the surfaces which fill with fluid (usually air). Since fluids generally have much lower thermal conductivities than solids used for heat conduction, this presents an additional thermal resistance to the flow of heat. To minimize thermal contact resistance surfaces should be as smooth as possible and the voids should be filled with a material with the highest thermal conductivity feasible. Typically a paste is used between metal parts to fill voids.

Convection consists of the transfer of heat by bulk fluid motion including liquids and gases and is broken down into forced convection and natural convection. Forced convection occurs when a fluid has an externally induced velocity relative to the heat transfer surface, usually imposed by a pump or fan. Natural convection occurs when the

fluid density varies due to a temperature change and induces a flow via buoyancy forces exerted on and by the surrounding fluid. Regardless of the type of convection it can be described by Newton's Law of Cooling

$$q = h_c A \Delta T \,, \tag{2.4}$$

where h_c, is the convection heat transfer coefficient, A, is the surface area and ΔT, is the temperature difference between the surface and a point far away in the fluid, referred to as the bulk fluid temperature. The heat transfer coefficient is used to relate the heat flow rate, q, to the temperature difference, ΔT. It can be calculated using the Nussult number as described in a following paragraph.

Dimensionless numbers are formed by combining variables from a problem to give a quantity without units. Specific dimensionless variables are useful to compare the characteristics of two different systems. There are several dimensionless parameters used in the calculation of convection coefficients in this study.

The Reynolds number (Re) represents the ratio of inertia forces to viscous forces and is defined as

$$\mathrm{Re} = \frac{U_\infty x}{\nu} \tag{2.5}$$

where U_∞ is the free stream velocity, x is the characteristic dimension, and ν is the kinematic viscosity of the fluid. The characteristic dimension is defined differently for different types of problems. For example, for flow inside a pipe the characteristic dimension, x, is the inner diameter of the pipe whereas for flow past a vertical plate the characteristic dimension used is the height of the plate.

The Prandtl number is the ratio of momentum diffusivity to thermal diffusivity and is made up of the kinematic viscosity of a fluid, ν, and thermal diffusivity of the fluid, α, and is defined as

$$\mathrm{Pr} = \frac{\nu}{\alpha}. \tag{2.6}$$

The Prandtl number is a dimensionless fluid property and is determined based on the fluid used and its temperature.

The Nusselt number is a dimensionless heat transfer coefficient and is the ratio of convection heat transfer to conduction in a layer of fluid x thick. It is of critical importance in finding the convective heat transfer coefficient. It is defined as

$$Nu = \frac{h_c x}{k_f} = f(\mathrm{Re}, \mathrm{Pr}) \tag{2.7}$$

where h_c is the convective heat transfer coefficient, x is the characteristic dimension and k_f is the thermal conductivity of the fluid. Nu is usually also related to Re and Pr experimentally by some function which depends on the geometry of the system. To account for natural and forced convection as well as different problem geometries, different functions are used to correlate Nu with Re and Pr to find h_c based on relevant experimental data.

A critical dimensionless number for natural convection is the Grashof number, which is the ratio of buoyancy to viscous forces

$$Gr = \frac{g\beta(T_s - T_\infty)L^3}{\nu^2}. \tag{2.8}$$

Often the Grashof number is combined with the Prandtl number to form the Raleigh number

$$\mathrm{Ra} = \mathrm{Gr}\,\mathrm{Pr}. \tag{2.9}$$

The Raleigh number is typically used predict onset of turbulence (Ra > 10^9) and to correlate experimental data with the Nusselt number with the relation

$$\mathrm{Nu} = \phi(\mathrm{Ra}). \tag{2.10}$$

Radiation heat transfer depends on the surface absolute temperature, the surrounding absolute temperature and the physical properties of the surface. The heat transferred by radiation from a gray body to a black enclosure is given by the Stephan-Boltzman law

$$q = A\varepsilon_1\sigma\left(T_1^4 - T_2^4\right) \tag{2.11}$$

where A is the surface area, ε_1 is the emissivity of the gray surface, σ is the Stefan-Boltzmann constant which has a value of 5.67 x 10^{-8} W/m^{2}K^4, T_1, and T_2, are the temperatures of the surface and enclosure respectively. The emissivity of a gray body is the ratio of the emission from the gray surface to the emission from a black surface at the same temperature. Equation (2.9) is valid when the surface does not see any of itself but only its surroundings. When considering a surface which is concave the equation must be modified to account for the radiation which is coming back to the surface and not reaching the surroundings. This can be accounted for using a shape factor, or view factor, a scalar value which represents how much of the radiation leaving a surface A_i reaches another surface A_j, denoted $F_{i\text{-}j}$. Using the shape factor, the heat radiated from a gray surface A_1 to a gray surface A_2 in a medium that does not absorb or emit radiation is

$$q_{1-2} = \sigma A_1 F_{1-2}\left(\varepsilon_1 T_1^{\ 4} - \varepsilon_2 T_2^{\ 4}\right) \tag{2.12}$$

where ε_1 and ε_2 are the emissivities of surface 1 and 2 respectively. Shape factors can be calculated analytically or calculated using published equations for common geometries.

Although not all modes of heat transfer can be easily transposed to give thermal resistance directly, local resistance can be calculated by dividing ΔT for a given section by q once the system is solved. Converting each part of the system into a thermal resistance value allows a comparison to determine the greatest thermal resistances and therefore the areas with the most potential to increase overall heat transfer.

2.2 Heat Pipes

A heat pipe is a two phase passive heat transfer device involving heat transfer by evaporation and condensation. It consists of a sealed tube lined with a wick structure and is partially filled with a working fluid (Dunn and Reay, 1982; Faghri, 1995; Peterson, 1994). Working fluid at the evaporator section where heat is applied evaporates and flows down the hollow centre of the tube to the condenser, section which is at a lower temperature compared to the evaporator, and condenses on the walls of the tube (Figure 2-1). The wick structure inside is integral in the functioning of a heat pipe because it provides the capillary pumping action which is the driving force for the heat pipe. A secondary function of the wick is that it helps distribute the fluid evenly around the circumference to give more evaporation area inside the heat pipe. Capillary force generated inside the wick structure that lines the wall pumps the condensed working fluid back to the evaporator. The cycle is continuous as long as there is a temperature

difference between the evaporator section and the condenser section and the operating parameters for the heat pipe are satisfied.

A vapour chamber is a heat pipe with a non-circular geometry (Prasher, 2003). An example of a vapour chamber is a flat plate where heat is applied to an area on the bottom and is removed from another area on the top as illustrated in Figure 2-2.

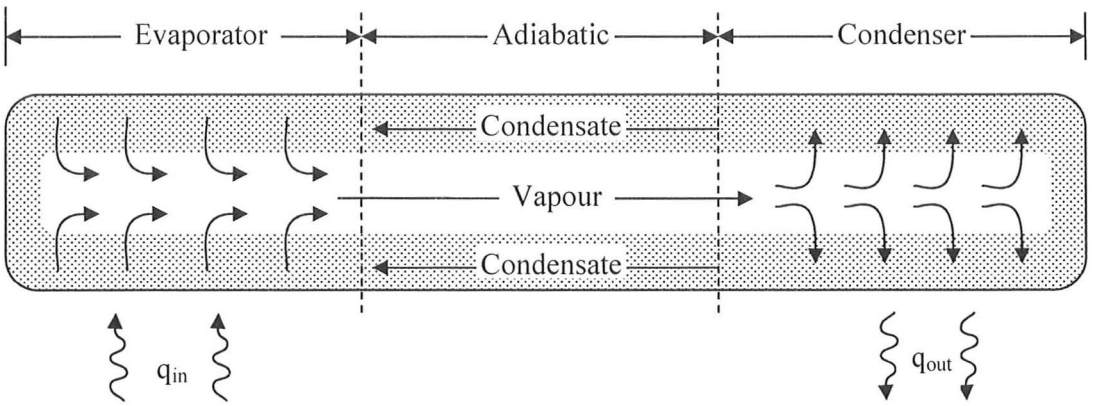

Figure 2-1: Basic Operating Schematic of a Heat Pipe

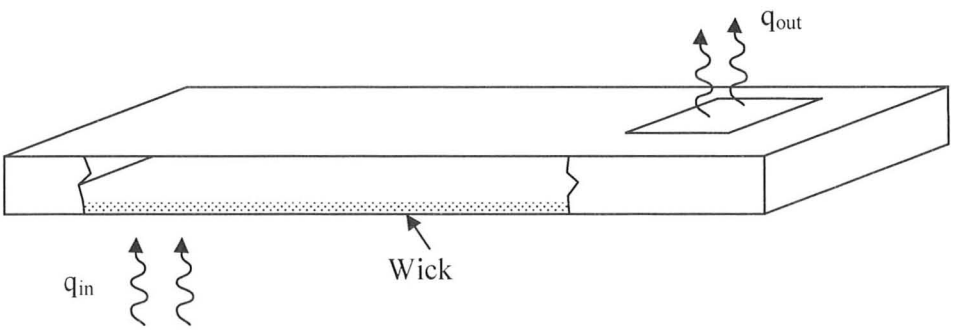

Figure 2-2: An Example of a Flat Plate Vapour Chamber

There are several conditions that limit the total power that can be conducted through a heat pipe. The vapour pressure limit happens when the pressure generated by the evaporator is not enough to drive the vapour all the way to the end of the condenser. The sonic limit occurs when the vapour flow at the exit of the evaporator is choked. The entrainment limit is caused when the vapour flow in the channel exerts a shear force on the condensate flow in the wick and moves droplets of condensate back to the condenser. Burnout can happen in cases of high radial heat flux when the thermal resistance in the radial direction becomes non-trivial and when boiling occurs in the wick and vapour bubbles become trapped in the wick (Dunn and Reay, 1982). For heat flux levels and temperatures typically encountered in computers, the capillary limit is usually the first limit that is reached (Faghri, 1995). The capillary limit occurs when the capillary pumping force is not great enough to overcome the total pressure drop in the system and the evaporator section dries out due to lack of working fluid. The capillary limit is the only limiting condition which is affected by gravity and hence the only limit that is affected by orientation of the heat pipe.

To determine the analytical limit of a heat pipe based on the governing pressure equation (Faghri, 1995)

$$\left(\Delta p_{cap}\right)_{\max} \geq \Delta p_e + \Delta p_v + \Delta p_g \tag{2.13}$$

where Δp_{cap} is the capillary pressure generated, Δp_e is the pressure drop in the liquid phase, Δp_v is the pressure drop in the vapour phase and Δp_g is the pressure drop due to gravity.

Wick properties control the capillary pressure generated. The key properties of the wick that influence the heat pipe performance are the wick area, A_w, the wick permeability, K_w, and the effective pore radius of the wick structure, r_c. The area and permeability determine the liquid pressure drop and the radius of curvature determines the capillary pressure. Designs under consideration in this investigation include grooved and sintered. For grooves with a rectangular profile (Figure 2-3) the permeability, K_w, is calculated as (Faghri, 1995)

$$K_w = \frac{D_h^{\,2}\varphi}{2\left(f\,\mathrm{Re}_{l,h}\right)} \tag{2.14}$$

where D_h is the hydraulic diameter given by

$$D_h = \frac{4D_g W}{2D_g + W} \tag{2.15}$$

and (Shah and Bhatti, 1987)

$$f\,\mathrm{Re}_{l,h} = 24\left(1 - 1.355\alpha^* + 1.9468\alpha^{*2} - 1.7012\alpha^{*3} + 0.9564\alpha^{*4} - 0.2537\alpha^{*5}\right) \tag{2.16}$$

where

$$\alpha^* = \frac{W}{D_g} \tag{2.17}$$

The area of the wick needs to be measured from the actual heat pipe under consideration. The effective radius of curvature for rectangular grooves is

$$r_c = D_g \tag{2.18}$$

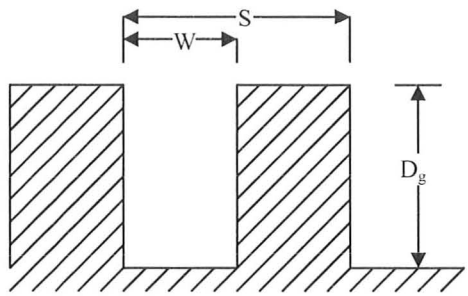

Figure 2-3: Dimensions of Rectangular Grooves

Sintered wick heat pipes operate in a similar manner to grooved wick except for the shape of the wick structure. Sintered wicks are created by lining the tube wall with metal powder, compacting and sintering it together. The porosity, permeability, cross section area and effective radius of curvature determine the performance. The wick area can be directly measured by examining the heat pipe, but the other parameters require more sophisticated tools. Total porosity can be measured with a mercury intrusion porosimeter, and the permeability can be calculated using the porosity and average powder diameter (Leong et al., 1997). Typical values for these values are published (Dunn and Reay, 1982) and they are used for the analysis (Table 2-1).

Table 2-1: Typical Sintered Wick Properties (Dunn and Reay, 1982)

Copper Powder	Pore Radius (m)	Permeability (m^2)	Porosity (%)
45-56 μm	0.0009	1.74×10^{-12}	28.7
100-125 μm	0.0009		30.5
150-200 μm	0.0021		35

The maximum heat that can be transferred by the heat pipe can be determined by rearranging the governing pressure balance equation for a heat pipe and is (Faghri, 1995)

$$q_{\max} = \left(\frac{2\sigma_l}{r_c} - \rho_l g \Delta h \sin\varphi \right) \frac{\rho_l A_w K}{\mu_l L_{eff}} \times h_{fg} . \tag{2.19}$$

where σ_l is the surface tension, ρ_l is the fluid density, g is the gravitational constant, Δh is the difference in height between the evaporator and condenser, φ is the inclination angle from the horizontal, is the fluid viscosity and L_{eff} is the effective length from the evaporator to the condenser. L_{eff} is taken to be half the evaporator length, plus the adiabatic length plus half the condenser length (Kreith and Bohn, 2001).

2.3 Computer Cooling

Cooling and thermal management of computer systems and components has been a topic of study since the first computers were created. Chu et al. (2004) present a very thorough review of computer cooling technology and research beginning with the ENIAC system built in 1946 up to the time of publishing, covering both desktop computers and servers. Three scales of the problem are covered: module (chip) level cooling; system cooling; and data centre cooling. As discussed in the scope of work, the analysis and review here will be limited to system level cooling. System level cooling encompasses the cooling of the computer casing and can be accomplished by air cooling, using airflow through the case; a hybrid air water system where an air to water heat exchanger is used to lower the temperature of the air inside the system; a liquid cooling solution where cooling water is used to cool the chips and/or system components and finally refrigeration cooling where a refrigeration system is used to achieve very low temperatures. Most commonly used is a finned heat sink that is air cooled by forced convection as shown in Figure 2-4 (Webb, 2005). Many different concepts of two phase cooling using heat pipes and vapour chambers exist and are reviewed.

Typical finned heat sinks have a base area which contacts the chip and distributes the heat to the fins. Air is forced past the fins by a fan and this convects the heat away. Much work has been published on optimization of forced convection heat sinks for chip cooling. It will only be briefly referenced (Culham and Muzychka 2001, Holahan 2005) here since it is not directly applicable to this project since it is based on forced convection. Work has been done to optimize the fin pattern for maximum heat removal and minimum pressure drop. An optimization method based on entropy generation minimization was developed by Culham and Muzychka (2001) that allows the optimization of all parameters for a plate fin heat sink operating under with forced convection.

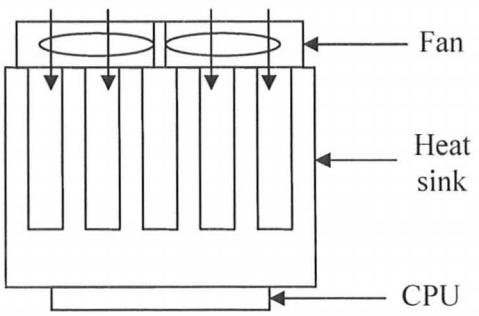

Figure 2-4: Diagram of a Typical Forced Convection Cooled Finned Heat Sink

Holahan (2005) extended the performance of a single fin over an array of fins to find the maximum volumetric system cooling performance. Heat sink base spreading losses were not taken into account.

The limits of direct air cooling have been explored by Saini and Webb (2002) and Webb (2005) and discussed by Wang (2008). It is found that there is a certain maximum that can be removed from a heat sink unit with specific overall dimensions.

2.3.1 Passive Phase Change Cooling Technologies

A design is discussed (Webb, 2005) which use vapour phase heat transport (heat pipes) to move heat to fins located farther away which increases the maximum heat that can be removed, an example of which is shown in Figure 2-5.

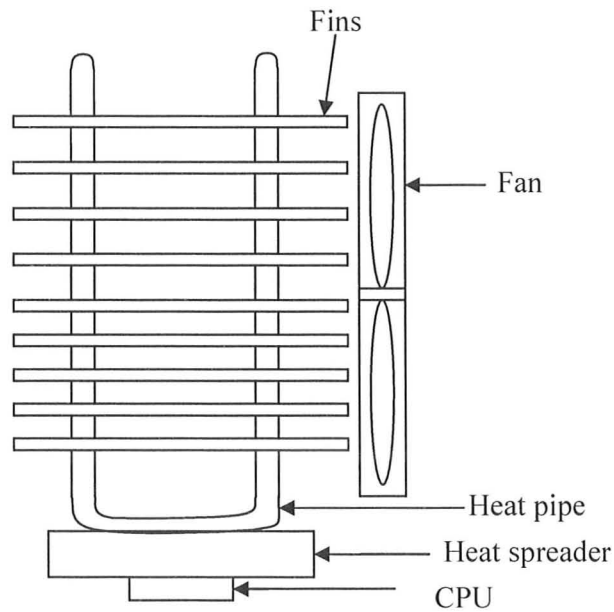

Figure 2-5: Diagram of a CPU Cooling Unit which uses Heat Pipes to Distribute Heat to Fins Located Some Distance Away from the CPU

Gao and Cao (2003) proposed and tested a system using a flat plate vapour chamber as a heat sink base to reduce temperature variations across the heat sink base (Figure 2-6). By changing from a copper spreader to a vapour chamber type heat spreader of the same dimensions the maximum temperature difference was reduced from 32°C to

3.3°C. They also tested a similar design using a U shaped vapour channel with positive results (Figure 2-7).

Roknaldin and Sahan (2003) conducted a computer simulation of a heat sink unit subjected to forced convection. It was designed with two flat heat pipes embedded in the base to increase heat spreading. It was found that an aluminum base with embedded heat pipes provided a lower chip temperature than either aluminum fins bonded to a copper

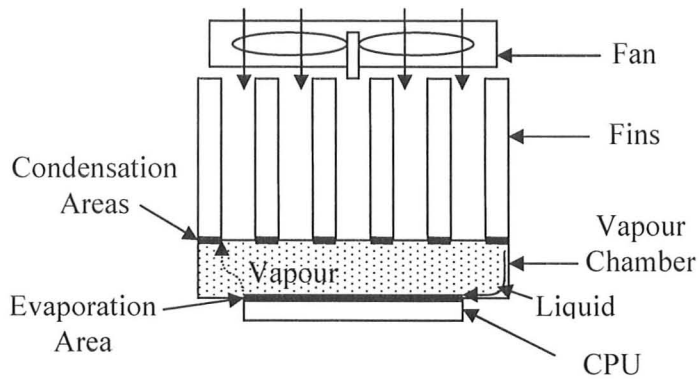

Figure 2-6: Heat Sink which uses a Vapour Chamber Base to Distribute Heat More Evenly to the Fins (Gao and Cao, 2003).

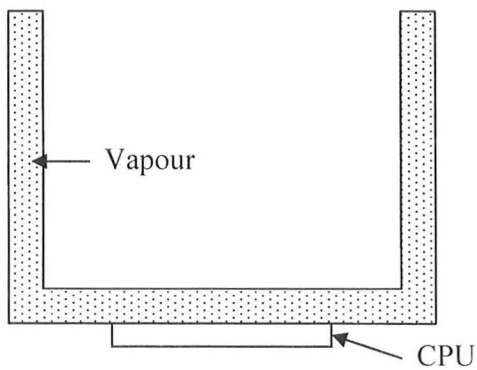

Figure 2-7: U Shaped Vapour Chamber Used as a Fin Surface for Heat Removal from a Processor (Gao and Cao, 2003)

base or a solid extruded aluminum heat sink unit. They also tested a case with an angled heat sink base that increases thickness in the flow direction to enable better spreading in the area with higher air temperature. Adding an angled base decreases chip temperature by about 4% compared to the solid aluminum heat sink, but only by about 2% compared to a base with embedded heat pipes.

Sauciuc et al. (2002) compared the spreading resistance of heat sink bases made using phase change systems such as vapour chambers to those made of solid metals. Two types of phase change systems were considered, those without wicks such as thermo-siphons and those with wicks (i.e. heat pipes). For systems that have no wick and the evaporation of the working fluid occurs on a smooth surface, the heat transfer limit is based on the nucleate boiling limit on the evaporator surface. For wicked heat pipes, the thermal resistance is based on the resistance through a fully saturated wick structure. It was found that as thickness of a solid metal base plate is increased, the spreading resistance decreases compared to a phase change base plate. For each heat source size, there is a critical plate thickness beyond which the solid metal base offers lower spreading resistance than the phase change plate. An equation was found to allow fast analysis of the effective thermal conductivity of vapour in a vapour chamber.

Xie at al. (1998) review the use of heat pipes in computer cooling applications. They looked at various notebook cooling designs and the use of a heat spreader plate for a processor chip package that uses heat pipes to distribute the heat more evenly. It was found to have half the spreading resistance of a copper plate of equal size and less than half the weight.

2.3.2 Microchannel Liquid Cooling

To adequately cool chips with high heat flux density that are packaged in closely spaced arrays, the concept of etching fins on the same silicon as the chip was first discussed and tested by Tuckerman and Pease (1981). Although high heat flux densities can be cooled by direct air cooling, when chips are packaged in closely spaced arrays there is insufficient space for air cooling. The design consisted of microchannels embedded in the same silicon substrate as the chip itself to enable direct heat removal without any intermediate materials and the associated contact resistance (Figure 2-8). Constant temperature water flow at about 23°C was passed through the microchannels. They fabricated and tested several different silicon microchannel heatsinks and successfully dissipated 790 W/cm^2.

Schmidt (2004) and Kandlikar and Grande (2004) each reviewed work done on microchannel cooling and describe and test example designs. Microchannel cooling techniques as presented are beyond the scope here since they must be implemented at the module level. A system could use a microchannel heat exchanger that is external to the processor silicon, an example of which is shown in Figure 2-9. However, such a system would require piping, a pump and a heat exchanger to cool the water bring added complexity which should be avoided if possible.

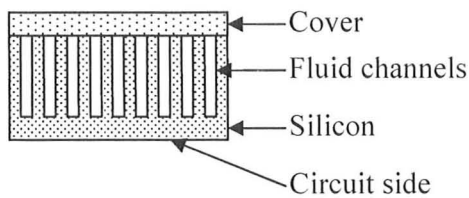

Figure 2-8: Diagram of a Microchannel Array Made from the Same Silicon Substrate as the CPU

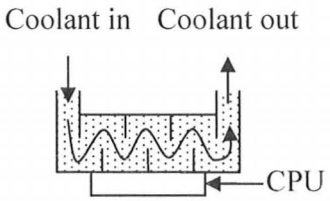

Figure 2-9: Diagram of a Chiller Block which Transfers Heat from the CPU to Coolant

2.3.3 Mobile Computer Cooling

Requirements for cooling for mobile computers (i.e. notebook computers) present many similarities to the cooling requirements for sealed systems. With the exception that mobile computers use forced air convection, they both need cooling in a limited space and with variable environmental conditions and possibly different orientations. Mobile cooling solutions are reviewed since many unique ideas are presented which can possibly be adapted for sealed systems. Wuttijumnong et al. (2004) reviewed present and future notebook cooling solutions. The systems considered, listed from lowest power dissipation to highest are a heat spreader with heat pipe, a hinged heat pipe system, a hybrid system with both a heat spreader and a fan, a remote heat exchanger and vapour chamber.

Kobayashi et al. (2002) discussed optimization of a thermal solution for a slim notebook computer running a CPU with a power dissipation of 4 W. Due to packaging constraints, fans and heat pipes are not considered for the solution. They determine that it can be adequately cooled by dissipating the heat to a cast magnesium heat spreader on the bottom of the chassis. Computer simulation was used to find the effect of the thermal conductivity of the heat spreader on the temperature of the processor.

Nakayama (2000) outlines the creation of a computer program to enable rapid analysis of heat spreading through different shapes of heat spreaders. The basis of the program is to create a database of general heat spreader layouts, and for each specific case the program will find an entry in the database that most closely resembles the specific case. The purpose is to create a system that is faster than full scale CFD and allows quick estimates during the design phase. Despite the ease of use of the proposed program, its creation involves a large amount of work which makes it only feasible if it was going to be used very heavily.

When using chips with TDP of up to 100 W forced air convection provides adequate cooling and two-phase cooling is only necessary when TDP exceeds 100 W (Webb, 2005). As suggested by Prasher (2003), heat pipes and vapour chambers can be modelled by assuming a low conductivity for the wick, on the order of 26 W/mK and a very high conductivity for the vapour phase area. For the geometry Prasher studied with an adiabatic length of 95 mm, the effective thermal conductivity of the vapour (k_{vapour}) was on the order of 267000 W/mK. Prasher notes that although it is always very high, k_{vapour} depends on the adiabatic length and it will decrease for longer distances. Although the chip TDP does not exceed 100 W, since the sealed computer system requires moving heat over a distance of about 40mm and temperature drops should be minimized from the chip to the fin surface, two-phase solutions (i.e. heat pipes and vapour chambers) show the most promise due to the very high effective thermal conductivity.

2.4 Natural Convection from Vertical Fins

Since the final resistance in the thermal path from the CPU to the ambient is the fins, parallel plate fins will be reviewed. The first study of natural convection from parallel plates was by Elenbaas in 1942. The convection coefficient was investigated for various spacing between plates. For closely spaced plates the coefficient was found to approximately equal that for fully developed laminar flow and for widely spaced plates the coefficient approached the value for flow over a flat plate.

Bodoia and Osterle (1962) numerically solved the equations of motion for natural convection of fluid between two heated plates. When compared with the experimental data of Elenbaas a good agreement was found.

Experiments on parallel rectangular fins were also conducted by Starner and McManus (1963). They tested four fin sets with spacing (S) 6.35 mm and 7.95 mm and heights (H) of 6.35 mm, 12.7 mm, 25.4 mm and 38.1 mm, where the spacing and height dimensions are defined in Figure 2-10. Tests were conducted with the plate oriented vertically, at 45° and horizontally. The heat transfer coefficients were found to be about 5 to 20% lower for fins than for similarly spaced parallel plates due to base effects and end effects. Heat transfer coefficients were highest for the vertical orientation, followed by the 45° orientation and lowest for the horizontal orientations.

Experimental investigations on rectangular vertical fins were conducted by Welling and Wooldridge (1965). They tested four different distances of fin spacing and three fin heights for a total of 12 fin configurations and tested a flat plate with the same base area size, all of which are listed in Table 2-2. Each of the fin parameters, fin height,

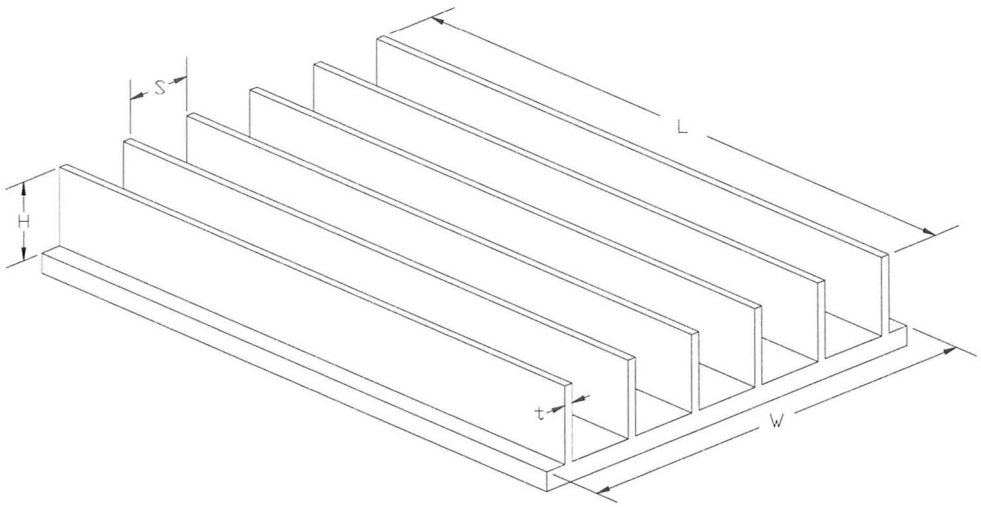

Figure 2-10: Fin Array Tested by Starner and McManus (1963)

Table 2-2: Fin Configurations tested by Welling and Wooldridge (1965)

Configuration	H (mm)	S (mm)	L (mm)	W (mm)
1	19.05	19.05	203.2	66.294
2	19.05	10.52	203.2	66.294
3	19.05	6.858	203.2	66.294
4	19.05	4.826	203.2	66.294
5	12.7	19.05	203.2	66.294
6	12.7	10.52	203.2	66.294
7	12.7	6.858	203.2	66.294
8	12.7	4.826	203.2	66.294
9	6.35	19.05	203.2	66.294
10	6.35	10.52	203.2	66.294
11	6.35	6.858	203.2	66.294
12	6.35	4.826	203.2	66.294
13 (Flat Plate)	0	-	203.2	66.294

and fin spacing had an impact on the heat transfer rate. It was found that for all fin dimensions the convective heat transfer coefficient was below that of a flat plate but above that for parallel plates or a square duct. However despite the heat transfer

coefficient being below a flat plate, the added surface area increases the total heat transfer above that for a flat plate of the same size as the fin base (Figure 2-12).

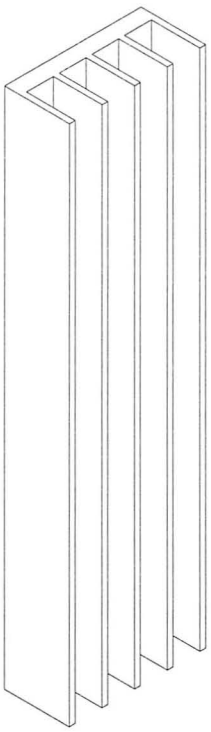

Figure 2-11: Fins Tested Experimentally by Welling and Wooldridge (1965)

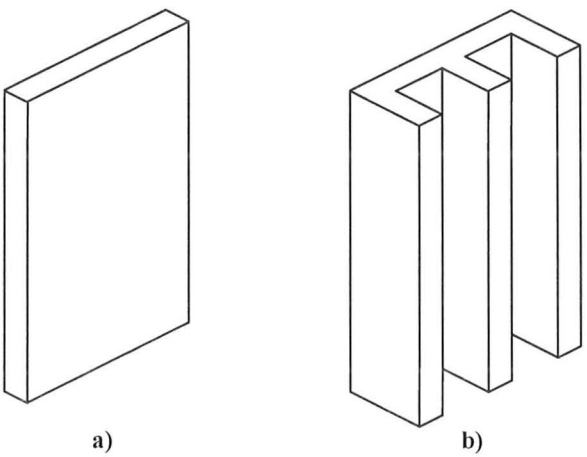

Figure 2-12: a) Flat Plate and b) Fin Plate with Equal Base Area

Aung et al. (1973) studied natural convection in electronic cabinets experimentally. They found that the results can be approximated quite well with two dimensional theoretical models. They studied staggering of heat generating electronic circuit boards in component cabinets (Figure 2-13) and found they can help heat transfer by exposing the top cards to cooler air from the centre of the lower channels, however they are helpful only in certain situations as long as the channels were not too long and/or narrow. They also studied baffles and found they are only useful when the drag on the flow is low.

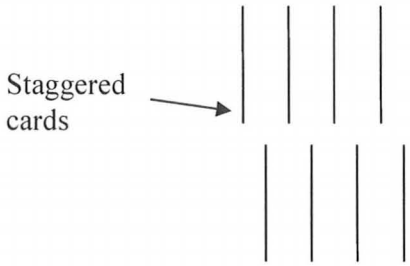

Figure 2-13: Staggered Cards as Investigated by Aung et al., (1973)

Bar-Cohen and Rohsenow (1983; 1984) detailed the development of equations for Nusselt numbers for flow between parallel plates. They presented equations for symmetrically isothermal, asymmetrically isothermal, symmetrically isoflux and asymmetrically isoflux channels. They described the optimization process for card spacing to achieve the lowest card temperatures. In 2003, Bar-Cohen et al. detailed how to optimize plate-fin heat sinks for different criteria including maximum heat transfer, maximum heat transfer with respect to heat sink mass and maximum heat transfer with respect to heat sink volume.

Sparrow and Bahrami (1980) compared the effects of open and closed edges on natural convection from parallel plates. They noted that the effect of the assumption of constant fluid properties can make a significant impact on the Nusselt number that is calculated when there is a large difference between the surface temperature and the ambient air temperature as was the case in Elenbaas's work. Further discrepancies with Elenbaas's work were found and are attributed to corrections made by Elenbaas to account for heat losses in the system. Differences with two dimensional models are attributed to the significant edge/end effects which require three dimensional models to capture properly.

Karagiozis et al. (1994) experimentally studied the natural convection heat transfer from horizontal and vertical triangular fins on a vertical surface. A correlation equation was found which allowed estimation of their results with less than 5% error. Results for horizontal fins were not correlated due to strong dependence on number of fins, although the authors state that horizontal fins have a significantly lower Nusselt number than vertical fins.

Khan et al. (2006) used entropy generation minimization to determine the heat transfer and pressure drop simultaneously in different fin configurations. Using entropy generation minimization they optimized fin geometry, and compared the performance of different shapes of pin fins and plate fins.

The previous experimental studies most relevant to the current work are the work done by Starner and McManus (1963) and Welling and Wooldridge (1965) since their geometries most closely resemble the current system. All of the fins tested by Starner and

McManus had a spacing of either 6.35 mm or 7.95 mm, well below the current spacing of 10.5 mm. Welling and Wooldridge tested a far broader range of fin dimensions including one with a height of 19.05 mm and spacing of 10.52 mm which is very close to the current height of 22.3 mm and spacing of 10.5 mm.

The model presented by Bar-Cohen and Rohsenow (1983) detailed in Bar-Cohen and Rohsenow (1984) and extended in Bar-Cohen et al. (2003), is also of great interest since it allows analytical estimation of the performance of any fin spacing. The Nusselt number for a symmetrically isothermal channel is given as

$$Nu_O = \left[\frac{576}{(Ra')^2} + \frac{2.873}{(Ra')^{-1/2}} \right]^{-1/2} \tag{2.20}$$

where Ra' is the channel Raleigh number given as

$$Ra' \equiv \overline{\rho}^2 \frac{g\beta c_p b^4 \theta_o}{\mu k L} \tag{2.21}$$

where b is the fin spacing, in m, c_p is the specific heat of the fluid, g is the gravitational acceleration, k is thermal conductivity of the fluid, L is the channel height, β is volumetric expansion coefficient, ρ is the fluid density, θ_o is the temperature difference, and μ is the dynamic viscosity.

Another mechanism of heat transfer from the fins to the surroundings is by radiation heat transfer. Ellison (1979) studied vertical rectangular fin channels and noted that a substantial amount of the total heat dissipated could be moved to the surroundings by radiation. He assumed that the heat sink material is a gray, diffuse, isotemp surface and presented a series of figures to find the gray body shape factor for different values of H/L. Shabany (2008) solved for a complete analytical formula for the view factor from a

U channel of dimensions S, L and H. The shape factor for a set of U channel fins is given by Shabany (2008), in terms of normalized dimensions $\overline{H} = H/S$ and $\overline{L} = L/S$ as

$$F_{s-surr} = \frac{A_1}{A_{123}}\left[F_{1-4} + 2F_{1-5}\right] + 2\frac{A_2}{A_{123}}\left[F_{2-4} + 2F_{2-5}\right] \tag{2.22}$$

where

$$F_{1-4} = \frac{2\overline{H}^2}{\pi\overline{L}}\left\{\ln\left[\frac{\left(\overline{H}^2+1\right)\left(\overline{H}^2+\overline{L}^2\right)}{\left(\overline{H}^2+\overline{L}^2+1\right)\overline{H}^2}\right]^{1/2} + \frac{\left(\overline{H}^2+\overline{L}^2\right)^{1/2}}{\overline{H}^2}\tan^{-1}\frac{1}{\left(\overline{H}^2+\overline{L}^2\right)^{1/2}} + \frac{\overline{L}\left(\overline{H}^2+1\right)^{1/2}}{\overline{H}^2}\tan^{-1}\frac{\overline{L}}{\left(\overline{H}^2+1\right)^{1/2}} - \frac{1}{\overline{H}}\tan^{-1}\frac{1}{\overline{H}} - \frac{\overline{L}}{\overline{H}}\tan^{-1}\frac{\overline{L}}{\overline{H}}\right\}, \tag{2.23}$$

$$F_{2-4} = \frac{\overline{L}}{\pi\overline{H}}\left\{\frac{\overline{H}}{\overline{L}}\tan^{-1}\frac{\overline{L}}{\overline{H}} + \frac{1}{\overline{L}}\tan^{-1}\overline{L} - \frac{\left(1+\overline{H}^2\right)^{1/2}}{\overline{L}}\tan^{-1}\frac{\overline{L}}{\left(1+\overline{H}^2\right)^{1/2}} + \frac{1}{4}\ln\left[\left(\frac{\left(\overline{L}^2+1\right)\left(\overline{H}^2+\overline{L}^2\right)}{\left(\overline{H}^2+\overline{L}^2+1\right)\overline{L}^2}\right)\left(\frac{\overline{H}^2\left(\overline{H}^2+\overline{L}^2+1\right)}{\left(\overline{H}^2+1\right)\left(\overline{H}^2+\overline{L}^2\right)}\right)^{\frac{\overline{H}^2}{\overline{L}^2}}\left(\frac{\overline{H}^2+\overline{L}^2+1}{\left(\overline{L}^2+1\right)\left(\overline{H}^2+1\right)}\right)^{\frac{1}{\overline{L}^2}}\right]\right\}, \tag{2.24}$$

$$F_{1-5} = \frac{1}{\pi\overline{L}}\left\{\overline{L}\tan^{-1}\frac{1}{\overline{L}} + \overline{H}\tan^{-1}\frac{1}{\overline{H}} - \left(\overline{H}^2+\overline{L}^2\right)^{1/2}\tan^{-1}\frac{1}{\left(\overline{L}^2+\overline{H}^2\right)^{1/2}} + \frac{1}{4}\ln\left[\left(\frac{\left(1+\overline{L}^2\right)\left(1+\overline{H}^2\right)}{\left(\overline{H}^2+\overline{L}^2+1\right)}\right)\left(\frac{\overline{L}^2\left(\overline{H}^2+\overline{L}^2+1\right)}{\left(\overline{L}^2+1\right)\left(\overline{H}^2+\overline{L}^2\right)}\right)^{\overline{L}^2}\left(\frac{\overline{H}^2\left(\overline{H}^2+\overline{L}^2+1\right)}{\left(\overline{H}^2+1\right)\left(\overline{H}^2+\overline{L}^2\right)}\right)^{\overline{H}^2}\right]\right\}, \tag{2.25}$$

$$F_{2-5} = \frac{\overline{H}}{\pi\overline{L}}\left\{\frac{\overline{L}}{\overline{H}}\tan^{-1}\frac{\overline{H}}{\overline{L}} + \frac{1}{\overline{H}}\tan^{-1}\overline{H} - \frac{\left(1+\overline{L}^2\right)^{1/2}}{\overline{H}}\tan^{-1}\frac{\overline{H}}{\left(1+\overline{L}^2\right)^{1/2}} + \frac{1}{4}\ln\left[\left(\frac{\left(\overline{H}^2+\overline{L}^2\right)\left(1+\overline{H}^2\right)}{\left(\overline{H}^2+\overline{L}^2+1\right)\overline{H}^2}\right)\left(\frac{\overline{L}^2\left(\overline{H}^2+\overline{L}^2+1\right)}{\left(\overline{L}^2+1\right)\left(\overline{H}^2+\overline{L}^2\right)}\right)^{\frac{\overline{L}^2}{\overline{H}^2}}\left(\frac{\overline{H}^2+\overline{L}^2+1}{\left(\overline{H}^2+1\right)\left(\overline{L}^2+1\right)}\right)^{\frac{1}{\overline{H}^2}}\right]\right\}. \tag{2.26}$$

A simplified version is given which can predict the shape factor to within 11%:

$$F_{s-surr} = 1 - \frac{2\overline{H}\left[\left(1+\overline{L}^2\right)^{1/2} - 1\right]}{2\overline{H}\overline{L} + \left(1+\overline{L}^2\right)^{1/2} - 1}. \tag{2.27}$$

Due to the broad scope of the review presented, not all reviewed material is relevant to the present work. Concepts for new computer cooling techniques provide interesting solutions to many problems but due to the design of this system they would not solve the final bottleneck of the fins and are not investigated further. The effective thermal conductivity equation for vapour presented by Sauciuc (2002) appears quite useful if future work is done on vapour chamber heat spreaders. Carbon foam properties tested by Klett (1999), Klett et al. (2000) and Gaies and Faber (2002), are all quite useful to understand the properties of the foam. Since the foam is not being investigated for use as a fin material the studies on forced convection are not used further.

The experimental results of Welling and Wooldridge (1965) are quite relevant to analysis of the fin plate along with the model developed by Bar-Cohen and Rohsenow (1983; 1984) since it allows prediction of fin performance for any fin geometry. Radiation analysis prediction can be estimated using the model of Shabany (2008). The experiments on horizontal fins by Starner and McManus (1963) suggest horizontal orientation of the fin plate will reduce natural convection. The experiments of Karagiozis et al. (1994) describe the significant reduction in Nusselt number for a vertical fin plate with horizontal fins compared to a vertical plate with vertical fins. These studies indicate that the computers should only be operated with the fins in the vertical orientation unless special care is taken in the design and analysis.

Chapter 3 Test Facility and Data Reduction

3.1 In-Situ Test Facility

3.1.1 Components and Instruments

The application based nature of this project dictates that many tests be conducted in a computer system so that results are immediately applicable to the end use. By instrumenting the system to take internal temperature measurements not only can the system performance be determined but the performance of each component can be isolated. Type T thermocouples were used and calibrated to an accuracy of 1°C and a precision of 0.125°C. Thermocouples were either 30 or 36 gauge with bare ends and were held in place with tape and a thermally conductive paste was used to reduce contact resistance between the junction and the surface being measured. Thermocouples were placed throughout the system. One was placed on the CPU package substrate, next to the silicon die (Figure 3-1). Another was placed on the base of the fin plate in approximately the centre of the plate (Figure 3-2) and another was located well away from the fin to measure the surrounding air temperature.

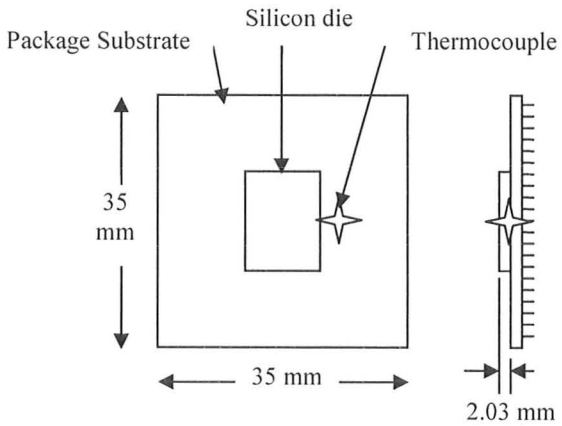

Figure 3-1: Placement of Thermocouple on CPU Package Substrate

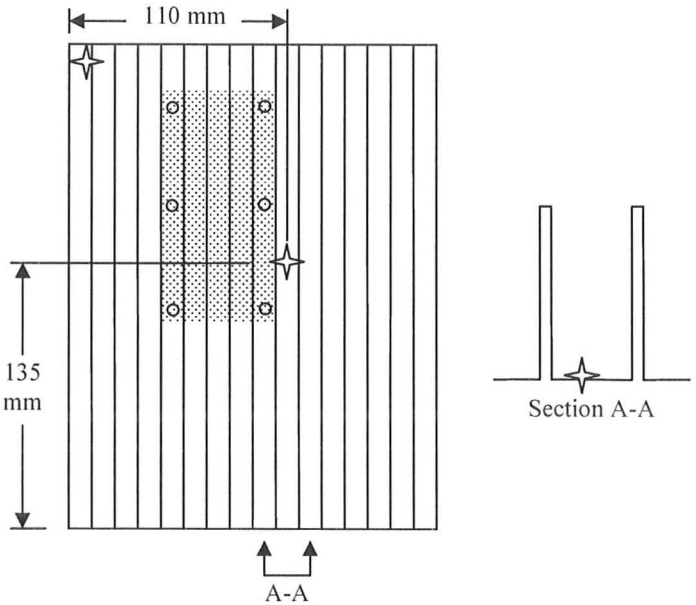

Figure 3-2: Placement of Thermocouple on Fin Plate

The temperature gradient and rapid increases in power output that can occur inside the silicon that forms the processor core can cause temperatures inside the silicon that exceed the maximum temperature and are not detected with an externally mounted temperature sensor. The temperature inside the processor is measured using Digital

Thermal Sensors (DTS) located at the hottest points inside the silicon substrate to prevent thermal failure (Intel, 2009a). The DTS is designed to enable active thermal management to prevent failure using techniques including switching the processor cores off and on at a 50% duty cycle to control the processor power consumption and completely cutting off power to the processor. Accuracy of DTS sensors is typically ± 5°C from 80°C to 110°C and decreases below 80°C (Intel, 2009c). Due to the relatively poor accuracy of the DTS sensor, values from it will not be used for analysis but just to ensure readings from thermocouples are in the correct range.

Power drawn by the computer was measured using an Extech True RMS Power Multimeter using the AC Voltage and AC Current modes and multiplying voltage and current. Voltage was measured to an accuracy of ± (0.8 % + 0.3) and current was measured to an accuracy of ± (1.5 % + 0.003) (Extech, 2001). For the voltage and current readings the percentage error comes from the analog measurement circuit and the whole value offset comes from error in the analog to digital converter.

3.1.2 Heat Pipe Test Section

In addition to the apparatus described in the preceding section, for testing the heat pipes two thermocouples were placed on the heat pipe unit, one on the heat spreader on the evaporator side of the heat pipe and the second on the heat spreader on the condenser side of the heat pipe (Figure 3-3). The evaporator heat spreader is screwed to the motherboard to provide a strong clamping force against the CPU and *northbridge* and the condenser heat spreader is screwed to the fin plate to reduce contact resistance (Figure

3-4). Due to the slight flexibility of the heat pipes, both spreaders can be successfully screwed down to reduce contact resistance.

Testing of the heat pipes was conducted at different orientations. The computer system was physically turned 180° to change the orientation during the testing. At all times a distance of between 150 mm and 200 mm was between the bottom of the fin plate and the computer mounting surface to allow flow development.

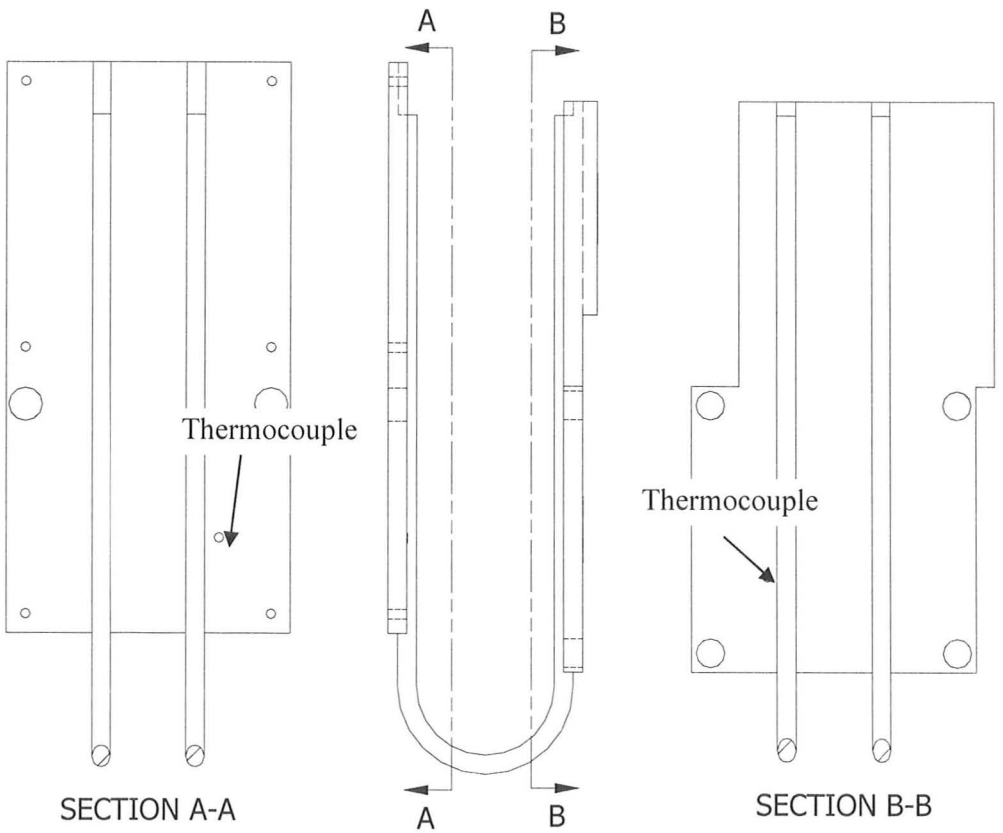

Figure 3-3: Placement of Thermocouples on Heat Pipe Unit

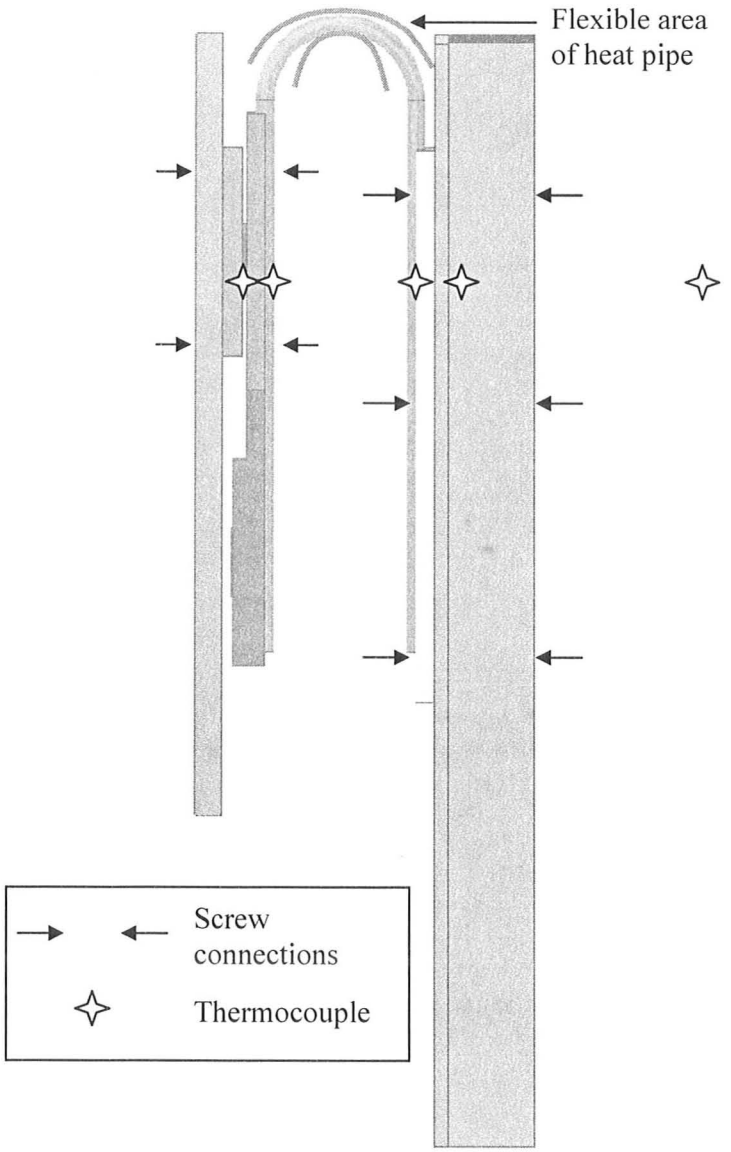

Figure 3-4: Fastening of Heat Pipe Unit to CPU and Fin Plate and Placement of all Thermocouples on Heat Pipe Test Section

3.2 Controlled Heat Flux Test Facility: Components and Instruments

A test apparatus was designed to simulate the in-situ conditions while at the same time providing more control over the experiment. The main unknown in the in-situ testing was how much power was being dissipated through the conduction medium since the CPU and *northbridge* each produce a different amount. In order to quantify the properties of the carbon foam, the exact power dissipated must be known. The test apparatus consisted of a polyimide film insulated flexible heater connected to an aluminum heat spreader, which represents the CPU and *northbridge*, bolted to the fin plate (Figure A-8) with the conduction medium in the middle. This design allowed the distance between the heat spreader, which represents the CPU and *northbridge*, to sit at any distance to the fin plate. The carbon foam and copper blocks were also placed in the test apparatus in their thinnest orientation to determine if the carbon had anisotropic thermal properties. At all times the fin plate had a clearance of 910 mm to the surface below, which allowed flow to develop.

Type T thermocouples were used and calibrated to an accuracy of 1°C and a precision of 0.125°C. Thermocouples were either 30 or 36 gauge with bare ends and were held in place with tape and a thermally conductive paste was used to eliminate contact resistance between the junction and the surface being measured. A thermocouple was placed on the center of the heater, on the front surface of the fin plate, in the centre, on the end of one fin and another was located well away from the fin to measure the surrounding air temperature (Figure 3-5).

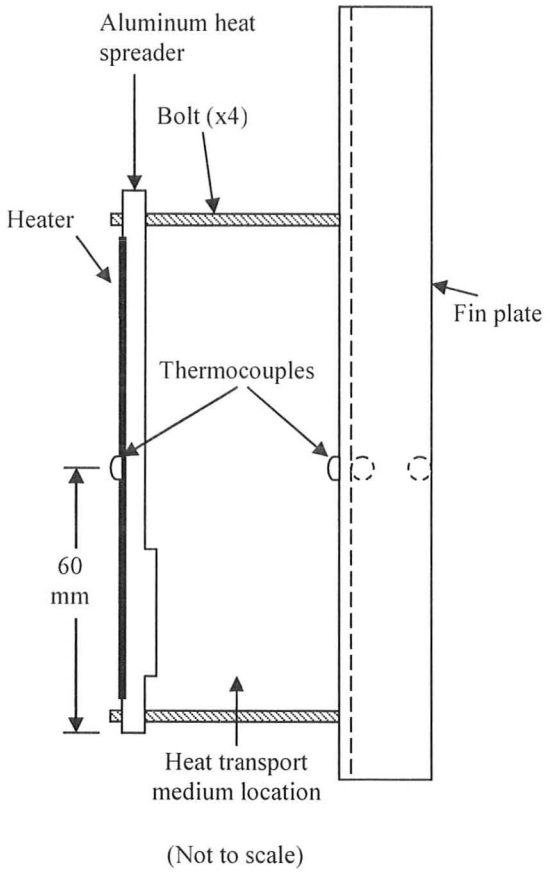

Figure 3-5: Controlled Heat Flux Test Facility

Power drawn by the computer was measured using an Extech True RMS Power Multimeter using the AC Voltage and AC Current modes and multiplying voltage and current. Voltage was measured to an accuracy of ± (0.8 % + 0.3) and current was measured to an accuracy of ± (1.5 % + 0.003) (Extech, 2001). For the voltage and current readings the percentage error comes from the analog measurement circuit and the whole value offset comes from error in the analog to digital converter.

To prevent heat loss to the ambient, 20mm fibreglass insulation was placed tightly around all components behind the fin plate. It was not placed between components so radiation could occur between the heat spreader and the fin plate.

3.2.1 Heat Pipe

The procedure for studying the heat pipe in a controlled heat flux test facility was developed by M. K. Russel as part of the project and is detailed in Russel et al. (2010). A 50 mm x 100 mm flexible heater with a maximum heat flux of 1.55 x 10^{-3} W/mm^2 controlled by a variable transformer was used to provide the thermal load on the heat spreader on the evaporator side. The heater was connected through a power meter to measure the power input to the system. The other heat spreader was attached to the fin plate as depicted in Figure 3-6. The system was tested in five orientations with respect to gravity, shown in Figure 3-6.

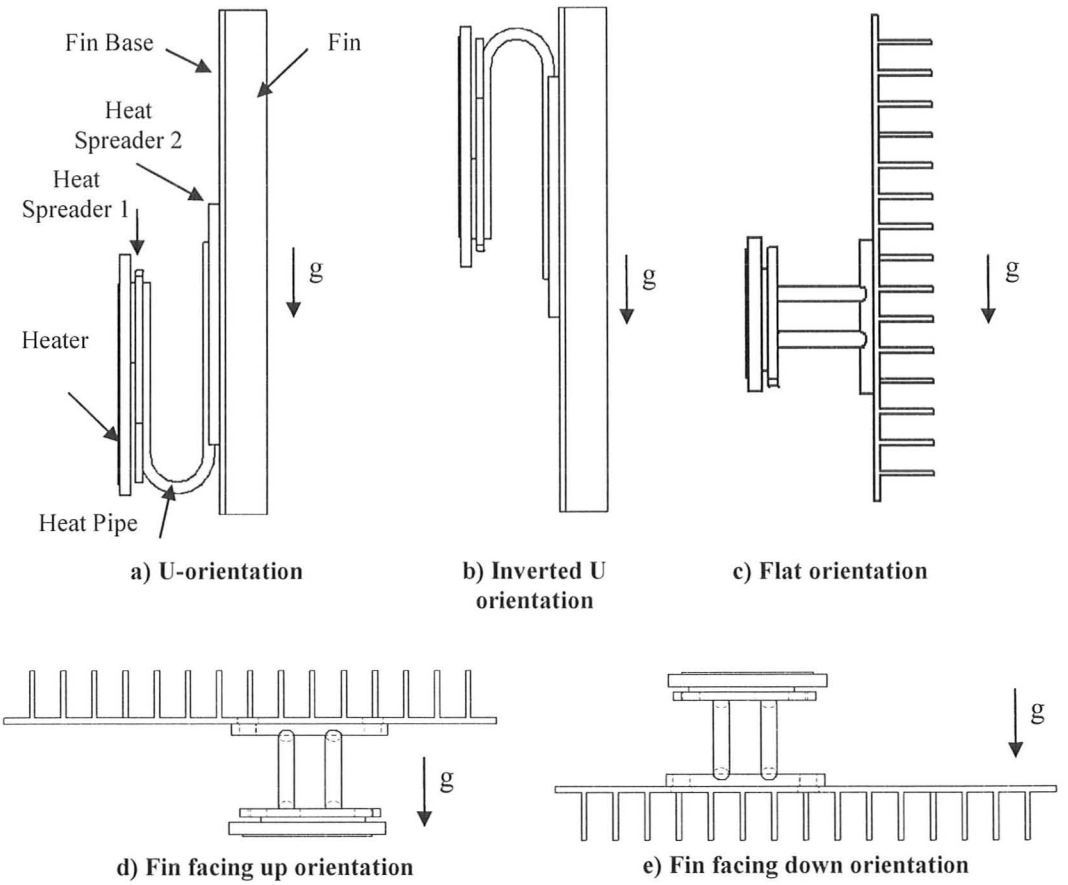

a) U-orientation

b) Inverted U orientation

c) Flat orientation

d) Fin facing up orientation

e) Fin facing down orientation

Figure 3-6: U Heat Pipe Orientations

Five T-type thermocouples were attached along the length of each heat pipe using thermal paste with a thermal conductivity of 8.7 W/mK to reduce thermal contact resistance. Fibreglass insulation was used to insulate the whole system to reduce heat losses to the surroundings. Temperature measurements for each orientation were taken after the system was allowed to fully reach steady state and the thermocouples readings did not fluctuate by more the 0.5°C over 5 minutes.

3.3 Fin Heat Transfer Spreading Measurements

Heat transfer spreading measurements were taken concurrently with the testing of the heat pipe in the in-situ and controlled heat flux test facility. Using an infrared camera, temperature contour images of the fin plate were recorded.

A Flir SC-3000 infrared thermal imaging camera was used with a thermal sensitivity of 0.02 K and accuracy of ± 1% or ± 1°C up to 150°C. ThermaCAM Researcher software running on a PC enabled viewing and recording of thermal images. Accurate measurements require the emissivity of the surface under investigation to be known. By viewing the fin plate with thermocouples attached by black vinyl tape, the emissivity of the tape could be seen to be approximately that of the anodised finish on the aluminum plate (Figure 3-7). The temperatures are 50.8°C and 51.2°C for SP01 and SP02 respectively. Using the temperature reported by the thermocouple as the known surface temperature and the temperature reported by the IR camera for the vinyl tape, the software automatically calculated the emissivity value of the surface and tape to be 0.99.

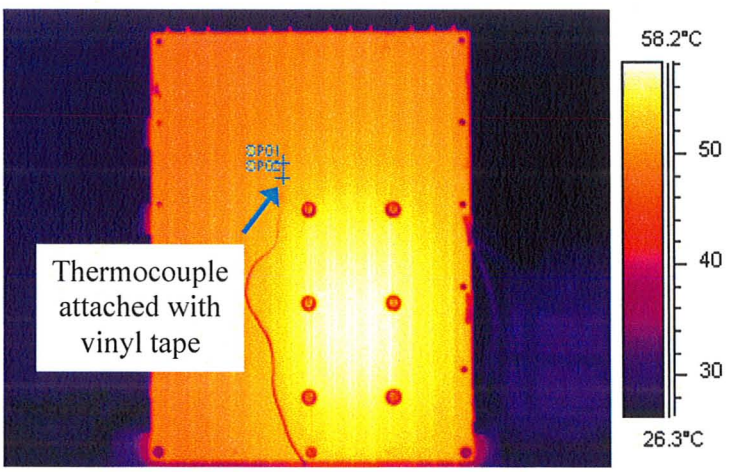

Figure 3-7: Thermal Image of Fin Plate showing Thermocouple

Provided the surface coating is uniform, the emissivity found at one point can be applied to the whole surface and allows temperatures to be found anywhere on the surface. The temperature of any holes, screws or bolts present on the surface are not reported correctly since their emissivity is different from that of the plate.

The conditions of the surroundings were monitored. The air conditioning system was detected in the results as the temperature would slowly climb until it came on and the temperature was reduced. Without the air conditioning running the room temperature would have climbed constantly throughout the day. Temperatures were always measured before the air conditioning switched on in its cycle. The temperature was approximately 25°C. The thermal imaging software corrected for the air temperature interfering with infrared readings.

3.4 Data Acquisition System

Thermocouple temperature measurements were recorded by a Measurement Computing Corp. PCI-DAS-TC data acquisition system and the recorded with Labview software. Sampling rate could be controlled and was set to record data at 5 second intervals.

Power measurements using the multimeter were recorded manually. Speedfan 4.38 software was loaded on the computer being studied to monitor and record the temperature from the DTS inside the CPU.

3.5 Experimental Procedure and Methodology

3.5.1 In-Situ

The first test performed was to characterize the system as it was received from the manufacturer. Thermocouples were mounted to parts of the system and software was used to read the DTS inside the processor. The power use and heat generated by the computer system varies based on the load applied to the processor. For testing, processing load was controlled using "Burn in" software which can individually load many different parts of the system (Table 3-1) and control the heat produced by the system. By setting the CPU Math processor, CPU MMX processor, memory, video, 2D graphics and 3D graphics to 100% load, the CPU and *northbridge* chip will produce the maximum heat possible giving a worst case scenario for real world use. Running the computer at idle was accomplished by booting to windows and not opening any programs. CPU usage stayed below 2% while running at idle. The computer was typically left for at least 1 hour

Table 3-1: Systems Which can be Individually Controlled using "Burn in" Software

CPU Math
CPU MMX
RAM
Video
2D Graphics
3D Graphics
Disk(s)
CD-RW/DVD
Sound
USB
Printer
Parallel Port
Com Port(s)
Network
Tape

to reach steady state when it was running at idle and for 3 hours when running at full load.

For testing the heat pipe, carbon foam and copper block benchmark, the system was started, data acquisition was started and once the system had booted the "burn-in" software was loaded and full load was applied to the system. Ambient temperatures in the room were steady between 22°C and 25°C. The system was run until steady state conditions were achieved. Steady state was defined as a change of less than 0.5°C over 5 minutes.

The power meter allowed measurement of the total power consumed by the computer during use. For calculations the CPU was assumed to consume its rated TDP while it was operating at full load. Baseline power consumption was found by subtracting the TDP of the CPU from the measured power consumption at full load. To estimate the CPU power consumption at idle, baseline system power was subtracted from the measured power consumption of the system at idle. The power budget of the system at idle and full load is shown in Figure 3-8.

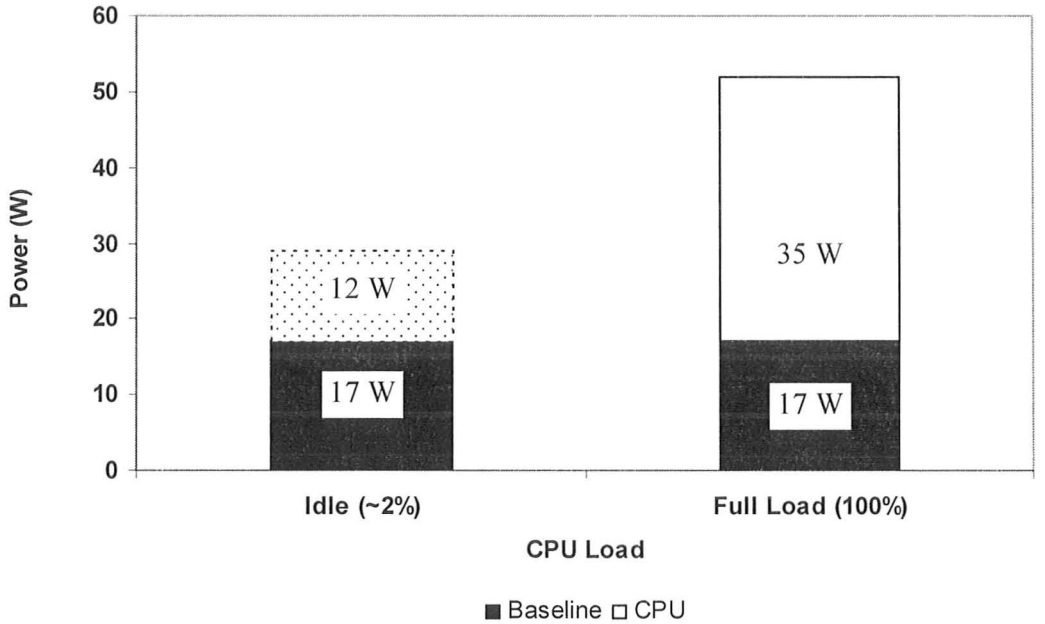

Figure 3-8: Breakdown of System Power Consumption at Idle and 100% Load.

3.5.2 Controlled Heat Flux Facility

For testing the heat pipe, carbon foam and copper block benchmark, each was installed into the controlled heat flux facility and power applied to the heater. The data acquisition system was started at the same time as power was applied. The system was run until steady state conditions were achieved, typically 1 hour. Steady state was defined as a change of less than 0.5°C over 5 minutes. In the case of the test apparatus, the power to the heater was set at 35 W to match the TDP of the CPU for the normal orientation and 25 W for the alternate orientation.

3.6 Data Reduction and Error Analysis

Temperatures from the data acquisition system were averaged over 5 minutes once steady state was reached and the average value was used for each point. Uncertainty

for each measured value is based on equipment specifications. Uncertainties for measured values are shown in Table 3-2. Uncertainties for calculated values are found using the formula provided by Kline and McClintock (1953)

$$\Delta f = \sqrt{\sum_{i=1}^{n}\left(\frac{\partial f}{\partial x_i}\Delta x_i\right)^2} \tag{3.1}$$

where x_i are the independent variables used to calculate the desired value f. Calculated uncertainties are listed in Table 3-3. When experiments were repeated, the results were comparable within a maximum of 5% when a variation of surrounding temperature of 6% was taken into account. Conducting a three point calibration of the thermocouples it was found they had an accuracy 0.6 K and the readings agreed within 0.125 K of each other. This close agreement is used to find the ΔT uncertainty.

Table 3-2: Uncertainty in Measured Values

Measurement	**Uncertainty**
AC Current	± 2.5%
AC Voltage	± 1.5%
Temperature – Thermocouple + Data Acquisition System	± 0.6 K – accuracy, ± 0.125 K precision
Distance	± 0.01 mm
Temperature – IR Camera	± 1 K or ± 1%
Mass	Readability 0.01g, Repeatability 0.01g, Linearity ± 0.02g

Table 3-3: Uncertainty in Calculated Values

Quantity	Equation	Uncertainty
Electric Power	$q_{elec} = IV$	± 3%
Temperature difference	$\Delta T = T_2 - T_1$	± 0.2 K
Thermal resistance	$R = \Delta T / q$	± 7 % for 3 K < ΔT < 5 K ± 5 % for 5 K < ΔT < 10 K ± 3 % for 10 K < ΔT < 20 K ± 2.5 % for ΔT > 30 K
Thermal conductivity	$k = q * t / \Delta T * A$	± 7 % for 3 K < ΔT < 5 K ± 5 % for 5 K < ΔT < 10 K ± 3 % for 10 K < ΔT < 20 K ± 2.5 % for ΔT > 30 K
Density	$\rho = m / l * w * h$	± 1 %
Evaporator temperature – Controlled heat flux heat pipe test	$T_e = (T_1 + T_2 + T_3 + T_4) / 4$	± 0.5 K
Condenser temperature – Controlled heat flux heat pipe test	$T_c = (T_5 + T_6 + T_7 + T_8) / 4$	± 0.5 K
Temperature difference – Controlled heat flux heat pipe test	$T_e - T_c =$ $[(T_1 + T_2 + T_3 + T_4)$ $- (T_5 + T_6 + T_7 + T_8)] / 4$	± 0.7 K

Chapter 4 Results and Discussion

Chapter 4 will review and discuss the results of the work done and what they mean in terms of overall system performance. Initially the work done to benchmark the systems will be covered to determine the starting place for subsequent research. Following that, detailed experimentation and analysis to characterize two heat pipe units is examined. Carbon foam is investigated next as a possible material to use to directly conduct heat from the CPU and *northbridge* to the fin plate. For the fin plate the natural convection is analyzed, optimization of the fin geometry is examined and numerical fluid modeling is conducted.

4.1 In-Situ – Computer Benchmarking of Current Designs

Computer benchmark testing consisted of instrumenting a computer system with thermocouples as described in section 3.1.1 and running the system at idle and full load as discussed in section 3.5.1. The results of the computer benchmark testing were analyzed to identify the magnitude of each thermal resistance in the system (Figure 4-1) and are shown in Figure 4-2.

The resistances measured are shown in Figure 4-2 and all resistances are calculated using values from thermocouples. The first resistance, $R_{CPU\text{-}Evaporator}$ uses the temperature difference between the CPU and the evaporator section of the heat pipe. This resistance includes the contact resistance between the CPU and the heat spreader as well as the resistance due to conduction through the heat spreader. The resistance denoted R_{HP} is based on the temperature drop from the evaporator of the heat pipe to the condenser.

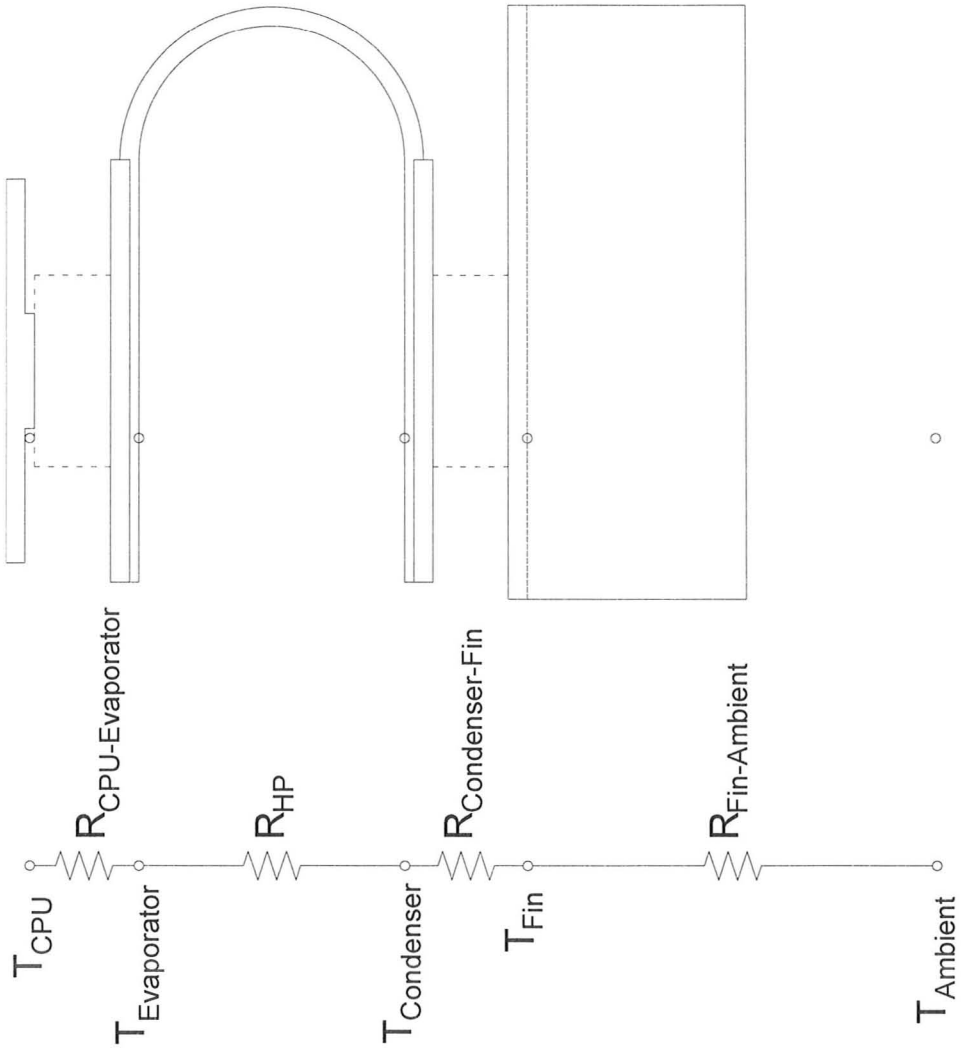

Figure 4-1: Thermal Resistance Diagram for Initial System Evaluation

$R_{Condenser\text{-}Fin}$ uses temperatures from the condenser of the heat pipe and the front side of the fin plate. This includes resistance from conduction through the condenser side heat spreader, contact resistance between the heat spreader and the fin plate and conduction through the fin plate. The final resistance is $R_{Fin\text{-}Ambient}$ and it includes the conduction through the fin plate, the fin efficiency and the convection from the fin base plate and from the fins to the surrounding air.

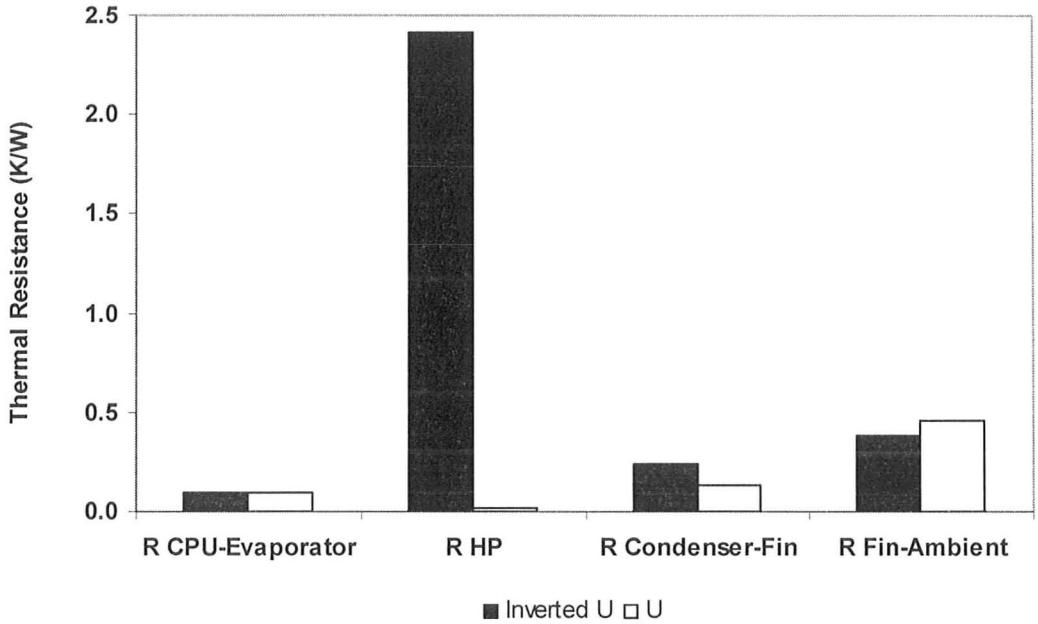

Figure 4-2: Thermal Resistances of System with Groove Wick Heat Pipe

Considering Figure 4-2, for a grooved heat pipe, R_{HP} varies by two orders of magnitude depending if the heat pipe is oriented as a U or an upside down U (inverted U). However considering the case of best orientation of the heat pipe, the next largest resistance is that of the natural convection, $R_{Fin\text{-}Ambient}$. The test was run with the CPU at idle while it is generating 12 W. The room temperature was 25°C ± 1°C. Although the idle power consumption is only an estimate, since the conditions were the same for both tests then it is a valid comparison. Temperatures at each thermocouple are summarized in Table 4-1.

Table 4-1: Temperature, in °C, of Components for the Initial Computer Benchmarking Test

	CPU	Evaporator	Condenser	Fin	Ambient
U	34	33	32	30	24
Inverted U	60	59	32	30	25

The system was not run at full load because a built-in system to prevent overheating was triggered by the high temperatures generated with the heat pipe in the inverted U orientation. This overheating protection system activates different modes depending on the temperature of the CPU. The first mode which is activated around 100°C reduces the processors power consumption and speed to lower the temperature, the second mode activates above 100°C and begins to shutdown the system to prevent damage and the third mode which activates at a higher temperature will immediately cut power to the CPU to prevent damage (Intel, 2009a). The temperatures that trigger each mode and the amount of power reduction are processor specific and not released by Intel.

Although typically contact resistance is cited as a major issue in thermal cooling (Grujicic, 2004) it can be seen that it is not the largest resistance in the system. This is due to the use of natural convection which presents a larger resistance compared to the more typical forced convection. The variation of heat pipe performance with orientation and mesh design is also apparent and will be covered in the next chapter.

Based on these initial results the topics of research moving forward have been identified. Heat pipe performance is of critical importance and the effect of orientation on grooved and sintered wick heat pipes will be investigated. A concept to remove variability of performance with changes in orientation is to use carbon foam for direct conduction to move heat from the CPU and *northbridge* to the fin plate. Following heat pipes the transport of heat from the fin plate to the surroundings is the next major focus and will be investigated.

4.2 U-Shaped Heat Pipe Design

Heat pipes currently provide the thermal path from the CPU and *northbridge* to the fin plate. Their performance is critical to the operation of the system and has shown variation with orientation. Performance of heat pipes with grooved wick structures was compared to performance of heat pipes with sintered wick structures. Each heat pipe unit consists of two heat pipes bent into a U shape connected between a heat spreader on the evaporator side and a heat spreader on the condenser side. The dimensions of the heat pipe in the heat pipe unit are shown in Figure 4-3. The heat pipes were tested at different power levels and orientations with respect to gravity (Figure 3-6) by M. K. Russel and described in detail in Russel et al., (2010). Analytical models are used to predict the

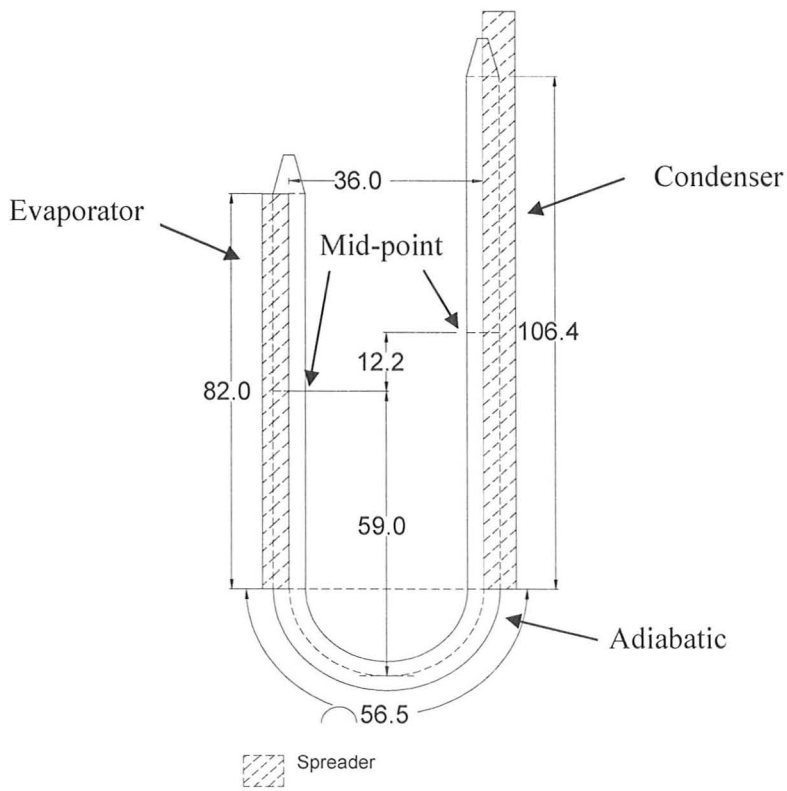

Figure 4-3: Dimensions of U Shaped Heat Pipe

maximum heat transport and are compared to experimental results. In section 4.2, all power values are for one heat pipe and the total power flowing through the heat pipe unit is twice what is stated, based on the assumption that the heat is spread evenly between the two pipes and their performance characteristics are identical. Having the heat pipes attached to copper heat spreaders allows heat to flow through the heat spreader instead of the heat pipe. However, since the evaporator and condenser section are each supposed to be at a constant temperature, the spreaders will not impact the performance. The spreaders help the heat pipe in that they will distribute the heat from the CPU and *northbridge* contact areas. With the assumption of constant condenser and evaporator temperature, by averaging the temperatures from 5 thermocouples placed along each evaporator and condenser, a greater accuracy is achieved through averaging the readings.

Performance of the groove wick heat pipe in the U and inverted U orientation showed striking differences in performance and temperature profile on the fin plate of the computer. When the groove wick heat pipe was in the inverted U orientation, no hot spot was present on the plate (Figure 4-4) but when it was in a U orientation, a hot spot was clearly visible (Figure 4-5). Additionally, the presence of a hot spot indicates that fin performance could be affected due to non-constant temperature across the plate.

The temperature difference between the evaporator and condenser was measured for a range of heat loads applied to the heat pipes. Temperature difference vs. power for the groove wick heat pipe is plotted in Figure 4-6 and temperature difference vs. power

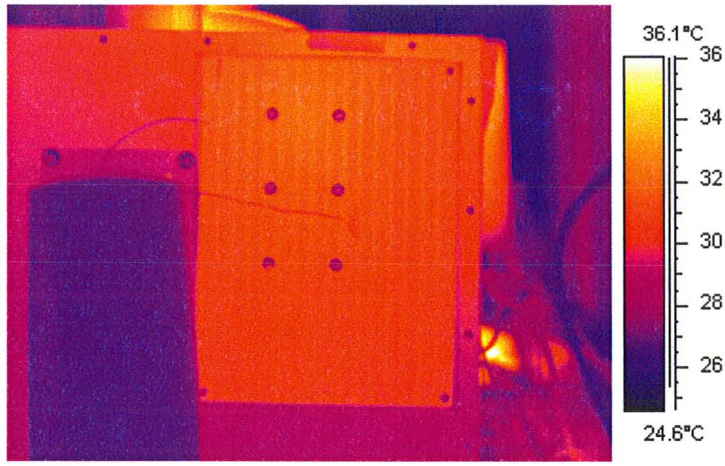

Figure 4-4: Temperature Distribution for Inverted U Orientation of Groove Wick Heat Pipe

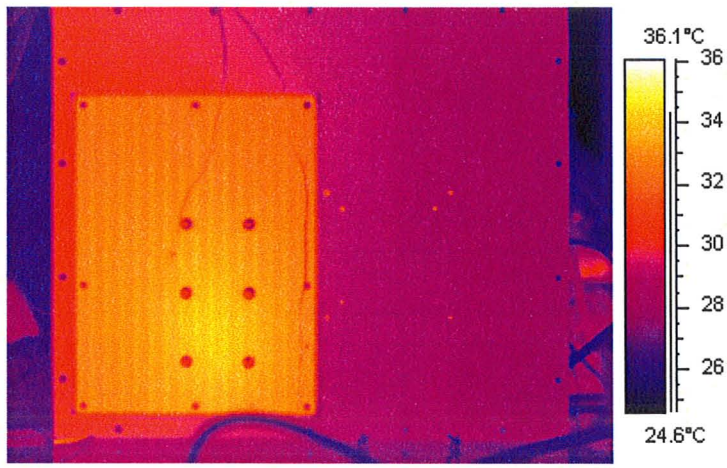

Figure 4-5: Temperature Distribution for U Orientation of Groove Wick Heat Pipe

for the sintered heat pipe is plotted in Figure 4-7. The thermal resistance of the heat pipes was calculated and is displayed for the groove wick heat pipe in Figure 4-8 and for the sintered wick heat pipe in Figure 4-9. In Figure 4-6 and Figure 4-7, the inflection point of each temperature curve is taken to be the q_{max} value for the respective heat pipe and orientation. The q_{max} values are summarized in Table 4-2. Each heat pipe has a certain q_{max} at which point its thermal resistance increases sharply. In addition to the q_{max}, each

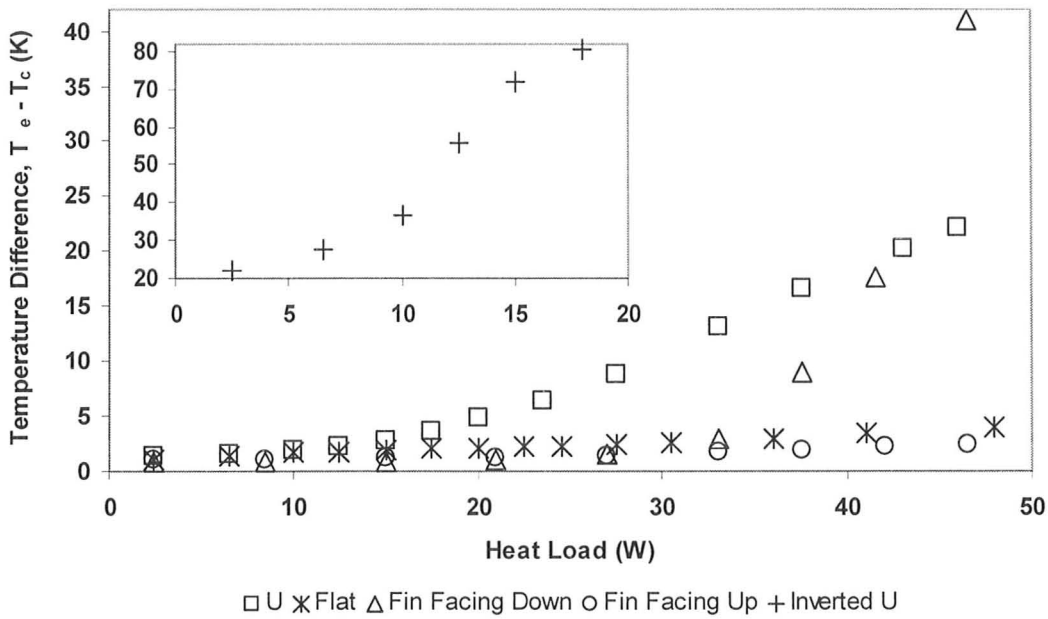

Figure 4-6: Temperature Difference for Different Heat Loads for the Groove Wick Heat Pipe

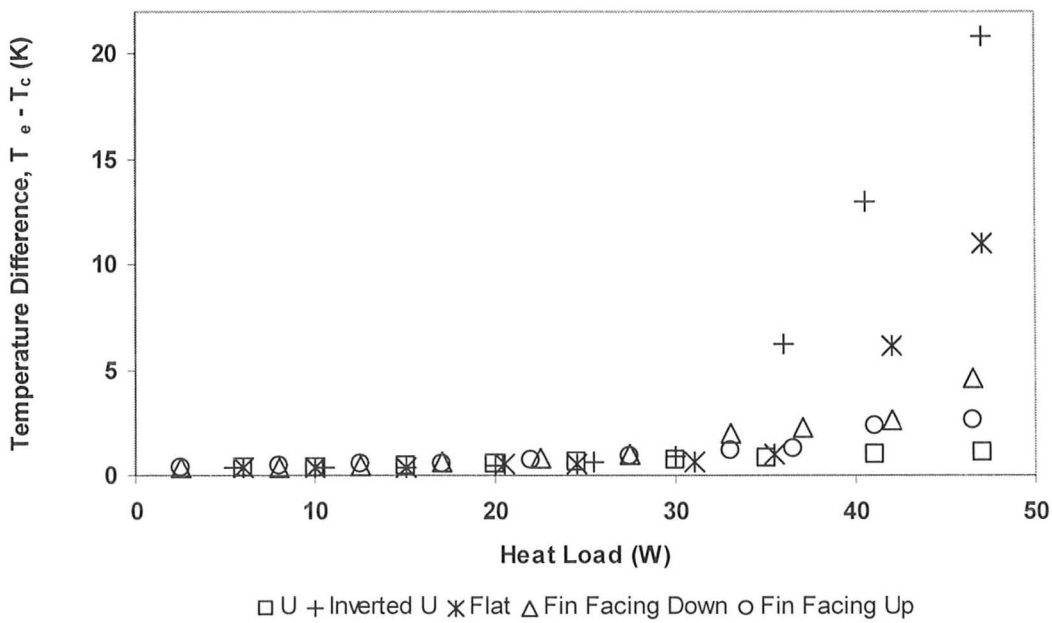

Figure 4-7: Temperature Difference for Different Heat Loads for the Sintered Wick Heat Pipe

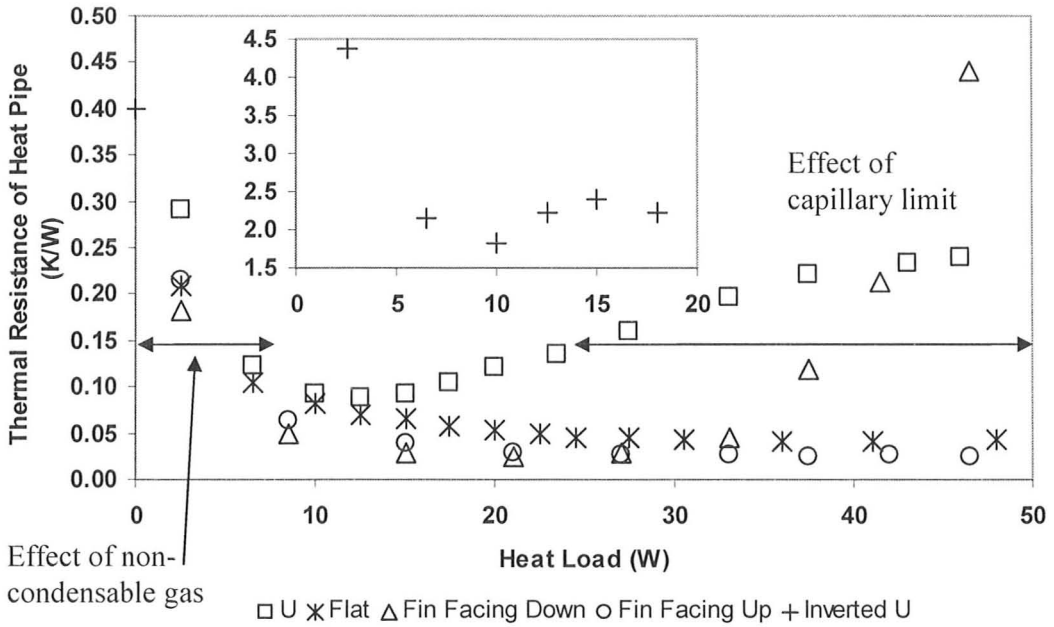

Figure 4-8: Thermal Resistance for Groove Wick Heat Pipe for Different Heat Loads

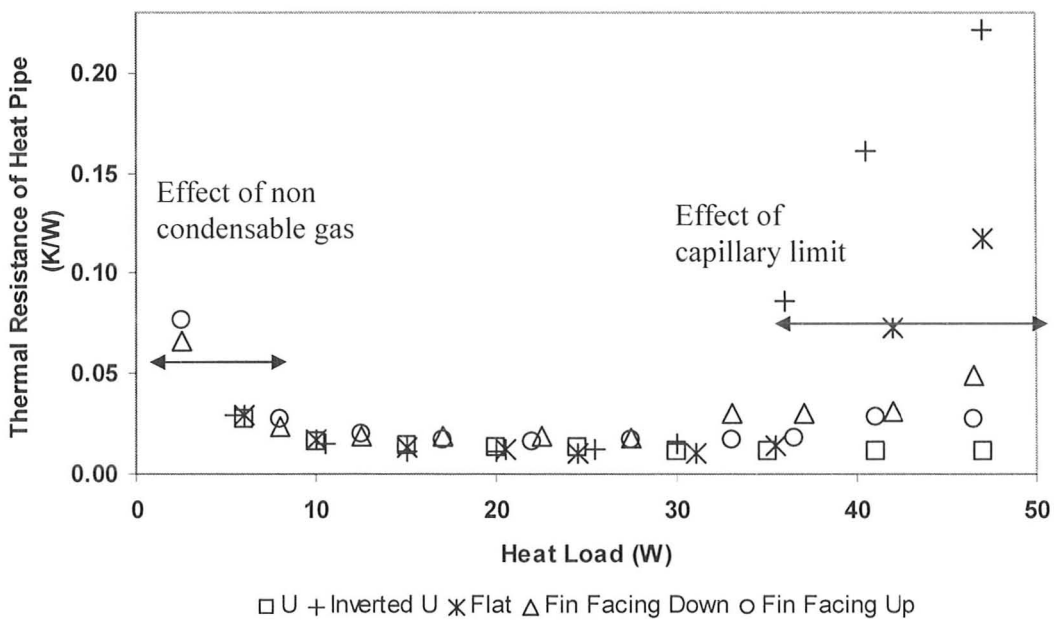

Figure 4-9: Thermal Resistance for Sintered Wick Heat Pipe for Different Heat Loads

heat pipe has a certain thermal resistance which is comprised of the resistance of the metal tube wall, the wick structure and the fluid inside the wick. This resistance causes the temperature drop across the heat pipe however since it is generally very small compared with the resistance that occurs once q_{max} is reached, analysis of it is neglected.

Table 4-2: Experimental and Analytical q_{max} for Groove Wick and Sintered Wick Heat Pipe

	Groove Wick		**Sintered Wick**	
Orientation	**q_{max} (W) experimental**	**q_{max} (W) theoretical**	**q_{max} (W) experimental**	**q_{max} (W) theoretical**
Flat	≥ 47	56.3	34.5	40.7
U	15	15	≥ 47	41.4
Inverted U	≈ 0	0.38	29	40.0
C fin up	≥ 47	82.5	36.5	42.9
C fin down	30	30	27.5	38.6

For the groove wick heat pipe, the change in temperature difference with heat load for all orientations is shown in Figure 4-6. The trend is similar to that of the sintered wick heat pipe for all orientations except the inverted U orientation (Figure 4-6 Inset). The temperature difference for the inverted U orientation is noticeably greater than the other orientations and it does not have a clearly defined sharp increase. The corresponding thermal resistance for different heat loads is shown in Figure 4-8. The inverted U orientation thermal resistance (Figure 4-8 Inset) is an order of magnitude higher than all of the other orientations. For power input up to about 10 W the thermal resistance decreases and again this is likely due to non-condensable gas inside the heat pipe blocking the condenser section and reducing its surface area. As heat loads increase, the increased vapour pressure moves the non-condensable gas away from the condenser.

The temperature difference between the evaporator and condenser ends for the sintered heat pipe with heat load for all five orientations is shown in Figure 4-7. The increase in the temperature difference with heat load is almost the same for all orientations. However, the maximum heat flux (q_{max}) as defined by the sudden increase in the temperature difference is significantly affected by the orientation. The orientations from lowest q_{max} to highest q_{max} are inverted U, flat, fin facing down, fin facing up and U.

The thermal resistance for the sintered heat pipe for all orientations is shown in Figure 4-9 for different heat loads. At heat loads from 0 W to about 10 W the thermal resistance decreases from about 0.07 K/W to 0.02 K/W and this is likely due to non-condensable gasses present in the heat pipe (Dube et al., 2004). At low heat loads (below 10 W) the non-condensable gas can occupy a significant portion of the condenser due to the low vapour pressure (Dube et al., 2004). When q_{max} is reached, the thermal resistance increases sharply because the evaporator temperature increases due to dryout of the evaporator.

The experimental q_{max} values for the sintered and groove wick heat pipe for the five orientations are listed in Table 4-2. Due to limitations of the heater, the q_{max} for some orientations were not reached. The maximum heat load that was tested was 47 W and the cases where the heat pipes did not fail before this point was reached are noted in Table 4-2 as "$q_{max} \geq 47$ W". For the grooved heat pipe the maximum occurs in either the flat orientation with no gravitational effect or the C orientation with the fin facing up. This contrasts with the maximum heat transfer for the sintered heat pipe which occurs in the U

orientation. The minimum heat transfer occurs for the inverted U orientation for each heat pipe.

Since geometry of the wick structure plays a large role in the performance of the heat pipe, exact measurements were required to accurately analyze the wick structure. Each heat pipe was filled with epoxy to hold the wick structure in place while cross sections were cut. The cross sections were then photographed using a microscope (Figure 4-10) and the images were scaled using the measured outer diameter of the pipe. The wick dimensions S, D_g, and W were measured from several wick channels in the grooved heat pipe from Figure 4-10a) and were averaged to calculate K_w using (2.14) and r_c using (2.18) and are listed in Table 4-3. The area of the sintered wick was measured from Figure 4-10b), while the wick permeability and radius of curvature were estimated from typical values given by Dunn and Reay (1982). All the wick values used for calculations for the sintered wick are listed in Table 4-3.

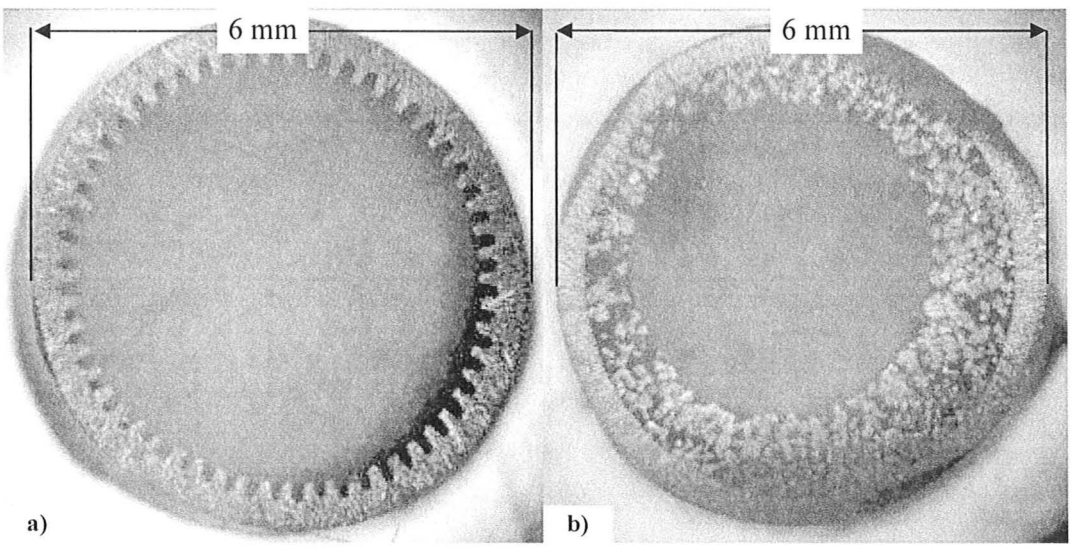

Figure 4-10: Cross Section of a) Groove Wick Heat Pipe and b) Sintered Heat Pipe

Table 4-3: Heat Pipe Wick Parameters used for Analysis

Parameter	Sintered	Grooved
K_w – Wick permeability	1.75×10^{-11} m^2	6.1×10^{-10} m^2 ± 40%
A_w – Wick Area	1.10×10^{-5} m^2 ± 5%	3.9×10^{-6} m^2 ± 5%
r_c – Radius of curvature	0.02 mm	0.20 mm ± 13%

Since the variation in performance occurs when orientation is changed, only the capillary limit is investigated since no other limits include the effect of gravity. The maximum power limited by capillary pressure is given by

$$q_{\max} = \left(\frac{2\sigma_l}{r_c} - \rho_l g \Delta h \sin\varphi \right) \frac{\rho_l A_w K}{\mu_l L_{eff}} \times h_{fg} \qquad (2.19)$$

where σ_l is the surface tension, ρ_l is the fluid density, g is the gravitational constant, Δh is the difference in height between the evaporator and condenser, φ is the inclination angle from the horizontal, μ_l is the fluid viscosity and L_{eff} is the effective length from the evaporator to the condenser. L_{eff} is taken to be half the evaporator length, plus the adiabatic length plus half the condenser length (Kreith and Bohn, 2001). Using equation 2.19 and the wick properties listed in Table 4-3, properties of liquid water and the appropriate Δh value for each orientation, given in Table 4-4, q_{max} for each orientation was calculated and is listed in Table 4-2.

The most variation is between the inverted U and U orientations. Since for both of these orientations the fins are vertical, the results are independent of the natural convection since it is the same in both cases. The groove wick heat pipe completely failed in the inverted U orientation because not enough capillary pressure was generated to

Table 4-4: Rise from Condenser mid point to Evaporator mid point (Δh) for each Heat Pipe Orientation used in Heat Pipe Analysis

Orientation	Groove Wick		Sintered Wick	
	Δh (mm)	Description of Δh	Δh (mm)	Description of Δh
Flat	0	No change in height for flat orientation	0	No change in height for flat orientation
U	59	Rise from bottom of U to midpoint of evaporator	-12.2	Drop from mid point on condenser to midpoint of evaporator
Inverted U	71.2	Rise from midpoint of condenser to top of U	12.2	Rise from midpoint of condenser to midpoint of evaporator
C fin up	-36	Drop from condenser to evaporator	-36	Drop from condenser to evaporator
C fin down	36	Rise from condenser to evaporator	36	Rise from condenser to evaporator

overcome the force of gravity acting on the fluid and move it from the mid point of the condenser to the top of the U where it could flow down to the evaporator. The groove wick heat pipe showed far more variation with orientation due to lack of pumping power compared with the sintered wick which was able to transfer 28 W per heat pipe in the inverted U orientation. This translates to the heat pipe unit being able to transport 56 W in the inverted U orientation, well above the current CPU rated TDP of 35 W. However, the theoretical values of q_{max} for the sintered heat pipe do not align perfectly with the experimental suggesting the model cannot completely account for the change in direction of flow present because of the U shape. The fact that variation can occur with heat pipes in different orientations and that U shaped designs are not well researched, suggests that an alternate solution to move the heat to the fin plate from the CPU and *northbridge* would increase reliability.

The effective thermal conductivity of a heat pipe can be calculated to allow simple modeling by choosing the distance as the effective length from the middle of the evaporator to the middle of the condenser and the conduction area as the cross section area of one tube. Using heat load and temperature drop values shown in Figure 4-6 for the groove wick heat pipe and from Figure 4-8 for the sintered wick heat pipe, the effective thermal conductivity of the heat pipe in several useful orientations is listed in Table 4-5. The variation of effective thermal conductivity with heat load shows a limitation of using effective thermal conductivity to estimate temperature drop. Effective thermal conductivity values for phase change heat transport systems need to be based on heat load.

Table 4-5: Effective Conductivity of Groove and Sintered Heat Pipes

Wick Structure	q (W)	Orientation	Effective Thermal Conductivity (W/mK)
Groove Wick	17.5	U	25435
Groove Wick	33	U	12968
Groove Wick	17.5	Flat	46420
Groove Wick	30.5	Flat	61059
Groove Wick	41	Flat	63974
Sintered Wick	17	*All*	138750
Sintered Wick	35	*All (except Inverted U)*	285663

4.3 Carbon Foam

Carbon foam is a new material with high specific thermal conductivity and the potential to have very high thermal conductivity when its porosity is reduced using new manufacturing techniques. This high thermal conductivity could be used to directly conduct heat with a temperature drop comparable to a heat pipe. Three types of carbon foam machined into a shape suitable for use in the sealed computer case (Figure 1-2) were tested. The three types of carbon foam are referred to as TC1813, TC1939 and TC1555. The temperature drop for each material and the calculated thermal conductivity value is listed in Table 4-6. Details of the experiments conducted on carbon foam are provided in Appendix A and Appendix B.

Table 4-6: Thermal Conductivity of Carbon Foam and Copper Calculated from Temperature Drop

Material	ΔT (K)	Thermal Conductivity (W/mK)
TC1813	21	59
TC1939	11	118
TC1555	17	72
Copper	3	370

The initial goal when carbon foam investigation began was to use carbon foam to replace the heat pipe unit in the system to conduct heat directly from the processor and *northbridge* to the fin plate. Testing on three samples in-situ revealed lower conductivity than expected which was confirmed by testing in a controlled heat flux test facility. The thermal conductivity values below the initially estimated values make the direct conduction solution not feasible for use in a computer system at this time.

4.4 Fins (Natural Convection)

The fin plate that forms one wall of the computer casing is the final part of the pathway of the heat from the CPU and *northbridge* to the surroundings. It is responsible for providing surface area for natural convection and radiation heat transfer to the ambient. The dimensions of the fin array control the amount of surface area available for heat transfer. Choosing the best dimensions and number of fins is not a trivial task as the minimum number of fins in an array is none which results in a flat plate and the maximum number results in an array spaced so closely together they are touching. Reviewing the literature revealed a model for estimating convective heat transfer coefficient for fin plates where each dimension is a parameter of the model. Using the model comprised of equations 2.18 and 2.19 from Bar-Cohen and Rohsenow (1983) to calculate the convective heat transfer coefficient for the geometry tested by Welling and Wooldridge (1965) is used as a check of the accuracy of the model. A comparison of the convective heat transfer coefficient for different fin spacings is shown in Figure 4-11. Although the heat transfer coefficients do not align exactly, the same trend is seen where the heat transfer coefficient increases from a spacing of about 5 mm to 10 mm after which it levels off and does not change with further increase in spacing. Good agreement between the data of Welling and Wooldridge (1965) and the model of Bar-Cohen and Rohsenow (1983) indicates that the model can be used to optimize the fin spacing.

Also of importance to optimizing the fin design is the effect of the dimensions on radiation heat transfer. Using equations 2.20-2.25 for shape factor from Shabany (2008), the power transferred to the surroundings by radiation was calculated for various fin

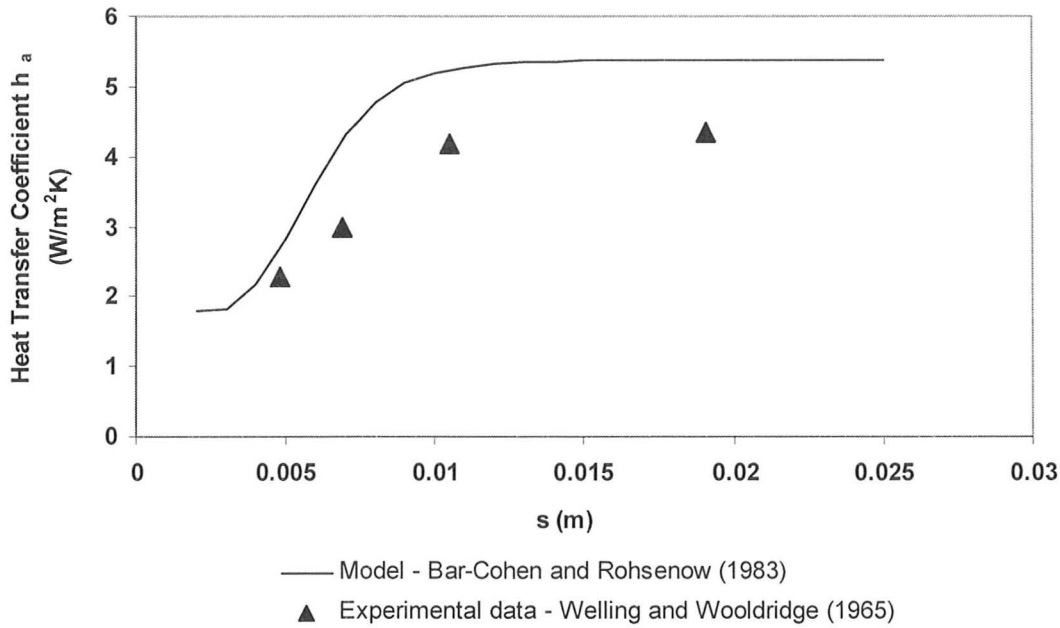

Figure 4-11: Convective Heat Transfer Coefficients for Different Fin Spacing

spacing distances. Combining the radiation calculations from Shabany (2008) and the natural convection model from Bar-Cohen and Rohsenow (1983) allows the fin geometry to be optimized for a combination of both mechanisms of heat transfer. The amount of heat transferred for different fin spacing, using the current fin plate dimensions is shown in Figure 4-12. Examining Figure 4-12 it is seen that the radiation heat transfer decreases slightly with increase in fin spacing, due to the decrease in total surface area that occurs as less fins are part of the array when they are spaced farther apart. Unlike radiation, heat transferred by natural convection is quite heavily influenced by the spacing distance with the peak heat transfer occurring at the spacing value of 8 mm. Figure 4-12 depicts analysis conducted with an air temperature of 25°C and a fin plate surface temperature of 62.6°C. Fin efficiency was experimentally found to be 95% and a value of 1 for fin

efficiency has been used to simplify analysis. The influence of the other fin parameters H, L, W, t and L, which are defined in Figure 2-10, are also tested using the model. Fin thickness, shown in Figure 4-13, causes performance to decrease slightly as it is increased; however the rate of decrease is so slight that thickness should just be chosen for structural reasons and not on the basis of efficiency. Fin plate width, shown in Figure 4-14, fin plate height, shown in Figure 4-15, and fin height, shown in Figure 4-16, all increase maximum heat transfer as they are increased, with no inflection point. Fin plate width, height and fin height should be maximized to as large as the geometry constraints will allow.

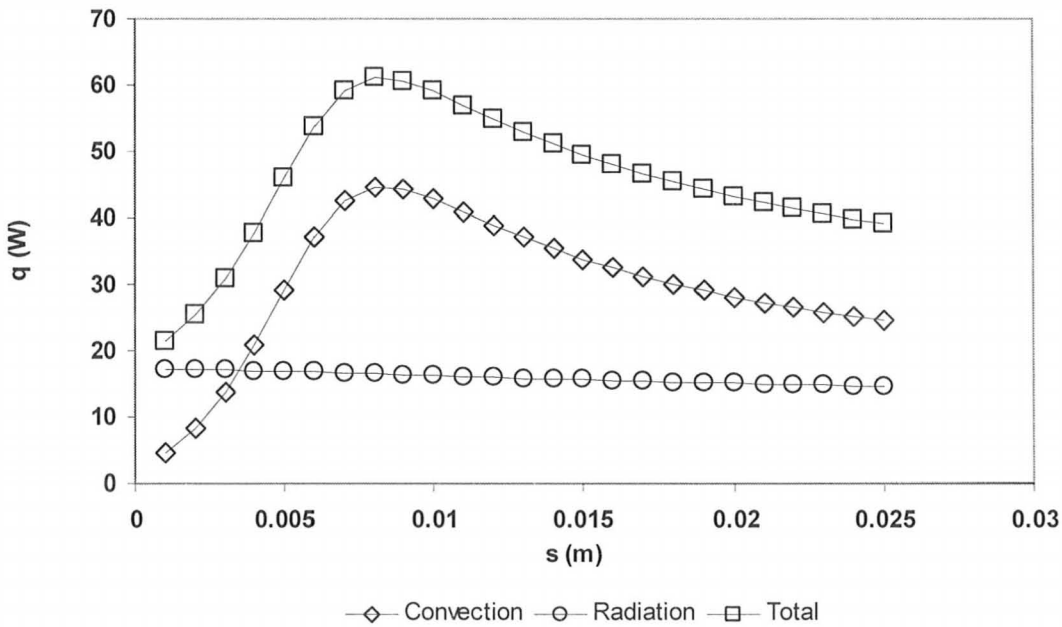

Figure 4-12: Heat Transferred for Different Fin Spacing Distances

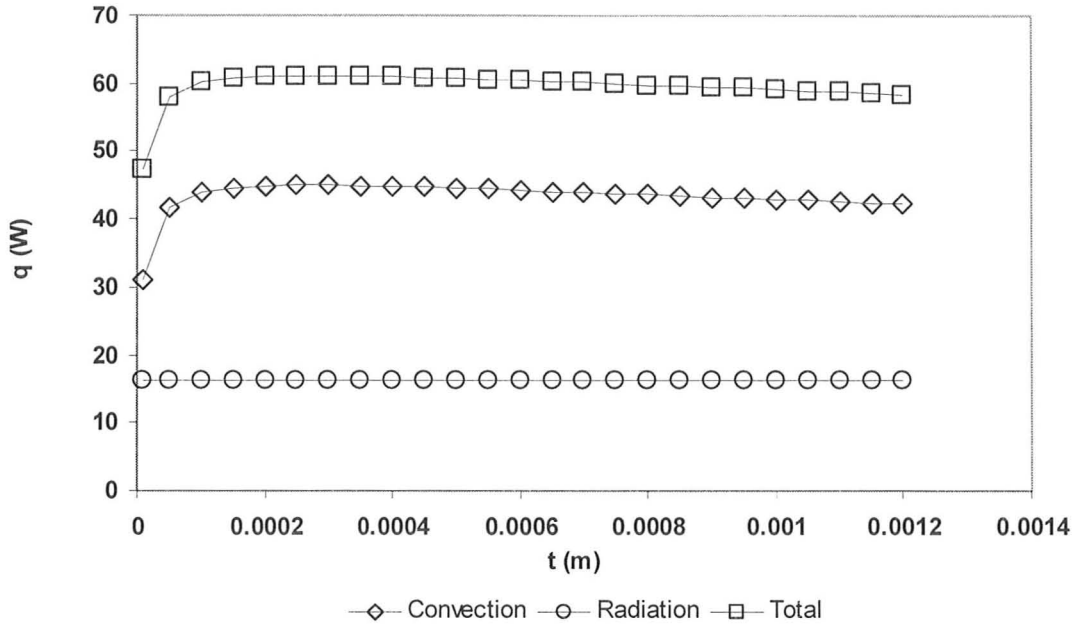

Figure 4-13: Heat Transferred for Different Fin Thicknesses

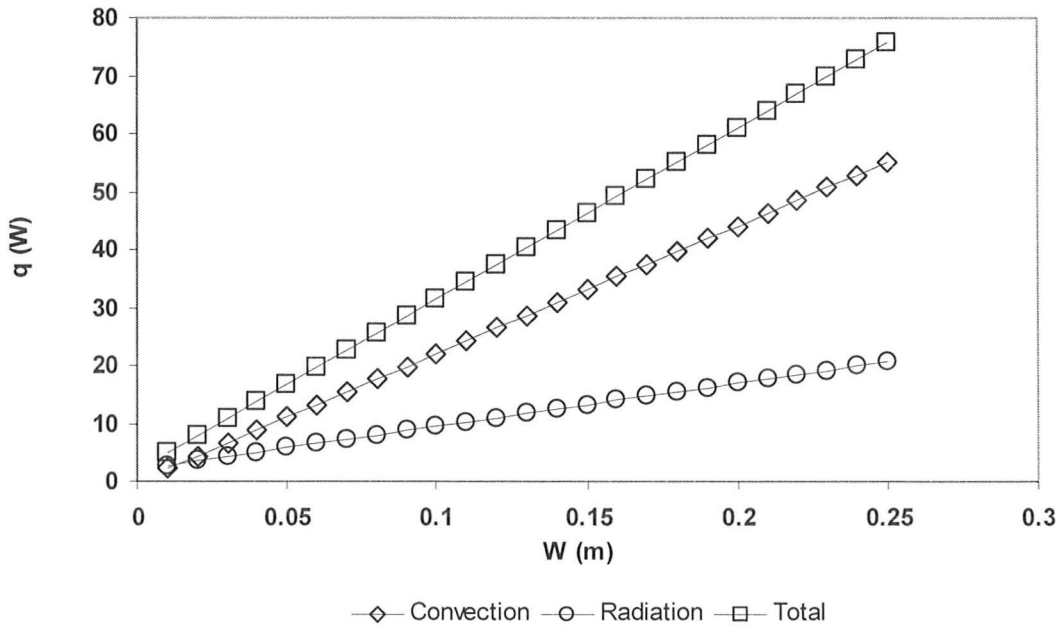

Figure 4-14: Heat Transferred for Different Fin Plate Widths

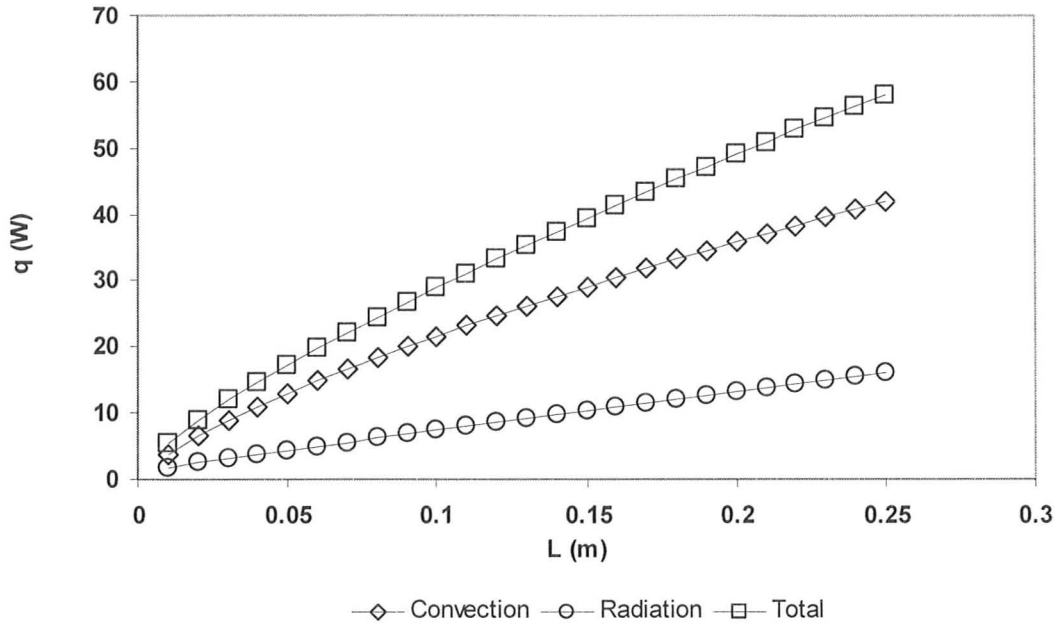

Figure 4-15: Heat Transferred for Different Fin Plate Heights

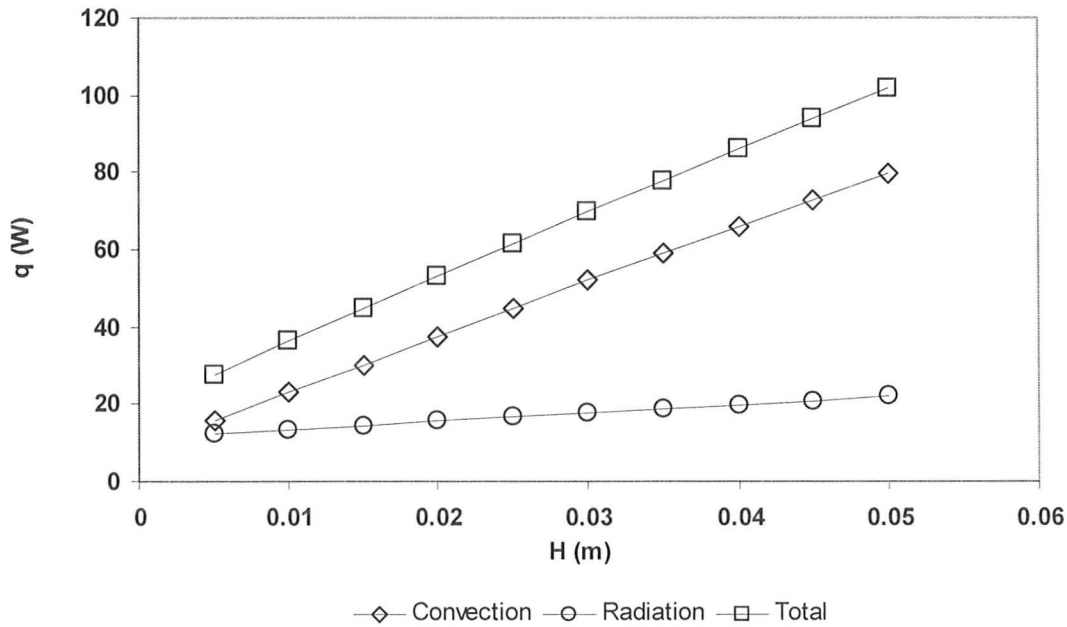

Figure 4-16: Heat Transferred for Different Fin Heights

Since the rate of heat transfer depends on the properties of air, which change with temperature, analysis had to be conducted to find the best fin spacing distance for a range of air temperatures from 25°C to 40°C. Also modeled were power levels of 25 W, 35 W, 45 W and 65 W. While keeping the outer dimensions the same as the current system as listed in Table 4-7, fin spacing distances from 5 mm to 15 mm were modeled. Fin spacing distances of 8 mm, 9 mm or 10 mm were found to be the best three cases. For each of these fin spacing distances, the minimum, maximum and average temperature which would occur over the range of four simulated power loads and two ambient temperature levels if fins were made with that dimension is given in 4-8. In 4-8 it can be seen that for a fin spacing distance of 8 mm, the lowest minimum temperature is achieved whereas for a spacing of 10 mm, the lowest maximum temperature is achieved. Since the maximum temperature is of primary concern, 10 mm would be the best spacing to use. However for all of the fin spacing distances from 8 mm to 10 mm, there is very little difference in the minimum and maximum temperature indicating that any of these dimensions could be

Table 4-7: Fin Geometry Parameters used for Fin Spacing Optimization Analysis

Parameter	Value (mm)
W	190
L	250
H	23
t	1.3

4-8: Effect of Fin Spacing Distance on Minimum, Maximum and Average Temperature of the Fin Plate for 25 W, 35 W, 45 W and 65 W at 25°C and 40°C

	Spacing distance		
Temperature	**8 mm**	**9 mm**	**10 mm**
Minimum	45.01	44.49	44.41
Maximum	64.50	64.75	65.64
Average	53.79	53.58	53.92

used successfully. If a computer would be operating in only a certain conditions, for example an ambient temperature of 40°C and not below 35°C, different optimization would result.

As first noticed while conducting the initial evaluation and shown in Figure 4-5, a temperature gradient is present on the fin plate. This is of concern since natural convection flow is driven by temperature difference and if the temperature distribution on the plate is not uniform the heat transfer may not be as effective as possible.

To analyze the complex interacting effects of heat spreading and natural convection and to allow for testing of new design ideas, computational fluid dynamic modelling was used. Computational Fluid Dynamics (CFD) is a software tool that solves the physical governing equations for a system and can include the equations of fluid motion, heat transfer and other more specialized properties including electrical fields and magnetism. It solves the equations over a specified area known as the domain which has the boundaries at each edge specified. The solution is found by discretizing the domain into a finite number of smaller volumes and iteratively solving discretized versions of the continuity, momentum and total energy equations for all of the volumes.

CFD analysis was performed using ANSYS CFX software. The software was used to model the flow of air over the fin surface, the heat transfer due to natural convection and conduction in the fin plate and fins. A domain was constructed with openings to air at a constant pressure and temperature at the top, sides, bottom and front of the fin plate shown in Figure 4-17. This allows air to flow against the fin as it rises due to natural convection and is similar to a domain shown by Zitzmann et al. (2005) for

natural convection modeling. The arc profile at the bottom was chosen so air can enter the domain generally perpendicular to the boundary. The temperature of the air at the opening is used as the bulk temperature for calculating the convective heat transfer coefficient.

To simplify the model of thermally induced buoyancy driven flow, the density is assumed to vary only based on temperature and not based on pressure. This assumption is known as the Boussinesq approximation (Kreith and Bohn, 2001) and implies that the hydrostatic pressure is constant in the vertical direction. A constant reference density is used in all equations other than the buoyancy source term (ANSYS, 2007).

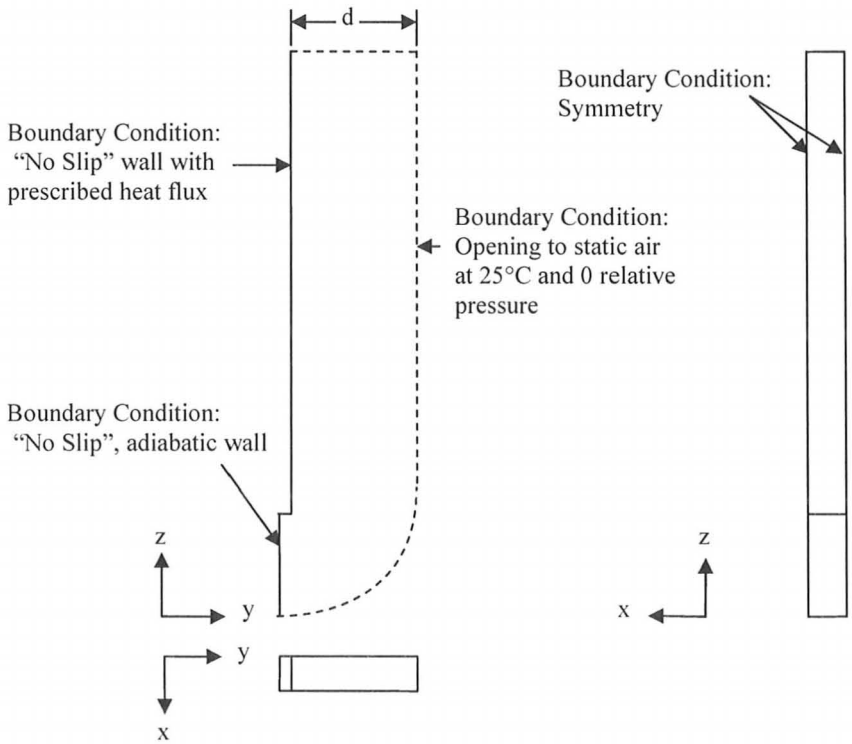

Figure 4-17: Domain with "Opening" Boundary Conditions

4.4.1 CFD Validation

To validate the numerical simulation, initial testing was done on simple flat plate geometry with opening boundary conditions with air at 25°C. Mesh parameters were varied and the resulting natural convection heat transfer coefficient was compared to that for a flat plate correlation (Rohsenow and Hartnett, 1973). Mesh parameters that were varied include element face spacing, which specifies the maximum length of an element in the model, the first prism height, which is the thickness of the first layer of the mesh used to resolve details of interaction between flow and a surface, and number of layers in the inflated boundary which defines the number of thin mesh layers to use in a boundary layer region. Maximum element spacing is seen in Figure 4-18 to have little influence on the convective heat transfer coefficient. The number of inflation layers used does not greatly impact convective heat transfer coefficient as shown in Figure 4-19. The first prism height has a clear correlation to the convective heat transfer coefficient which can be seen in Figure 4-20. As well the influence of the total number of elements on the convective heat transfer coefficient is shown in Figure 4-21 and is shown to not be directly related to the convective heat transfer coefficient. The results from this analysis were used as the initial parameters to generate the mesh on the fin surfaces. For the best case of mesh parameter with element spacing 10 mm, 15 inflation layers and 0.5 mm first prism height, the heat transfer coefficient value was found to vary by less than 2% from the analytical correlation for a natural convection flow over a flat plate.

Using the flat plate mesh parameters, element spacing 10 mm, 15 inflation layers and 0.5 mm first prism height, as a starting point, another grid independence test was conducted on single fin channel geometry shown in Figure 4-22. Applying symmetry

boundary conditions at the sides allowed simulation of an array of fins while reducing computing time. The outside edges of the domain were open to air at 25°C at a static relative pressure of 0 Pa. After refining the 1st Prism Height (Figure 4-23) and the Maximum element length (Figure 4-24), optimal values were found. A domain size independence study was conducted by varying the x dimension in Figure 4-17, and the results are shown in Figure 4-25. Since no variation is seen when increasing or decreasing the domain size in the range of 80 mm to 140 mm, a 100 mm domain is used for all further simulations.

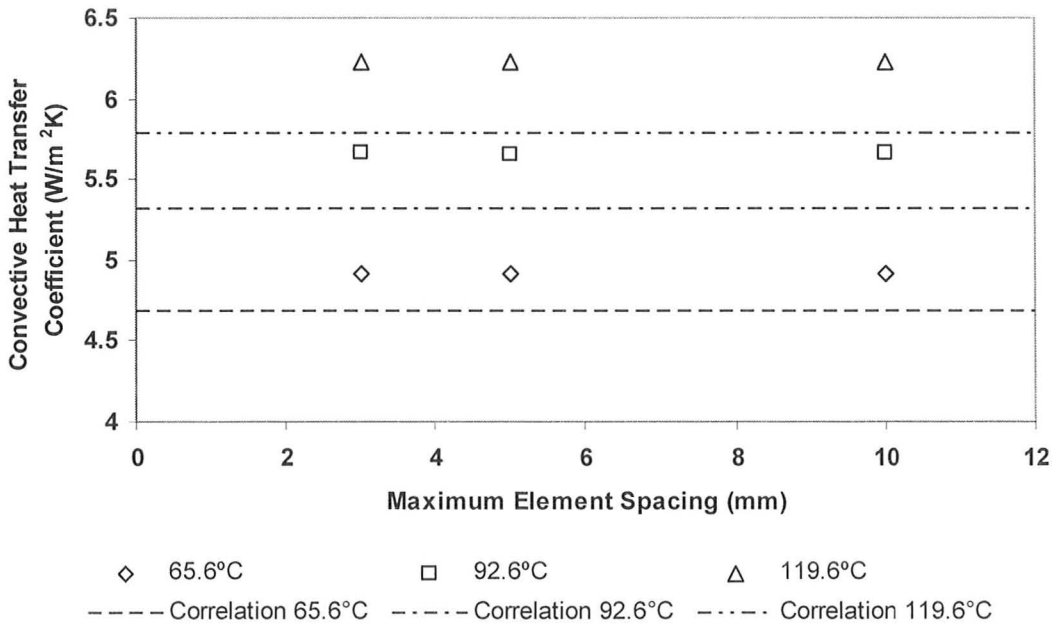

Figure 4-18: Effect of Maximum Element Spacing on Convective Heat Transfer Coefficient

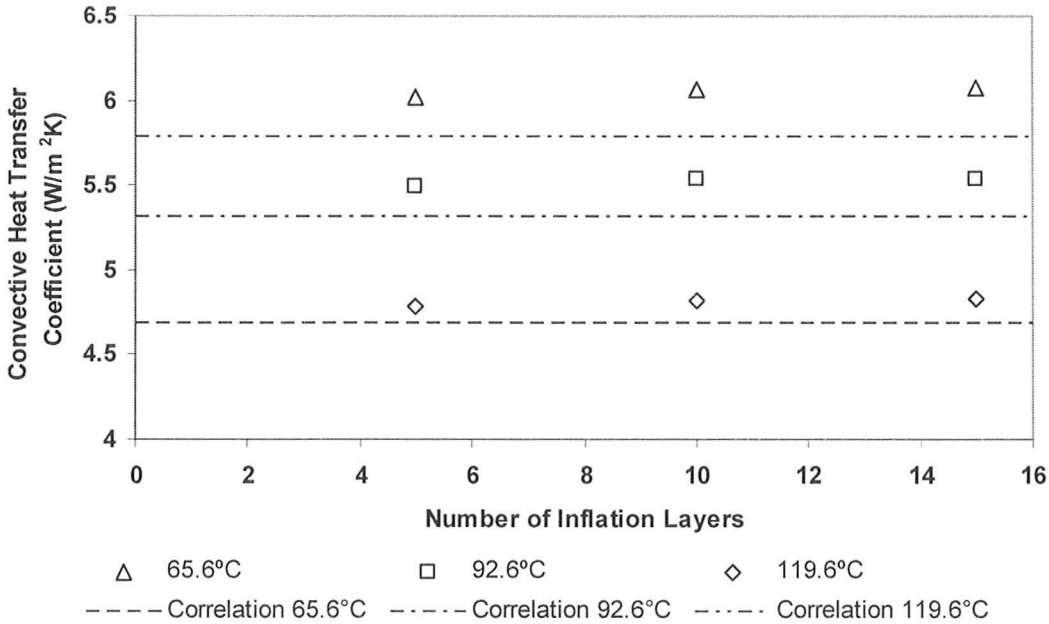

Figure 4-19: Effect of Number of Inflation Layers on Convective Heat Transfer Coefficient

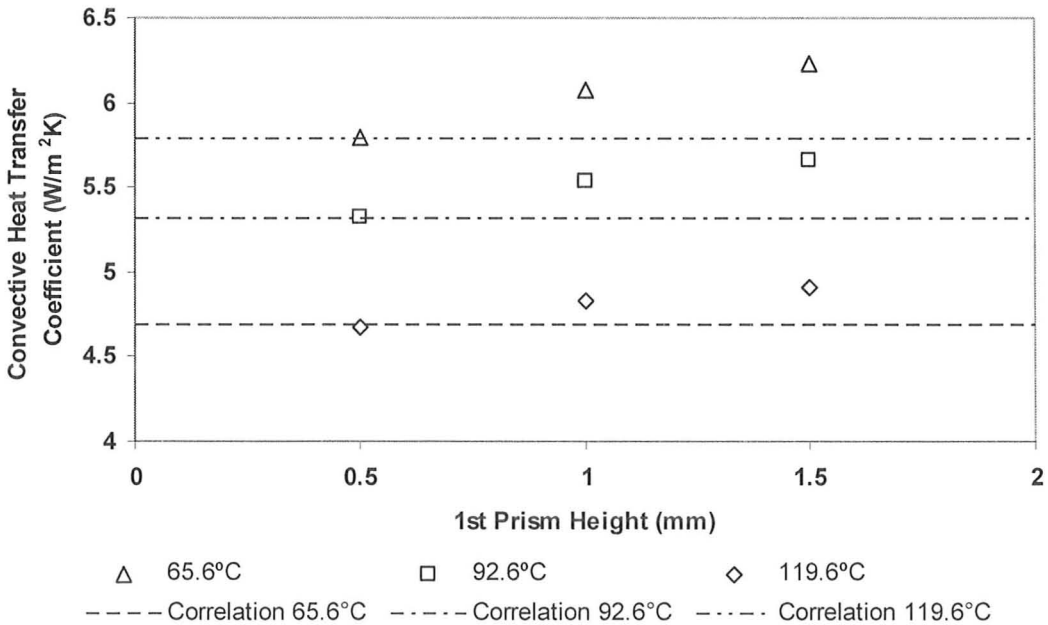

Figure 4-20: Effect of 1st Prism Height on Convective Heat Transfer Coefficient

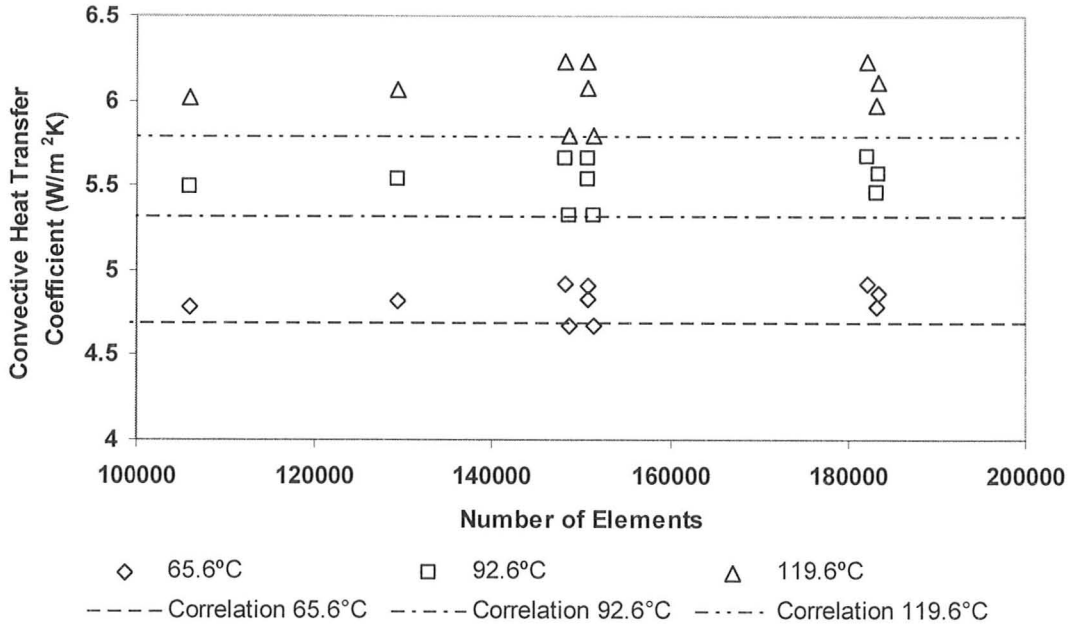

Figure 4-21: Effect of Number of Elements on Convective Heat Transfer Coefficient

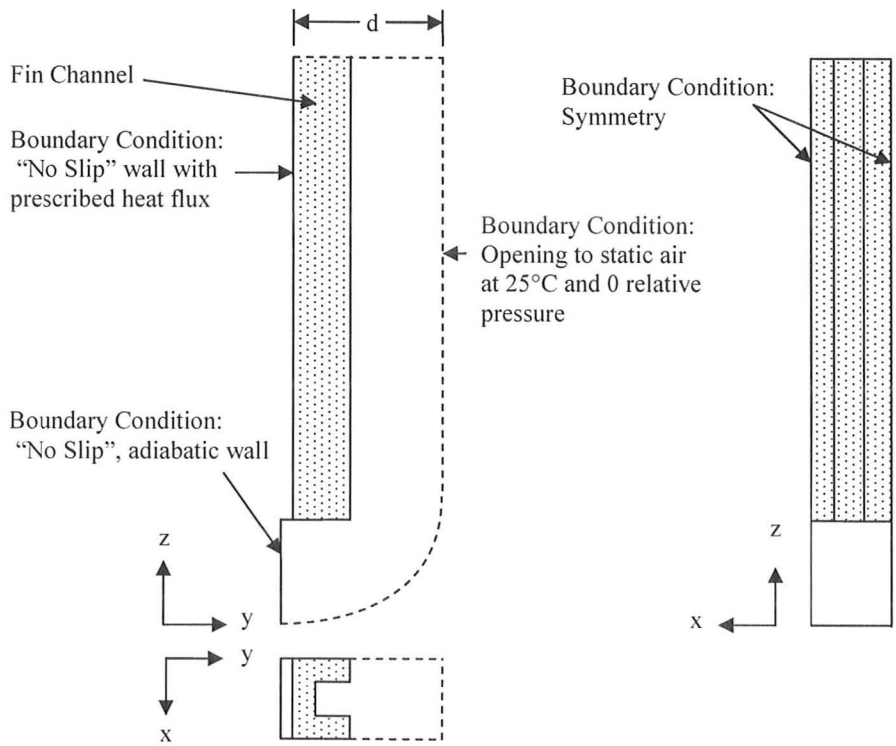

Figure 4-22: Isometric View of the Domain used to Simulate a Single Fin Channel

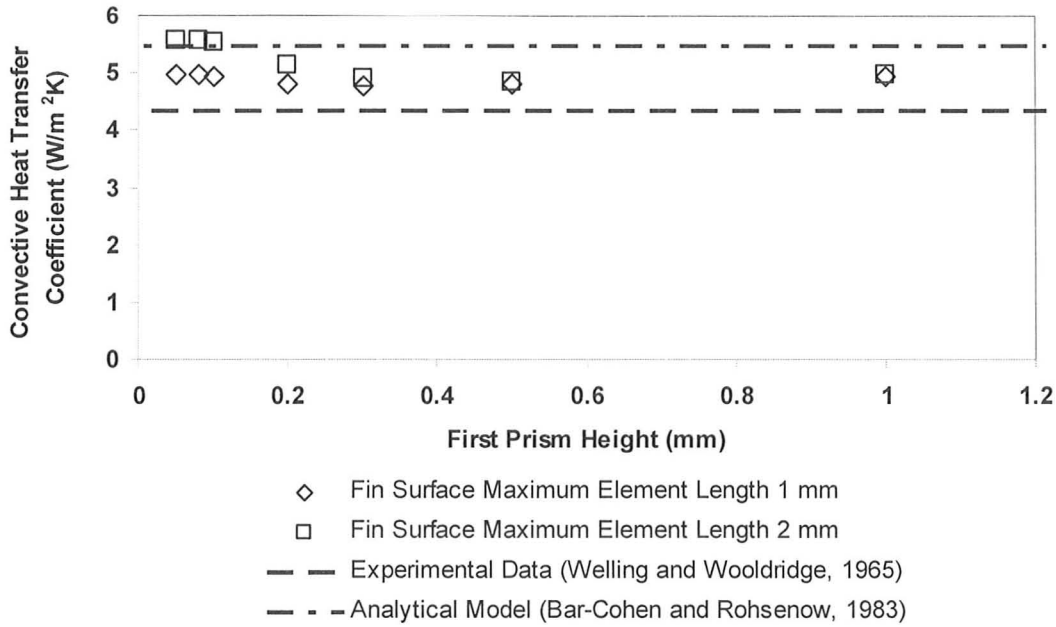

Figure 4-23: Effect of 1st Prism Height on Convective Heat Transfer Coefficient

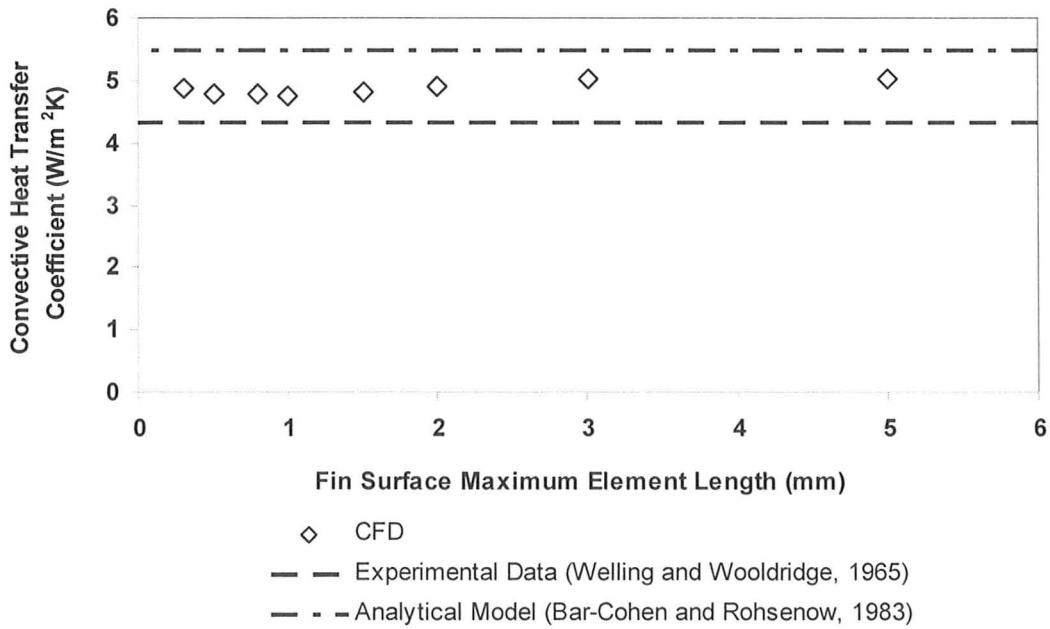

Figure 4-24: Effect of Maximum Element Length on the Convective Heat Transfer Coefficient

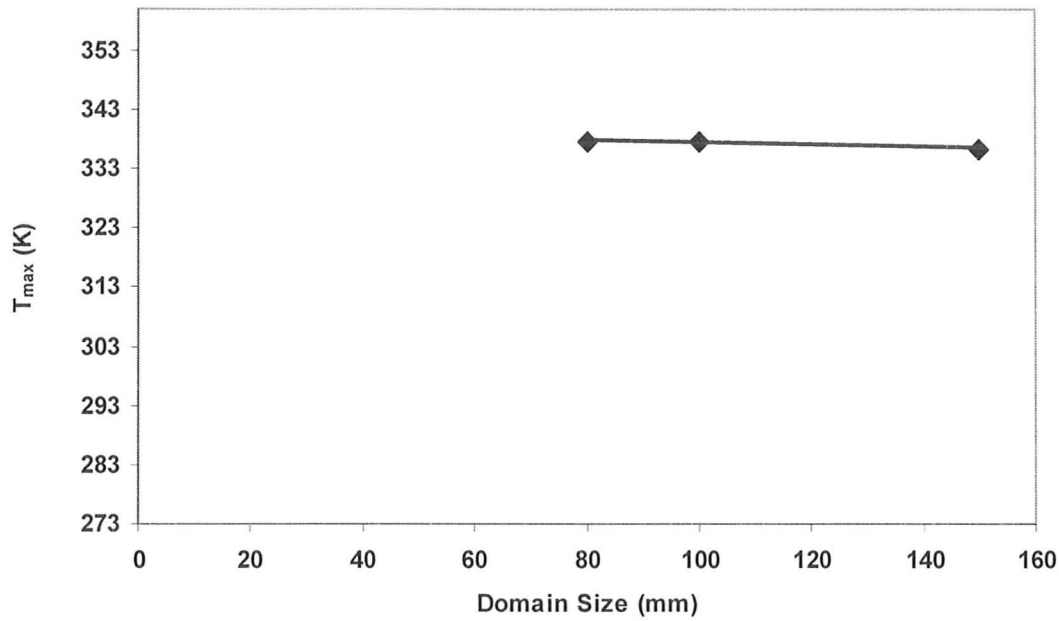

Figure 4-25: Effect of Domain Size on Maximum Temperature of Fin Plate

To see how well CFD captures the influence of different fin spacing distances on heat transfer coefficient, three aspect ratios of rectangular fin channels, listed in Table 4-9 were simulated. The results were compared with experimental results of fins with the ratio from Welling and Wooldridge (1965) and with the analytical model from Bar-Cohen and Rohsenow (2003). The comparison of the experimental results, CFD analysis and analytical model is shown in Figure 4-26 and show that the CFD results fall between the experimental results and the analytical model. The mesh used for all the simulations used maximum element spacing of 10 mm, 7 inflation layers and a first prism height of 0.5 mm. The fin surface was defined to have a fixed temperature of 62.6°C, 92.6°C or 119.6°C. The sides of the domain were set as symmetrical and the openings were open to air at static relative pressure of 0 Pa and 25°C. The surface temperature levels were

selected to allow comparison with the experimental data of Welling and Wooldridge (1965).

The purpose of conducting CFD simulation is to model heat spreading which plays an important part in the performance of the fin plate. When the heat is applied only to the contact area with the heat pipe unit, it must be conducted through the plate to

Table 4-9: Dimensions of Fin Channels Simulated

Configuration	H (mm)	s (mm)
1	19.05	19.05
2	19.05	10.52
3	19.05	6.85

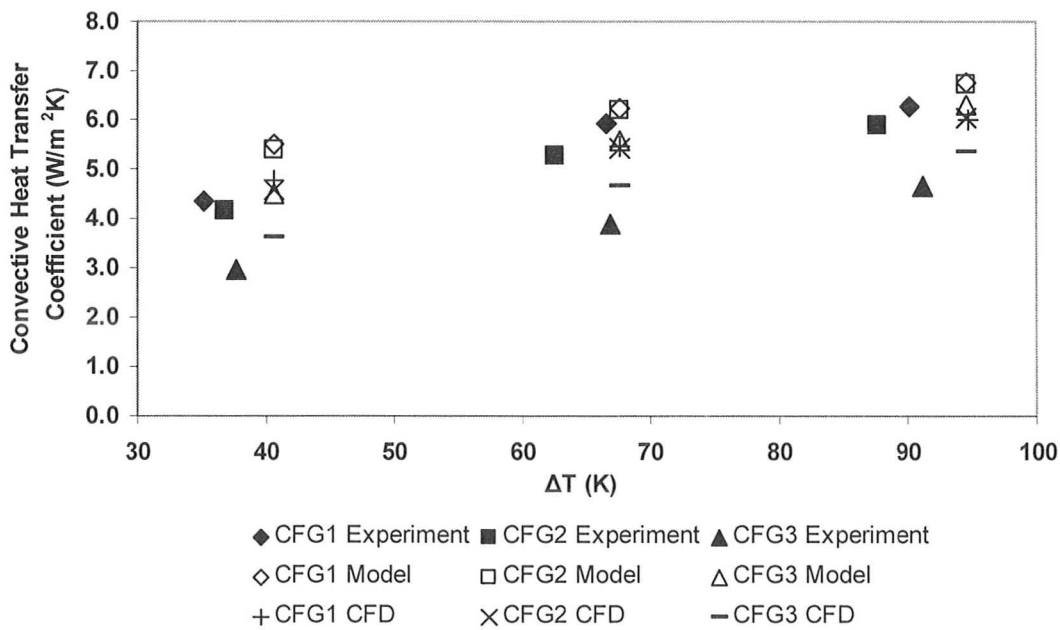

Figure 4-26: Comparison of Experimental Data, Model Predictions and CFD Results for Three Fin Configurations

spread out to the rest of the plate. Since the natural convection heat transfer coefficient is influenced by the temperature difference between the surface and the fluid, if the surface

temperature is reduced by thermal resistance inside the plate, the heat transfer coefficient will be lower farther away from the contact area of the plate. This temperature differential will also result in unusual flow patterns since the hottest area is not at the lowest part of the plate. In Figure 4-27 the temperature of the hot spot is 50°C and the temperature of the surrounding fin plate is 45°C. Using the model of Bar-Cohen and Rohsenow (1965), a fin plate at 50°C would transfer 24 W via natural convection to the surroundings while a fin plate at 45°C would only transfer 18 W.

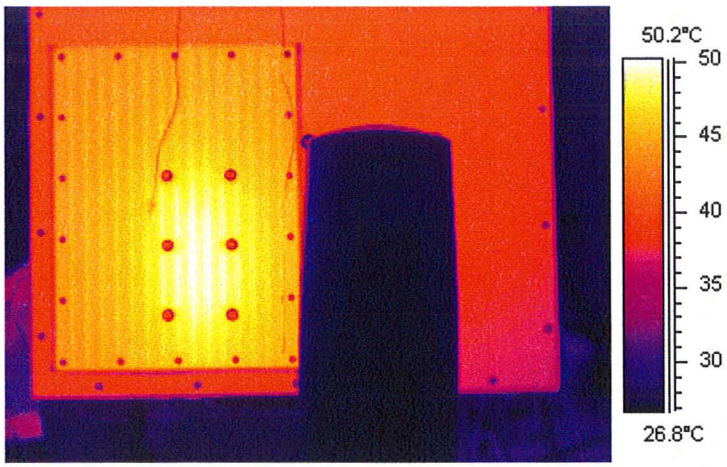

Figure 4-27: Infrared Thermal Image Showing Temperature Gradient Showing and Hot Spot on the Fin Plate

Investigation of improvements to heat spreading started by considering different material for the fin plate. A fin plate with the same dimensions as the plate that is currently used (Table 4-10) was simulated first. Simulations were conducted with total heat loads of 35 W, 50 W and 65 W on fin plates made of aluminum, steel and copper. For the simulation, thermal conductivity values of 60.5 W/mK, 237 W/mK and 401 W/mK were used for steel, aluminum and copper respectively. Plates were also simulated

with an even heat distribution on the back to remove the effects of spreading. Although heat spreading was eliminated, different materials still affect the maximum temperature by changing the fin efficiency by reducing temperature drop between the fin plate and the end of each fin. By increasing the fin end temperature, more heat will be transferred from the end of each fin.

The result of spreading can be seen in Figure 4-28, where a steel plate results in a maximum temperature 10°C higher than an aluminum plate and 15°C higher than a copper plate with an evenly distributed heat flux totalling 35 W. As the power input is increased up to 65 W the temperature difference increases up to 21°C between a steel plate and an aluminum plate. The heat distribution for a steel plate is shown in Figure 4-29 and can be compared to a more even distribution for an aluminum plate in Figure 4-30 and a copper plate in Figure 4-31.

Table 4-10: Dimensions of Current Fin Plate

W	190 mm
H	250 mm
S	10.5 mm
h	22.3 mm
t	1.3 mm
t_b	3 mm

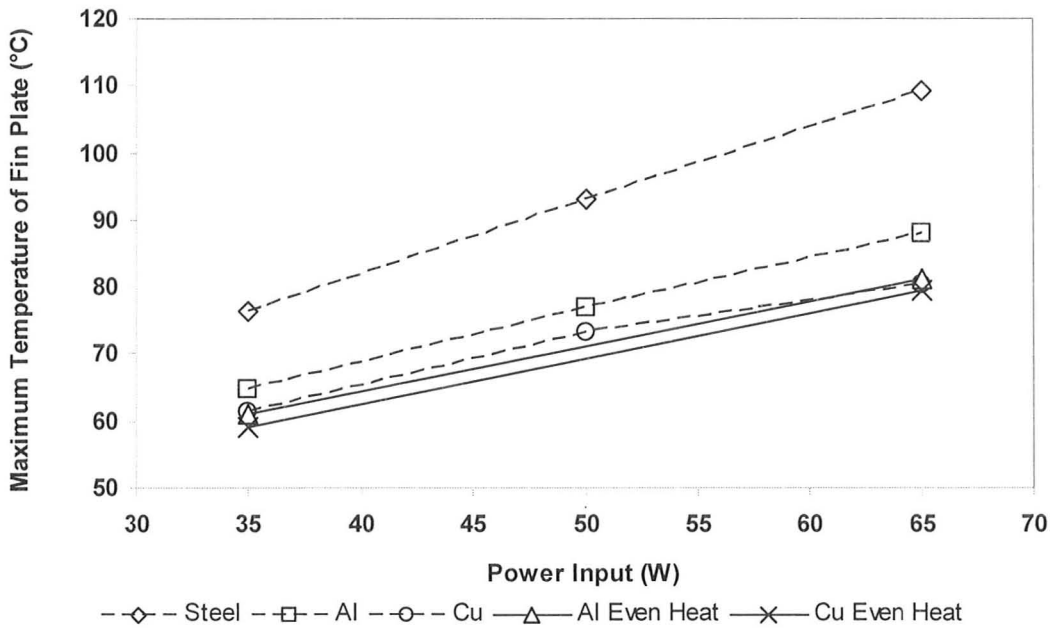

Figure 4-28: Maximum Temperature of Fin Plate for Three Power Inputs and Five Different Fin Plates

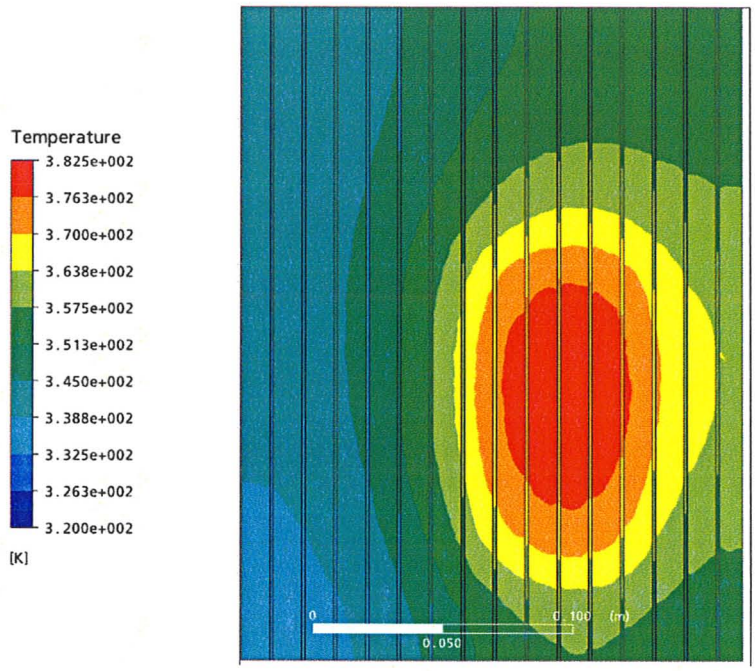

Figure 4-29: Temperature Distribution in 3 mm Steel Fin Plate Dissipating 65 W

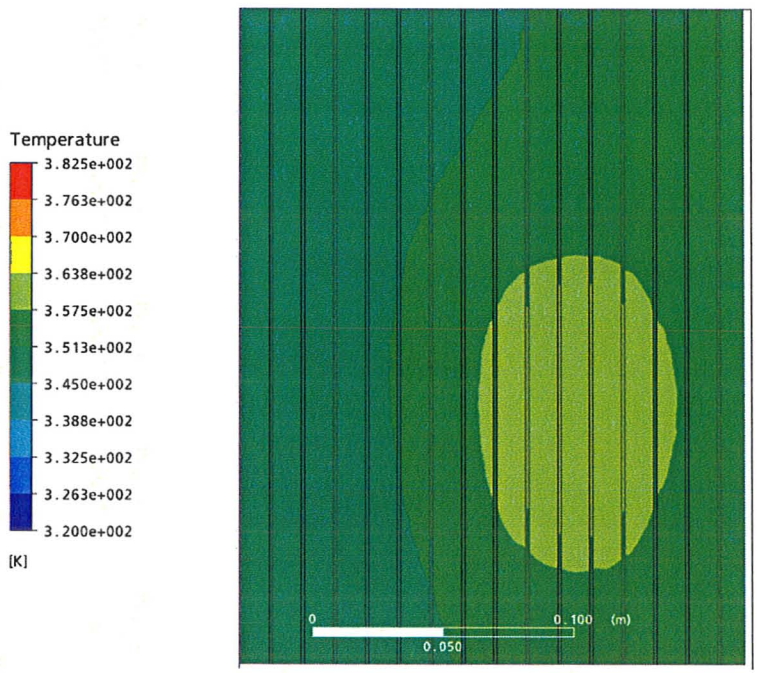

Figure 4-30: Temperature Distribution in a 3 mm Aluminum Fin Plate Dissipating 65 W

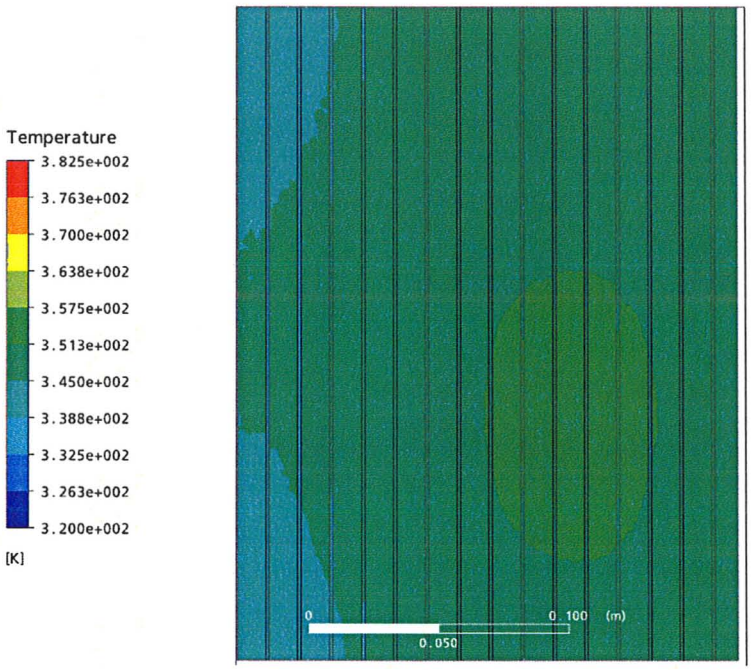

Figure 4-31: Temperature Distribution in a 3 mm Copper Fin Plate Dissipating 65 W

Figure 4-32 shows the temperature distribution for an aluminum fin plate dissipating 50 W simulated in CFD and Figure 4-33 shows the experimental results of dissipating 50 W through an aluminum fin plate. The overall scales are not aligned since radiation heat transfer was not included in the CFD analysis. When temperatures at specific points on the fin plate are compared between the IR image and the CFD analysis, the CFD temperatures are found to be higher by 5.2% ± 0.2%. The similar shape that is seen as well as the nearly constant increase of the CFD value over the experimental value indicates that the CFD is capturing the problem well.

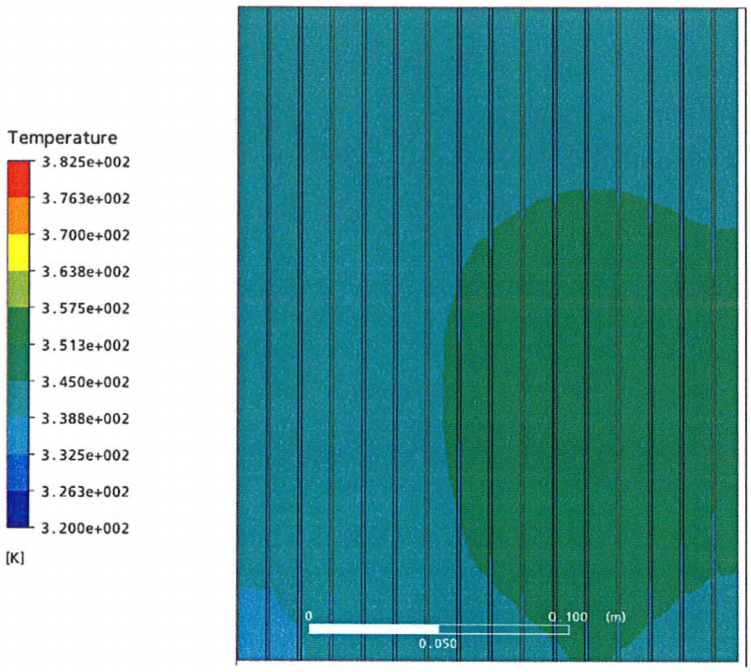

Figure 4-32: Temperature Distribution from CFD Analysis for 50 W Power Dissipation in an Aluminum Fin Plate

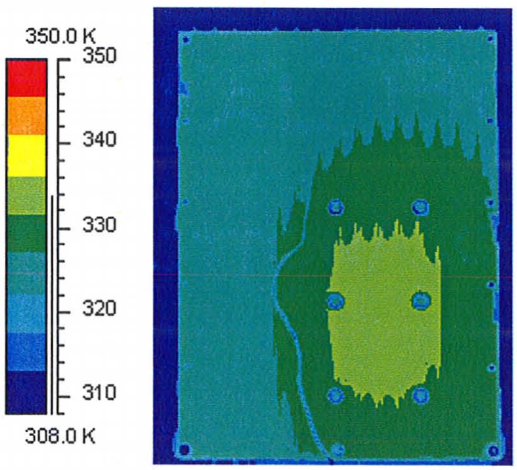

Figure 4-33: Temperature Distribution from an Infrared Image for 50 W Power Dissipation in an Aluminum Plate

One method to improve the heat spreading investigated was increasing the thickness of the fin plate. The same simulation was conducted for a fin plate with twice the base thickness (t_b = 6 mm) and the rest of the dimensions the same. The same three power levels were used (35 W, 50 W and 65 W) and steel and aluminum were simulated. The maximum temperature for each simulation is shown in Figure 4-34. The trends are the same as with the thinner plate (Figure 4-28) but the values are lower. The temperature distribution for a 6 mm steel plate dissipating 65 W is shown in Figure 4-35, and for a 6mm aluminum plate in Figure 4-36. The temperature distribution patterns are the same for the 3 mm and 6 mm plates; however as can be seen in Figure 4-28 and Figure 4-34, the temperatures are lower for the thicker plate.

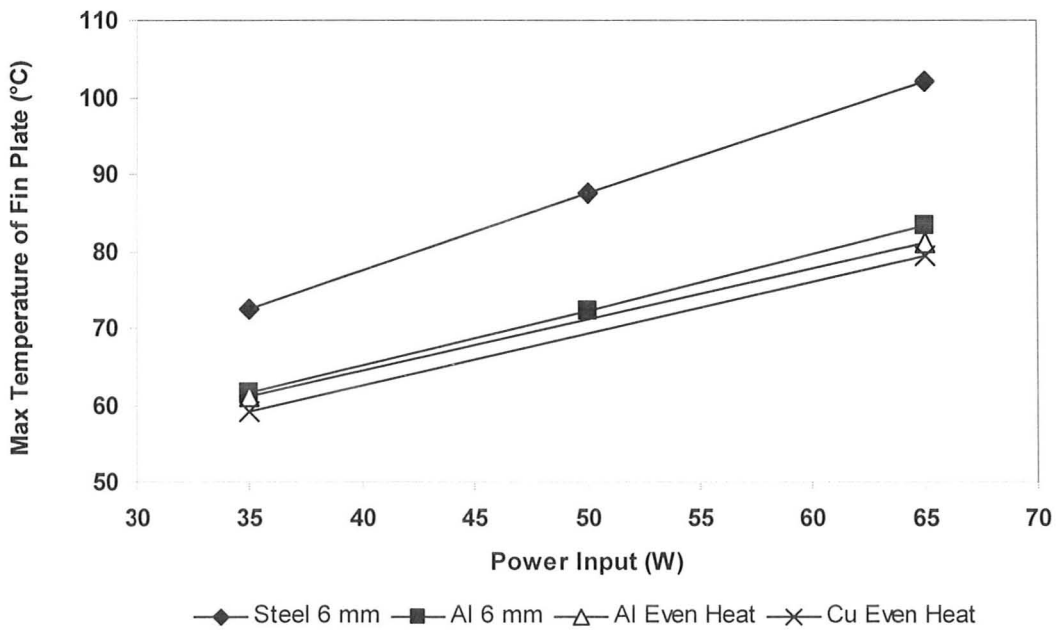

Figure 4-34: Maximum Fin Plate Temperature for Three Power Levels with 6 mm Thick Fin Plates

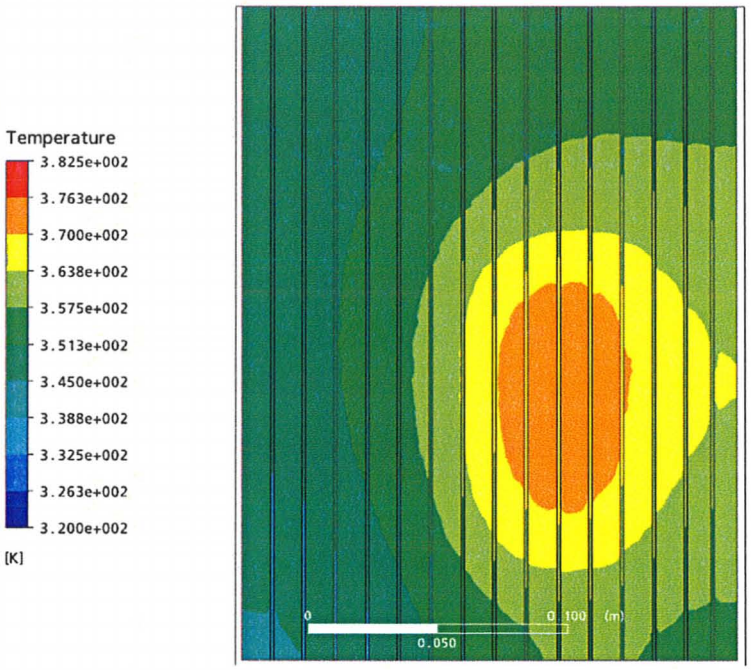

Figure 4-35: Temperature Distribution in a 6mm Thick Steel Fin Plate Dissipating 65 W

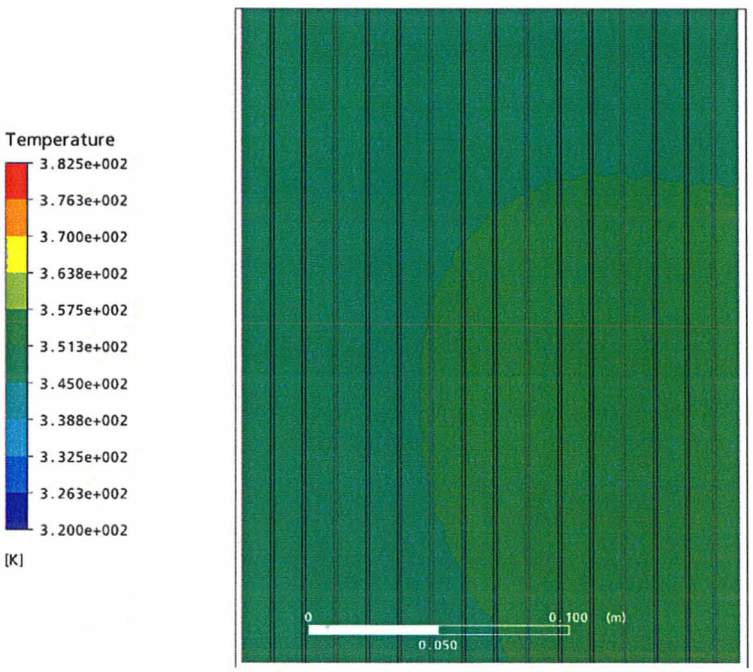

Figure 4-36: Temperature Distribution in a 6mm Aluminum Fin Plate Dissipating 65 W

Maximum temperature for an aluminum fin plate dissipating 65 W with even heat flux, a 3 mm plate and a 6 mm plate is shown in Table 4-11. By increasing the plate from 3 mm to 6 mm, temperature above a plate with even heat flux was reduced by 5°C from 7°C to 2°C or by 70%. This influence of heat transfer has an even larger impact for a material with a low thermal conductivity such as steel. A 6 mm steel plate has a maximum temperature of 109°C which is reduced to 102°C by increasing plate thickness to 6 mm but both values are still well above the temperature of an aluminum plate with even heat flux of 88°C.

Despite the performance increase available by using copper and by increasing plate thickness, additional design factors need to be considered before selecting the thickest plate possible. Increasing thickness of fin plates increases material cost, weight of the system and possibly manufacturing costs. Each specific application will need to be evaluated to optimize the balance between cost, weight and maximum temperature.

Table 4-11: Maximum Temperature for Different Thickness of Aluminum Fin Plate Heat Spreaders

Plate	Maximum Temperature (°C)
3 mm plate	88
6 mm plate	83
Even heat distribution	81

Chapter 5 System Model

The cooling system currently used in small, sealed computers contains many different components each with a thermal resistance. Each component must be evaluated independently to allow minimization of temperature drop, however to estimate the processor temperature accurately all components of the system must be combined into one model. Having all components in one model allows the operating temperature of each component to determine the operating temperature of the next component in the system. Since the processor temperature is the most critical temperature in the system which cannot exceed a certain limit, predicting it accurately is very important. This chapter will describe the formulas used for each part of the model and then detail several new possible designs and evaluate performance of the cooling system.

5.1 Model

Accurate use of the model requires the parameters of each component to be known so each temperature drop can be calculated. It also requires knowledge of how much power will be produced by the CPU and *northbridge* and the temperature of the surroundings. By entering the thermal resistance of each component in the system along with the power to be dissipated and the temperature of the surroundings, the temperature at each point in the system can be found. The model works by starting at the surrounding temperature and calculating each temperature in the path from the surroundings to the CPU.

Heat is transferred from the fin plate to the surroundings via natural convection and radiation, both of which are driven by the temperature difference. Using the equation of Bar-Cohen and Rohsenow (2003) for natural convection, discussed in Chapter 2, and the shape factor of Shabany (2008) for the radiation, also discussed in Chapter 2, the heat transferred to the surroundings can be found. The model uses an iterating loop to increase the surface temperature, assumed to be uniform, until the required amount of heat is dissipated. To facilitate comparison with the other components in the system, a thermal resistance value is calculated for the fin to surrounding section of the system using

$$R_{fin-surroundings} = \frac{\Delta T}{q}. \tag{5.1}$$

Thermal contact resistance that occurs where two components are in physical contact is modeled using a simple thermal resistance

$$R_{contact} = \frac{\Delta T}{q}. \tag{5.2}$$

A value for the resistance can be found in tables or determined based on experimental data for each situation.

The segment from the CPU to the fin plate can be constructed from many different elements including heat pipes or direct conduction through carbon foam or copper. When using a solid conduction medium the resistance can be found with

$$R = \frac{L}{kA} \tag{2.3}$$

where k is the thermal conductivity, in W/mK, L is the size of the conduction block in the flow direction, in m, and A is the cross sectional area of the conduction block, in m^2.

Any part of the system model can be modified using values from experimental analysis to quickly capture details which may not be possible to quickly capture using analytical models. This is employed when a sintered wick heat pipe is simulated. Based on experimental results, the heat pipe will not reach its q_{max} value, and its temperature drop is low enough compared to other system components so that it can be quickly estimated as a simple thermal resistance. Using the effective thermal conductivity values calculated in Chapter 5 and listed in Table 4-5, temperature drop across a heat pipe can be quickly estimated.

As with any analytical model, there are certain known limitations in the computer cooling system model. The most obvious is the lack of heat spreading analysis in the fin plate. Due to the complex nature of determining the temperature distribution in a fin plate, including it in the model was not feasible. When detailed spreading is required CFD can be conducted. Another limitation is that only the heat flow path through the fin plate is considered. Some amount of heat will flow from the CPU through the motherboard and be conducted into the other sides of the case. Alternate flow paths could account for a non-trivial amount of heat flow. However, they cannot be counted on for cooling since they will depend on where the system is installed and its surroundings, making this model conservative. Despite the limitations of the model it is believed to still provide a useful tool to quickly evaluate different system parameters and their effect on the CPU temperature. Regardless of the accuracy of the CPU temperature estimated, trends can be identified which will aid with design of new heat transfer systems.

5.2 System Analysis of Future Design Options

The performance of the current system will be estimated for processors that generate more heat. Processors are available that require power dissipation of 65 W and 130 W, both of which are tested. The current fin design will be used, with dimensions given in Table 4-10. Contact resistance of 0.1 K/W was used for both contact resistances in the model based on experimental data, which is on the same order of magnitude as reported values (Fried, 1969). Thermal resistance of the heat pipe was taken to be 0.025 K/W based on experimental data from the sintered heat pipe in the U orientation. The system parameters are summarized in Table 5-1. The resultant temperatures for a 65 W CPU are summarized in Table 5-2 and for a 130 W CPU in Table 5-3. Based on the

Table 5-1: Thermal Resistance Values used for System Model Analysis

$R_{contact}$	0.1 K/W
R_{HP}	0.025 K/W
Fins	Current design

Table 5-2: Temperatures Estimated by Model for 65 W CPU using Current Cooling System in 25°C Environment

T_{CPU}	82.1°C
$T_{Evaporator}$	75.6°C
$T_{Condenser}$	74.0°C
T_{Fin}	67.5°C
$T_{surrounding}$	25.0°C

Table 5-3: Temperatures Estimated by Model for 130 W CPU using Current Cooling System in 25°C Environment

T_{CPU}	127.7°C
$T_{Evaporator}$	114.7°C
$T_{Condenser}$	111.4°C
T_{Fin}	98.4°C
$T_{surrounding}$	25.0°C

model predictions, a 65 W CPU could successfully be used in a current system with a maximum temperature of 82.1°C, but a 130 W CPU could not as its temperature reaches 127.7°C which exceeds the maximum of 100°C. Expanding the fin plate to 300 mm wide and 350 mm high would allow a 130 W CPU to run at 96.4°C. Alternately, if the height of the fins was increased from 23 mm to 60 mm, the CPU temperature would be reduced to 97°C with a plate 190 mm wide and 250 mm high. These large sizes indicate the need to explore forced convection if high power CPUs are desired to be used.

Fin spacing effect on CPU temperature can also be investigated. For a 35 W CPU running with the current fin plate size (190 mm x 250 mm) and fin height (23 mm), the CPU temperature for fin spacing distances from 7 mm to 12 mm are shown in Table 5-4 and very little variation is seen.

Table 5-4: CPU Temperature for Fin Spacing Distances from 7 mm to 12 mm With Current Fin Geometry and 35 W CPU

Spacing Distance (mm)	CPU Temperature (°C)
7	59.37
8	58.25
9	57.87
10	58.02
11	58.50
12	59.14

Some systems are required to operate in areas where the temperature can approach 40°C. For the same system specifications as described in the previous simulation, summarized in Table 5-1, the temperatures for a 35 W CPU are listed in Table 5-5 and the temperatures for a 65 W CPU are listed in Table 5-6. The current system is more than capable to run a 35 W CPU below its maximum of 100°C however a

65 W CPU would reach 96°C if run in 40°C surroundings which is quite close to its maximum. A possible solution could be to increase the height of the fins from 23 mm to 40 mm in which case the CPU temperature is estimated to drop to 85.5°C permitting safe operation.

Conduction through a material such as carbon foam can be modeled to determine the final CPU temperature. If a piece of carbon foam with a cross section area of 400 mm^2, a height of 47.7 mm and a conductivity of 131 W/mK were used between a 35 W CPU and the fin plate, with contact resistance of 0.1 K/W, and the fins exposed to a 25°C environment, the CPU would reach a temperature of 82.6°C. If the height of carbon foam was reduced to 20 mm, by moving the fin plate closer to the CPU, the CPU temperature would be 64.5°C.

Table 5-5: Temperatures Estimated by Model for 35 W CPU using Current Cooling System in 40°C Environment

T_{CPU}	73.3°C
$T_{Evaporator}$	69.8°C
$T_{Condenser}$	68.9°C
T_{Fin}	65.4°C
$T_{surrounding}$	40.0°C

Table 5-6: Temperatures Estimated by Model for 65 W CPU using Current Cooling System in 40°C Environment

T_{CPU}	96.2°C
$T_{Evaporator}$	89.7°C
$T_{Condenser}$	88.1°C
T_{Fin}	81.6°C
$T_{surrounding}$	40.0°C

To achieve the same temperature drop as a sintered heat pipe in the U orientation with a piece of carbon foam with 400 mm^2 cross section over a distance of 20 mm, the carbon foam would require a thermal conductivity of 1925 W/mK.

If an aluminum fin plate, with a volume of 254.6 cm^3, ρ = 2.7 g/cm^3, were replaced with a carbon foam fin plate with the same volume but a density of 0.64 g / cm^3, the value for TC1556, the weight of the plate would be reduced from 687 g to 163 g. The thermal conductivity of TC1556 has been found to be 130.1 W/mK which is on the order of aluminum so performance would be similar. If weight savings were a priority, the design could be further investigated.

Using a model that applies heat transfer relations to analyze all the components of a computer cooling system simultaneously allows for quick and simple testing of effect of different parameters on the CPU temperature which is the most critical temperature in the system. Despite its short comings it is quite valuable for testing design ideas before reaching the experimental stage.

Chapter 6 Conclusions and Recommendations

The cooling system of a small sealed computer system was instrumented with thermocouples and the system was run at full capacity to find the current performance of the system. It was determined that the largest temperature drop was between the fins and the surroundings, provided the groove wick or sintered heat pipe were in the U orientation. When the groove wick heat pipe was in an inverted U orientation, the condensate was not returned to the evaporator from the condenser and produced the largest temperature drop. This initial research prompted the evaluation of heat pipes and the exploration of alternate solutions to remove the variable performance of heat pipes from the system. The next largest temperature drop, the fins was designated the second area of research after the heat pipe.

Testing types of heat pipes with sintered wicks and groove wicks to find the maximum heat which can be transferred in different orientations was conducted. It was determined that capillary force was not great enough in the groove wick heat pipe to move the condensate back to the evaporator for the inverted U orientation and limited the maximum heat load for the U orientation to 30 W. The sintered wick heat pipe was found to be affected by orientation as its qmax dropped to 44 W for the inverted U orientation but not to the same extent as the groove wick heat pipe which completely failed in the inverted U orientation.

Carbon foam was a proposed new material which, through new manufacturing techniques would achieve thermal conductivity approaching that of pure carbon

structures of 1925 W/mK. Using this material would allow for direct conduction of heat between the CPU and the fin plate with a similar temperature drop to a properly functioning heat pipe. This was appealing to remove the variability of heat pipes and the influence of orientation with respect to gravity. Testing of carbon revealed many interesting results. However the thermal conductivity was found to vary between about 30 W/mK and 131 W/mK depending on the manufacturing process. The thermal conductivity was found to vary by up to a factor of two in different directions of the same material. When no interface material was used, the thermal contact resistance between aluminum and carbon foam was lower than between aluminum and copper due to deformation of the carbon. Also of interest, the specific thermal conductivity of carbon foam was found to be just over four times greater than copper and three times greater than aluminum, which suggests that carbon foam could be a useful material in situations where weight was a primary concern.

The fin plate provides the final step, the transfer of heat from the CPU and *northbridge* to the surroundings. The dimensions of the fins were identified to influence the rate of heat transfer via natural convection and radiation. Using analytical models to predict performance allowed the optimum fin spacing to found to be 9 mm. The current fins have a spacing of 10.5 mm which provide a maximum temperature only 1°C higher than the optimum design. Another issue identified for analysis for the fin plate was the spreading of heat from the area where the heat pipe contacted the plate. This was investigated using CFD and it was found that increasing the thickness of an aluminum

plate from 3 mm to 6 mm lowered the temperature 5°C and brought it to within 2°C of the temperature of a plate with an evenly applied heat flux.

Another method of increasing heat spreading in a fin plate is by use of heat pipes embedded or partially embedded into the plate. By placing the heat pipes in contact with the contact area and having them lead to the areas away from the contact area, heat will be moved out towards the cooler parts of the plate and equalize the temperature. Simulations to determine the optimum number and arrangement of heat pipes on the plate can be conducted and compared with the cost of using a thicker aluminum plate or a copper plate. Another possibility is to use a vapour chamber as the plate to equalize temperature. This would require much research and is well beyond the scope of the current project. To achieve substantial weight savings, carbon foam could be used for the whole fin plate which would reduce the weight from 687 g to 163 g, or carbon foam could be used as a heat spreader fastened to the back of the fin plate. Carbon TC1556 shows potential since its thermal conductivity was measured to be 130 W/mK and it could have double that in the alternate orientation which would make it equal to aluminum. If weight savings were of primary importance, optimization of fin geometry for maximum heat transfer and minimum weight could be researched in the literature. If greater flexibility in placement is desired, alternate fin geometries could be considered including pin fins or staggered channels.

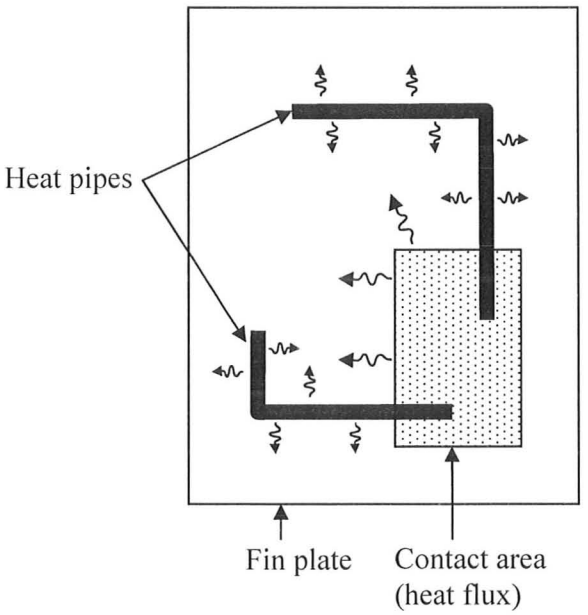

Figure 6-1: Concept Design using Heat Pipes to Spread Heat more Evenly on a Fin Plate

A simple analytical model was developed to predict system temperatures and CPU temperature by finding the temperature drop across the contact resistance, heat pipe or solid conductor (e.g. carbon foam), and from the fin plate to the surroundings by natural convection and radiation. The model allows fast analysis to see the effect of changing different parameters on the CPU temperature. The accuracy is dependent on the quality of data that is entered. Regardless of accuracy the model provides information on trends in the temperature of the CPU when any one parameter is varied and is useful as an initial design tool.

Appendix A Carbon Foam Analysis

A.1 Carbon Foam Literature Review

Carbon foam is a new material with high specific thermal conductivity and the potential to have very high thermal conductivity when its porosity is reduced using new manufacturing techniques. This high thermal conductivity could be used to directly conduct heat with a temperature drop comparable to a heat pipe. Also of interest is the potential for carbon foam to be used as a fin material or spreader due to its increased surface area because of exposed pores.

Graphitized carbon foam is a relatively new material with many unique properties including very high specific conductivity (Klett et al, 2000) and has been the subject of much research since it was first reported by Klett (1999). Properties have been found in some cases to be isotropic (Klett et al, 2000) and in other cases to be anisotropic (Gaies and Faber, 2002) with variation in the thermal conductivity of up to 3.5 times in different directions. Gaies and Faber (2002) noted that no visual difference could be seen in the foam structure for the different directions, but that the highest thermal conductivity occurred in the direction parallel with gravity during production.

Klett et al. (2000) described a new process which allows graphite foam to be produced in a much faster and cost effective process than previously possible. Using two different precursor pitches (synthetic and petroleum based), foams were produced at four different pressures, yielding eight samples. Scanning electron microscope, optical micrographs, x-ray analysis and thermal property measurements were presented and

discussed. The foam was found to have an isotropic thermal conductivity of up to 150 W/mK with a density of 57g/cc and depended on the operating pressure during manufacturing.

Gaies and Faber (2002) tested the thermal properties of several samples of graphite foam using the laser flash diffusivity method. Among their results, they found that the thermal conductivity varies with density, and that by using chemical vapour infiltration (CVI) tiny cracks in the carbon structure could be filled. CVI also added additional graphite to all surfaces of the foam and increased the density. The thermal conductivity of the samples was found to be highly anisotropic with the conductivity being 3.5 times greater perpendicular to the *xy*-plane compared to parallel to the *xy*-plane. They defined the *xy*-plane as the plane perpendicular to gravity during processing. It was also found that the thermal conductivity decreases by about 40% as the temperature is raised from 50°C to 300°C.

A very interesting and potentially useful application for carbon foam involves using the foam as a heat transfer surface in heat exchangers with liquids and gases being forced over or through foam to move heat into the fluid (Figure A-1). Gallego and Klett

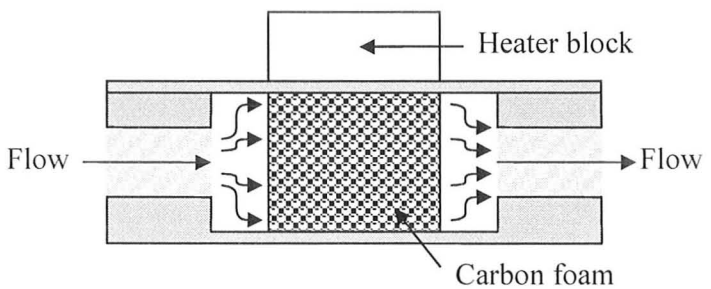

Figure A-1: Test Section used by Gallego and Klett (2003)

(2003) described the process used to make carbon foam and conducted tests to find the heat transfer coefficient for carbon foam in forced convection. Heat transfer coefficients were found using both water and air as the forced convection fluid. Several shapes were tested including rectangular fins, pin fins (Figure A-2), inverse pin fins (Figure A-3), corrugated and solid foam. The performance in forced air was compared for each shape of carbon and aluminum foam. It was found that the carbon achieves heat transfer coefficients up to 14 times greater than aluminum for certain configurations and at least 3 times greater for all configurations tested. The heat transfer coefficient was calculated based on the contact area of the foam block with the heater, so it was the same for each configuration and for the aluminum foam and carbon foam. A key difference between aluminum foams and carbon foams is the effective thermal conductivity. Although carbon foam has a similar thermal conductivity to that of solid aluminum (150-250 W/mK) (Klett et al., 2005, Poco, 2002) the effective conductivity of aluminum foam is much lower (5-50 W/mK) (Klett et al. 2000). The extra surface area of the smaller pores and the higher effective thermal conductivity are the two main factors why the carbon produces much higher heat transfer coefficients.

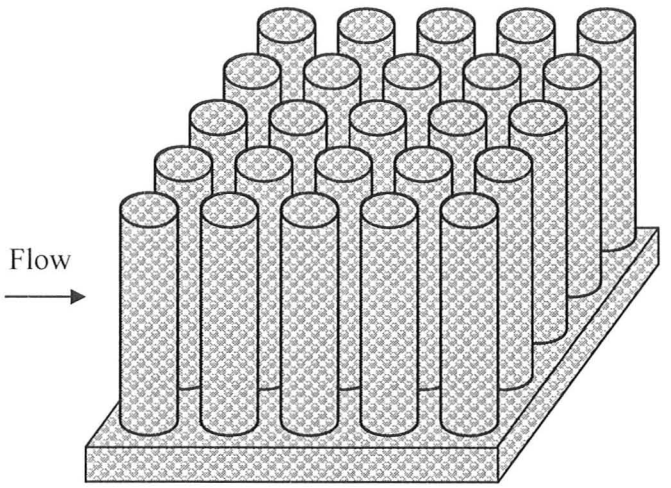

Figure A-2: Pin Fins Tested by Gallego and Klett (2003)

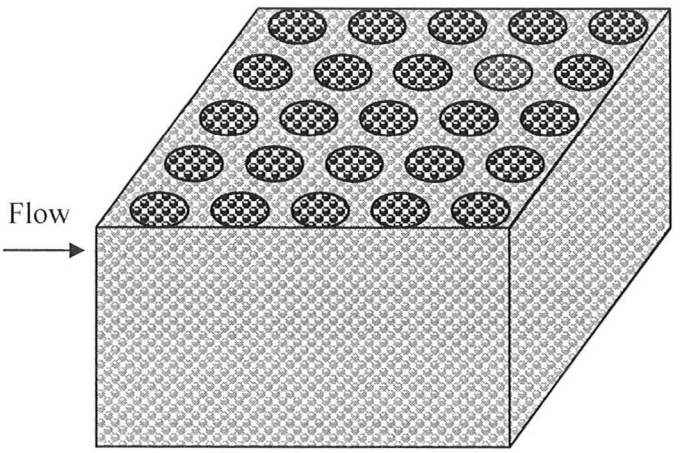

Figure A-3: Inverse Pin Fins Tested by Gallego and Klett (2003)

Yu et al. (2005) discussed the use of carbon foam in heat exchangers for compact recuperators for gas turbines. Simple models were presented to allow quick analysis of heat transfer from simple porous channels. Results indicated that a very light and small heat exchanger could be made by using a short section of carbon foam and passing air through the pores. This short carbon configuration gave similar heat dissipation, slightly

higher air side pressure drop and much lower mass compared to fins made of carbon foam.

Yu et al. (2006a) developed a model of a unit cube of porous carbon material to simulate porous carbon when using CFD and empirical models. Pressure drop and heat transfer were accurately found using the model.

Yu et al. (2006b) developed a thermal resistance model for a liquid to air heat exchanger using carbon foam fins on the air side of thin liquid channels. The model was compared with experimental results and found to be in good agreement. Optimization was performed using the model to find the effect of each parameter on the heat transfer. The porosity of the carbon and the fin density were found to have the greatest influence on performance. A performance improvement of 15% over aluminum heat exchangers was estimated to be possible.

Straatman et al. (2006a) conducted experiments to find the heat transfer coefficient for flow over rectangular pieces of carbon foam of different heights bonded to a surface at various flow rates. It was found that for heights greater than 3mm the height had no influence, indicating that the air penetrated the foam to a depth of 3mm. Heat transfer was enhanced most at the lowest flow rates and also by the foams with the highest porosity. However only sample heights of 1 mm, 3 mm, 5 mm and 10 mm were tested which suggests that the authors conclusion of flow penetration to 3 mm goes beyond the data available since the ideal thickness could be between 1 mm and 5 mm.

Betchen et al. (2006) presented a non-equilibrium model for conjugate heat transfer and fluid flow analysis. Solid, porous (containing solids and fluids) and fluid only domains were handled. The model was validated for a variety of cases.

Straatman et al. (2006b) tested pressure drop and heat transfer rates of water flowing through carbon foam. Pressure drop was found to be a function of the physical dimensions of the pores and heat transfer a function of the thermal conductivity and surface area.

Min et al. (2007) studied the anisotropic properties of pitch-derived carbon foams and discussed the foaming process in detail. Structural and microwave absorbing properties of the foams produced were tested and their variation with processing parameters was investigated. It was noted that bubbles in the foam extend in the direction of gravity during formation. Anisotropic bubble shape could be the cause of anisotropic thermal conductivity. Even if the bubbles appear isotropic, the graphitic structures could be orienting along the axis of gravity, enabling the high conductivity in that direction.

With the assumption that conductivity would scale as the porosity is reduced to the order of 20% with new manufacturing techniques, heat pipes could provide similar performance to heat pipes regardless of orientation. Current carbon foam has thermal conductivity in the range 150-250 W/mK (POCO, 2002 and Klett, 2000) and porosities of between 61%-78% (POCO, 2002 and Koppers Inc., 2006). Reduction of porosity was estimated by ThermalCentric to bring the thermal conductivity closer to that estimated for carbon ligaments (1950 W/mK, Klett et al., 2000) and achieve thermal conductivity on the order of 800-1200 W/mK.

A.2 Carbon Foam Test Section

Three types of carbon foam machined into a shape suitable for use in the sealed computer case (Figure 1-2) were tested. The three types of carbon foam are referred to as TC1813, TC1939 and TC1555. The carbon shape was designed to allow heat to flow from both the CPU and *northbridge* chip into the finned wall of the computer case (Figure A-4). An aluminum block (Figure A-5) fits around the carbon and was screwed to the fin plate to hold the carbon in place (Figure A-6). To validate results a copper block with known thermal conductivity of 401 W/mK was machined with the same dimensions as the carbon foam block. Thermal paste was spread between the carbon foam or copper and the CPU and *northbridge* as well as between the carbon foam or copper and the fin plate. The carbon and copper pieces were instrumented with four thermocouples, two placed near the fin plate and two near the chip side (Figure A-4).

Due to the design of the computer system with the motherboard being mounted to the bottom of the case and the fin plate mounting to the top of the case, the distance from the surface of the CPU and *northbridge* to the fin plate is fixed (Figure A-7). This fixed distance can present problems when the conduction medium connecting the chips to the fin plate is too short a gap can be left, and if the medium is too long, excess pressure can be applied to the chips when fastening the fin plate to the case.

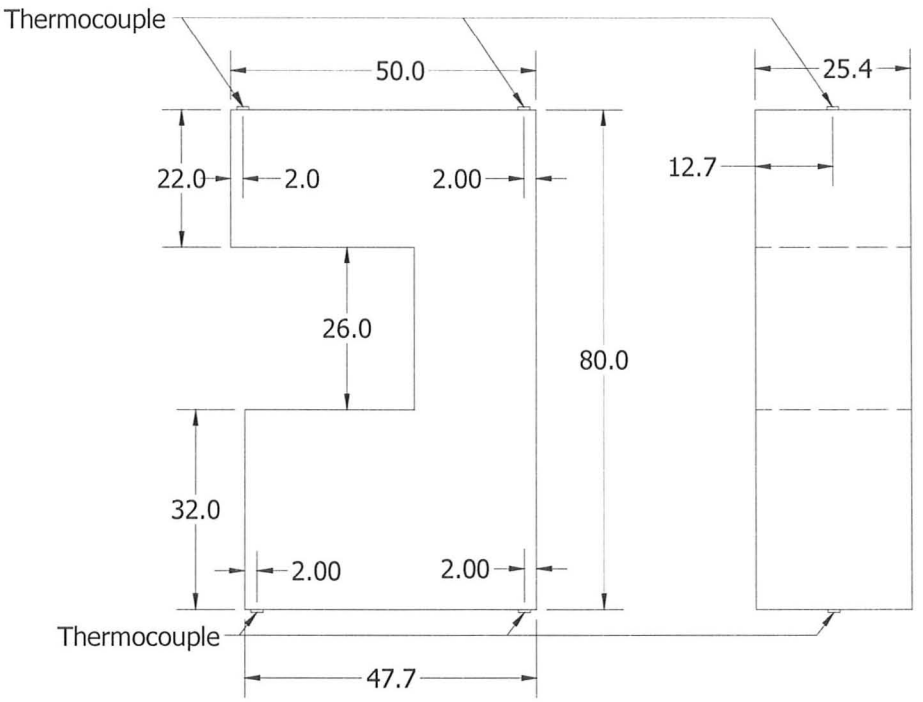

Figure A-4: Carbon Foam Computer Cooling Block (mm)

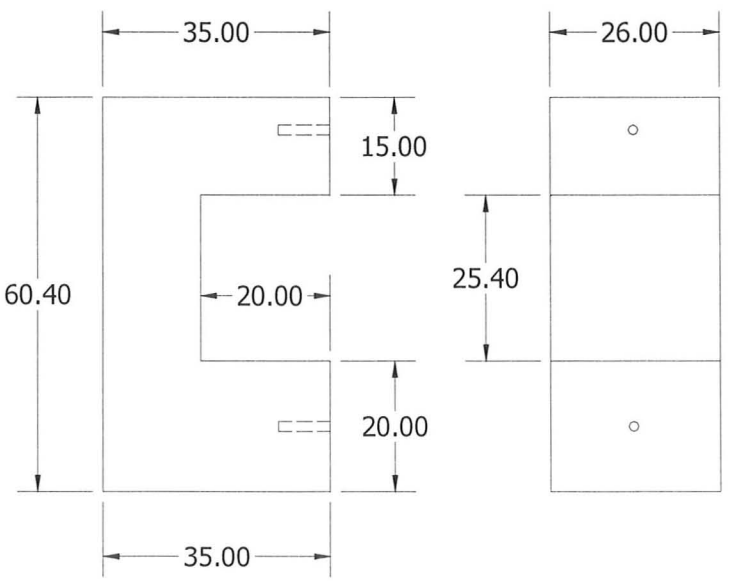

Figure A-5: Aluminum Clamping Block (mm)

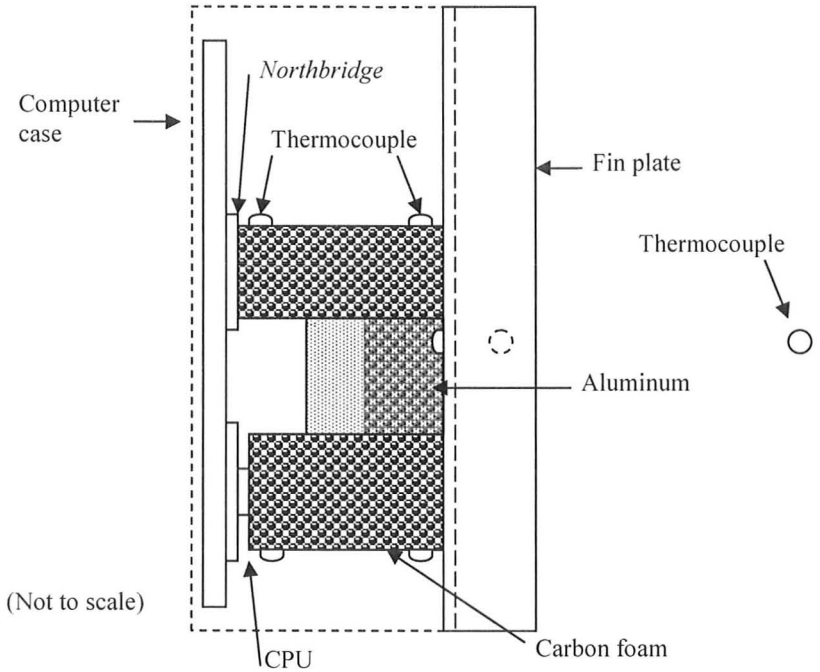

Figure A-6: Carbon Foam In-Situ Test Facility

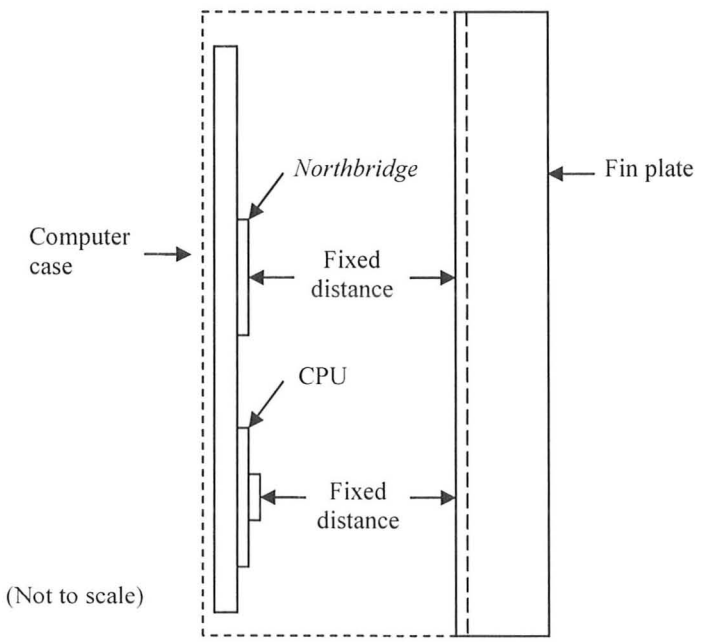

Figure A-7: Inside of Sealed Computer Case Showing Relation of CPU and *northbridge* to Fin Plate

Testing of carbon foam in the controlled heat flux test facility used thermocouples placed as shown in (Figure A-4). To test for possible anisotropic thermal conductivity of the carbon foam it was placed in the test facility to conduct heat along a different direction, refered to as the alternate orientation and is shown in Figure A-8 b) with the thermocouple placements shown in Figure A-9. In addition to thermocouples, an infrared thermal camera, as described in section 3.3, was used to view the carbon foam.

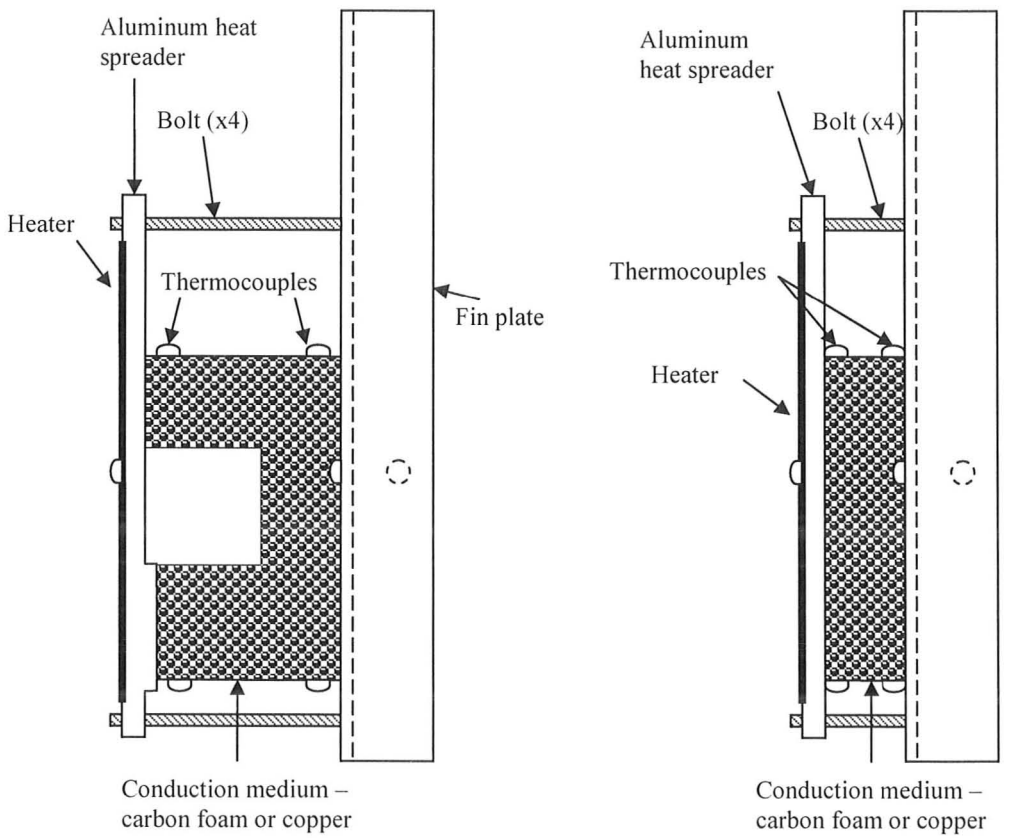

(Not to scale)

Figure A-8: Carbon Foam Test Apparatus Schematic

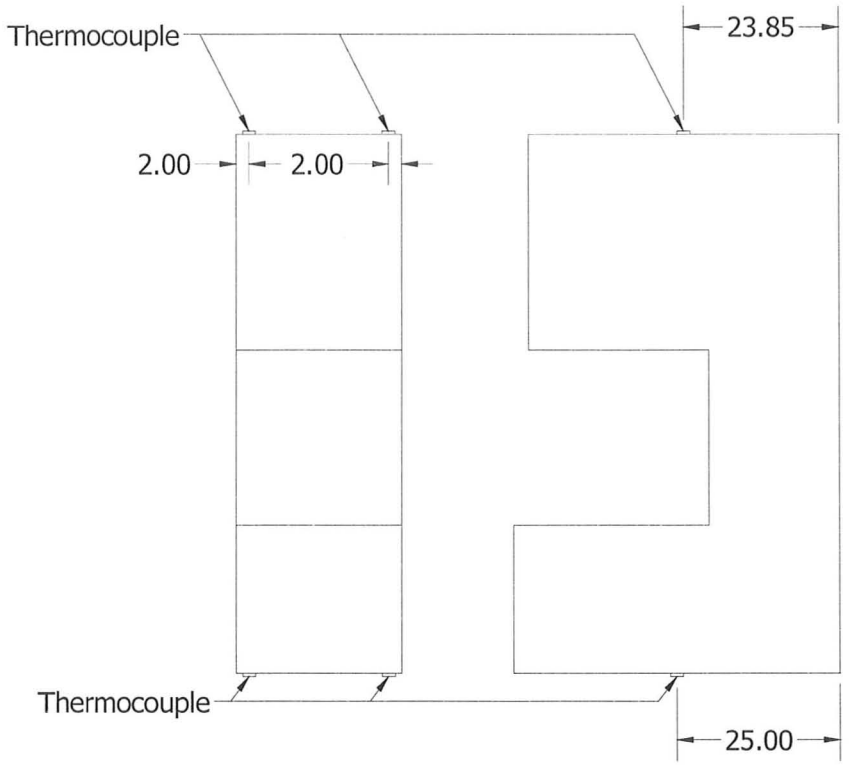

Figure A-9: Thermocouple Placements for Carbon in Alternate Orientation

To view the carbon with the thermal camera, insulation was quickly removed and an image was captured before the temperature of the heater dropped by more than 2°C. If the temperature did drop by more than 2°C, the insulation was replaced until the temperature increased to the previous steady state value. The emissivity of the carbon was estimated using ThermaCAM Researcher software and the temperature from thermocouples mounted as shown in Figure A-4 and Figure A-9.

A.3 Carbon Foam Results

Carbon foam is a new and unique material consisting of carbon pitch which has been foamed to create many interconnected voids in the material and then graphitized. Currently available foams have conductivity in the range 150-250 W/mK (POCO, 2002

and Klett, 2000) and porosities of between 61%-78% (POCO, 2002 and Koppers Inc., 2006). A new manufacturing technique developed by ThermalCentric promises to bring the porosity down to the order of 20% and the hypothesis is that conductivity will increase proportionally. Moving from a starting point of 250 W/mK at 61% porosity to 20% porosity should yield a conductivity of approximately 500 W/mK. Further proof of this concept lies in the estimates for thermal conductivity of carbon ligaments of 1950 W/mK (Klett et al., 2000) and the idea that as carbon foam approaches solid (0% porosity) the thermal conductivity will approach that of carbon ligaments. A solid material with very high thermal conductivity provides a potential solution to the orientation problem of moving heat from the CPU and *northbridge* to the fin plate. Using such a material it is possible to conduct heat directly from the CPU to the fin plate without having to rely on a more complex device such as a heat pipe which can have its performance affected by orientation with respect to gravity. Carbon foam was first tested in-situ to see directly how well it could transport heat away from the CPU.

For the in-situ test the computer burn-in software was used to load the computer to 100% capacity where the CPU was producing 35 W of heat and the *northbridge* 7 W. Thermocouples were placed as shown in Figure A-4. The temperature drop across each section and the temperature profile is shown in Figure A-10 for TC1813 carbon foam, the copper block and a sintered heat pipe in the U orientation. For details on heat pipe testing see section 4.1. For all three test pieces, the temperature rise from the ambient to the fins is quite close, the temperature rise to the fin side of the conductor is close but the temperature on the CPU side of the conductor is 68°C for the carbon foam and 47°C and

48°C for the heat pipe and copper block respectively. Since the carbon foam is 20°C higher than the copper, this indicates that the carbon foam has a much lower conductivity than copper. The CPU temperature was 83°C, 80°C and 50°C for the carbon foam, copper block and heat pipe respectively. The difference between the CPU – conductor side and the CPU temperature is due to contact resistance between the conductor and the CPU die surface. Since thermal paste is used between the die and conductor all values should be the same, however the temperature drop is 33°C and 15°C for the carbon foam and copper respectively which are both quite a bit higher than the drop of 3°C for the heat pipe. This large temperature difference for the copper and carbon foam indicates that there might be a small gap due to manufacturing tolerances and the inflexible nature of conductor design compared to the heat pipe. As discussed in section 3.1.3 and shown in Figure A-7, the distance between the CPU die and the fin plate is fixed. The heat pipe has some flexibility and is fastened to both the fin plate and the motherboard, no gap is possible and the low temperature drop reflects this.

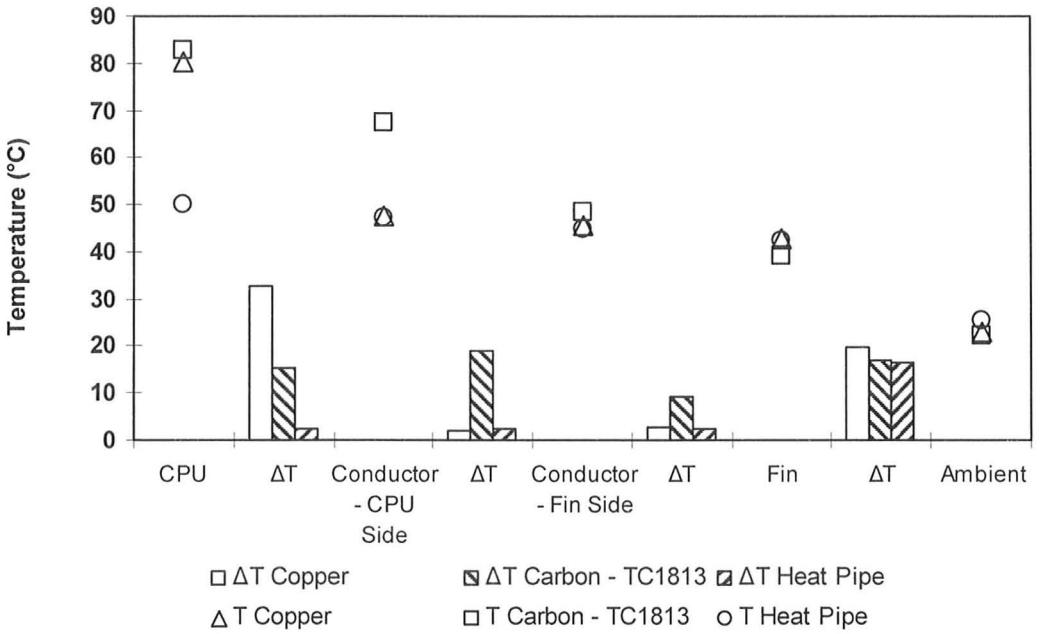

Figure A-10: Temperature Profile and Temperature Drops for In-Situ Testing for each Segment

Testing in the controlled heat flux test facility was done to overcome the limitations of testing in-situ including the fixed distance between the CPU and the fin plate and to achieve more control over the heat flux. By adjusting the mounting screws in the controlled heat flux test facility, the distance between the heat spreader used to represent the CPU and *northbridge* and the fin plate can be varied. The distance adjustment ensures that no gap is left and the contact resistance is reduced as much as possible.

Three samples of carbon foam, TC1813, TC1939 and TC1555 and copper were tested. The temperature profiles for the three carbon samples and copper in the test facility are shown in Figure A-11 and Figure A-12 for the upper and lower thermocouples respectively. The temperature drop between the top thermocouples was 25°C, 13°C, 20°C

and 4°C for carbon TC1813, carbon TC1939, carbon TC1555 and copper respectively. Temperature drop across the lower thermocouples was 17°C, 8°C, 14°C and 4°C for carbon TC1813, carbon TC1939, carbon TC1555 and copper respectively. The relative magnitude of temperature drops for both the upper and lower thermocouples are the same with the largest drop coming from carbon TC1813, followed by carbon TC1555, followed by carbon TC1939 and finally copper had the lowest temperature drop in both cases. This extreme variation is caused by unequal heat flow through each part of the carbon due to the three dimensional design. In addition to thermocouple measurements, infrared thermal camera images of the carbon TC1813 were also captured in order to validate the results. Using the temperature from the thermocouples located closest to the fin plate the emissivity was calculated to be 0.85. The thermal image shown in Figure A-13, displays the temperature gradient across the carbon foam. Using the analysis software the temperature profiles along three lines parallel to the direction of heat flow were measured. After calculating the emissivity using one point, the temperatures at the other points were compared and found to be within the range of error. To estimate the thermal conductivity of the carbon, numerical analysis was conducted to overcome the challenges of the three dimensional geometry. Using ANSYS software a model with the same geometry and dimensions as the test facility was created. A uniform heat flux was applied to the spreader plate with the total power equal to 40 W, the same as was applied in the experiment. To simplify modeling, a constant convective heat transfer coefficient was applied to the fin surface which was determined through iteration to make the fin surface temperature in the model correspond to the experiment. Contact resistance was

also iterated to make the model align with the experiment. The values measured from the thermocouples, infrared camera and calculated from the model are summarized in Table A-1. Using the average temperature drop across the carbon and the combined area of both the CPU and *northbridge* contact areas, the thermal conductivity was calculated as 59 W/mK. Using this as a starting value, thermal conductivity was then iterated in the model until the temperature drop in the model corresponded with the temperature drop seen in the experiment and was estimated to be 65 W/mK.

The close agreement of the calculation of thermal conductivity found using the average temperature drop and the combined area of the carbon foam and the calculation using the model suggests that the method of manual calculation is adequate for the remaining types of carbon foam. The temperature drop for each material and the calculated thermal conductivity value is listed in Table A-2. Copper, with a thermal conductivity of 401 W/mK, was included as a benchmark of the system and method. Its calculated thermal conductivity is within 8% of its known value suggesting the accuracy of the thermal conductivity values for the carbon foams can be expected to be within 10% of its real thermal conductivity value.

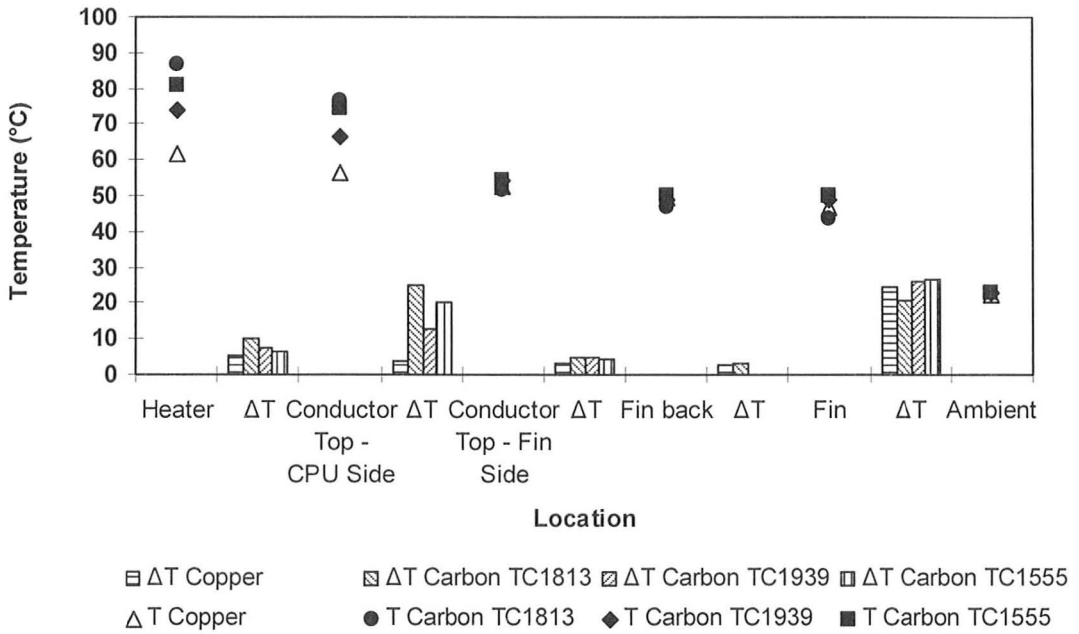

Figure A-11: Temperature Profile of Upper Thermocouples for Copper and Carbon Foams in the Normal Orientation in a Test Apparatus and Temperature Drops for each Segment.

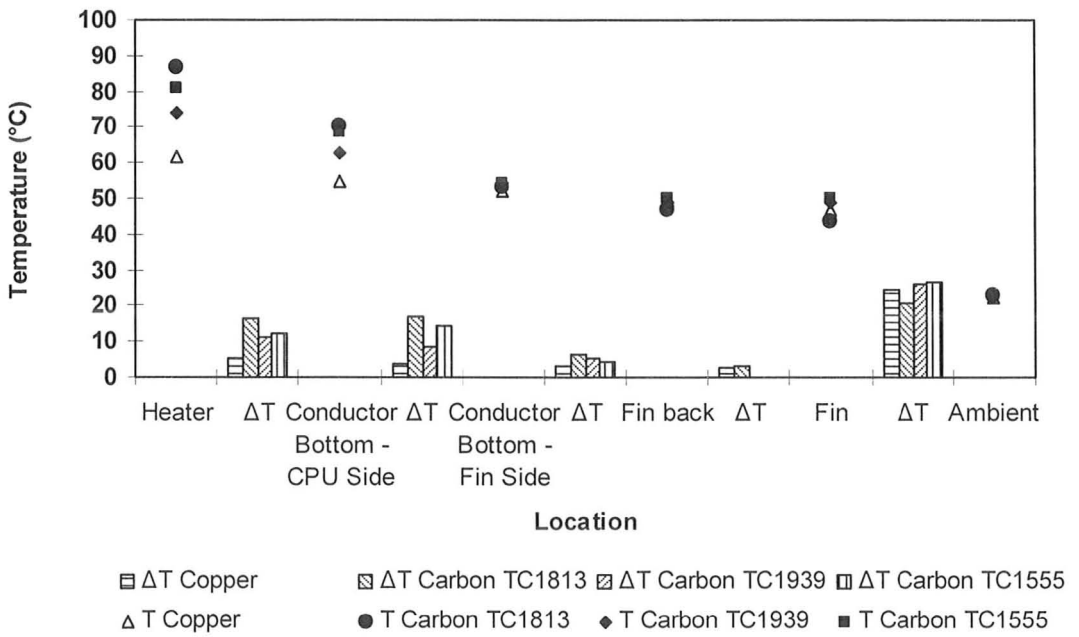

Figure A-12: Temperature Profile of Lower Thermocouples for Copper and Carbon Foams in the Normal Orientation in a Test Apparatus and Temperature Drops for each Segment.

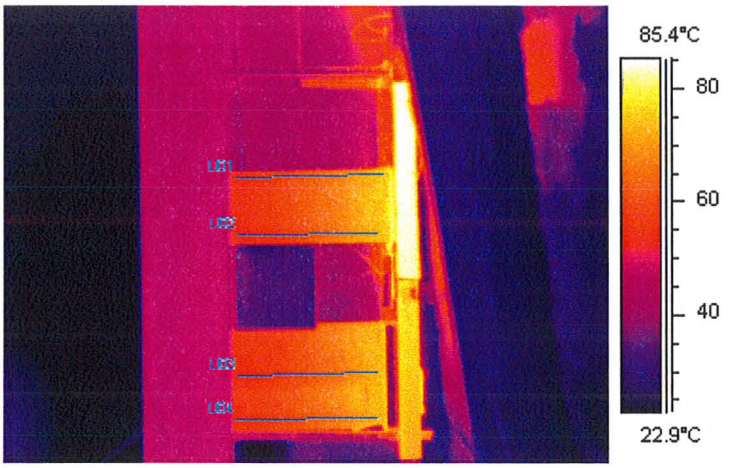

Figure A-13: Infrared Thermal Image of Carbon TC1813 in Controlled Heat Flux Test Facility

Table A-1: Temperatures of Carbon Foam TC1813 from Thermocouple, Infrared and CFD Analysis

Analysis	Conductor Bottom – CPU Side (°C)	Conductor Bottom – Fin Side (°C)	ΔT (K)
Thermocouple	70.3	53.5	16.9
IR	74.3	53.4	20.9
CFD	68.8	52.5	16.6

Table A-2: Thermal Conductivity of Carbon Foam and Copper Calculated from Temperature Drop

Material	ΔT (K)	Thermal Conductivity (W/mK)
TC1813	21	59
TC1939	11	118
TC1555	17	72
Copper	3	370

The thermal conductivity of the carbon foam estimated through measurements is well below the initially estimated values for new foams with reduced porosity but is in line with currently commercially available foams.

An aspect which requires consideration is the possibility that the carbon foam has anisotropic thermal properties. Currently commercially available foam is reported to have

different thermal conductivity depending on orientation (Poco, 2002; Koppers, 2006). To test for anisotropic thermal conductivity, carbon TC1813 was placed sideways in the controlled heat flux test facility to measure the temperature drop in the thinnest direction as shown in Figure A-8b). Thermal paste was not used where the carbon contacted the heat spreader or where the carbon contacted the fin plate due to practical considerations. Thermocouples were placed as shown in Figure A-9. Figure A-14 shows the temperature profile using the thermocouples located on the top of the conduction block and Figure A-15 shows the temperature profile of the thermocouples on the bottom of the conduction block. Copper was also tested in the same orientation to act as a benchmark. No thermal paste was used on the copper.

The results of testing indicate that the contact resistance is higher in this case due to the lack of thermal paste on the carbon and copper samples. An interesting result is that the contact resistance is lower for the carbon than for the copper for both the connection at the heat spreader and at the fin plate. This is thought to be due to the carbon foam deforming slightly and providing more surface area for heat conduction than in the connection between aluminum and copper (Figure A-16). The thermal conductivity of carbon TC1813 was calculated to be 31 W/mK in the alternate orientation (Table A-3), and is about half of what was found for the original orientation (Table A-2). The conductivity calculated for copper is 382 W/mK which is within 5% of its known value.

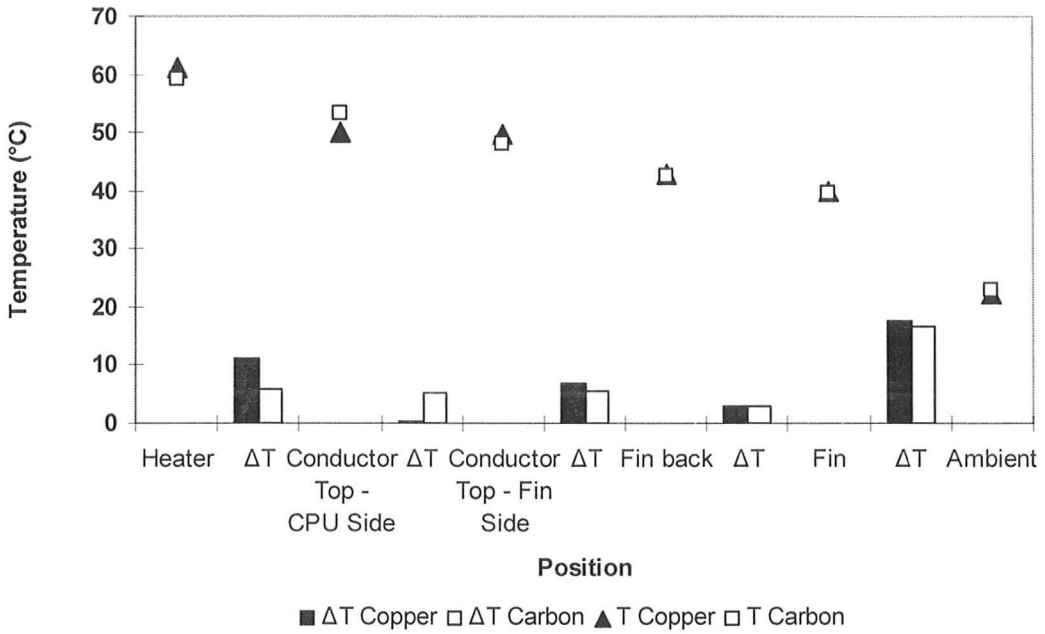

Figure A-14: Temperature Profile of Upper Thermocouples for Copper and Carbon Foam TC1813 in the Alternate Orientation in a Test Apparatus and Temperature Drops for each Segment.

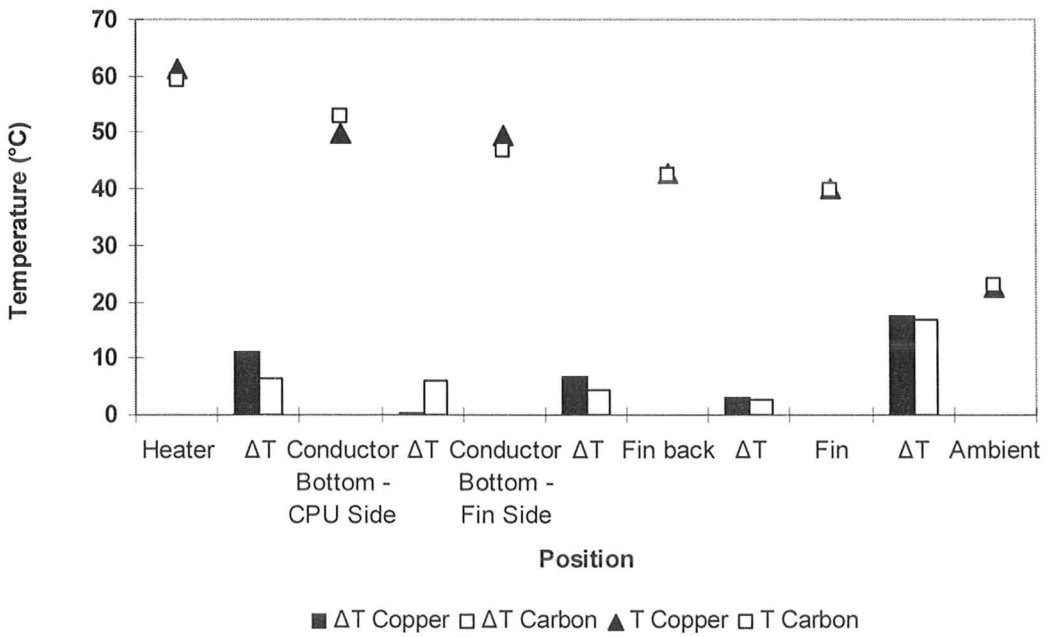

Figure A-15: Temperature Profile of Lower Thermocouples for Copper and Carbon Foam TC1813 in the Alternate Orientation in a Test Apparatus and Temperature Drops for each Segment.

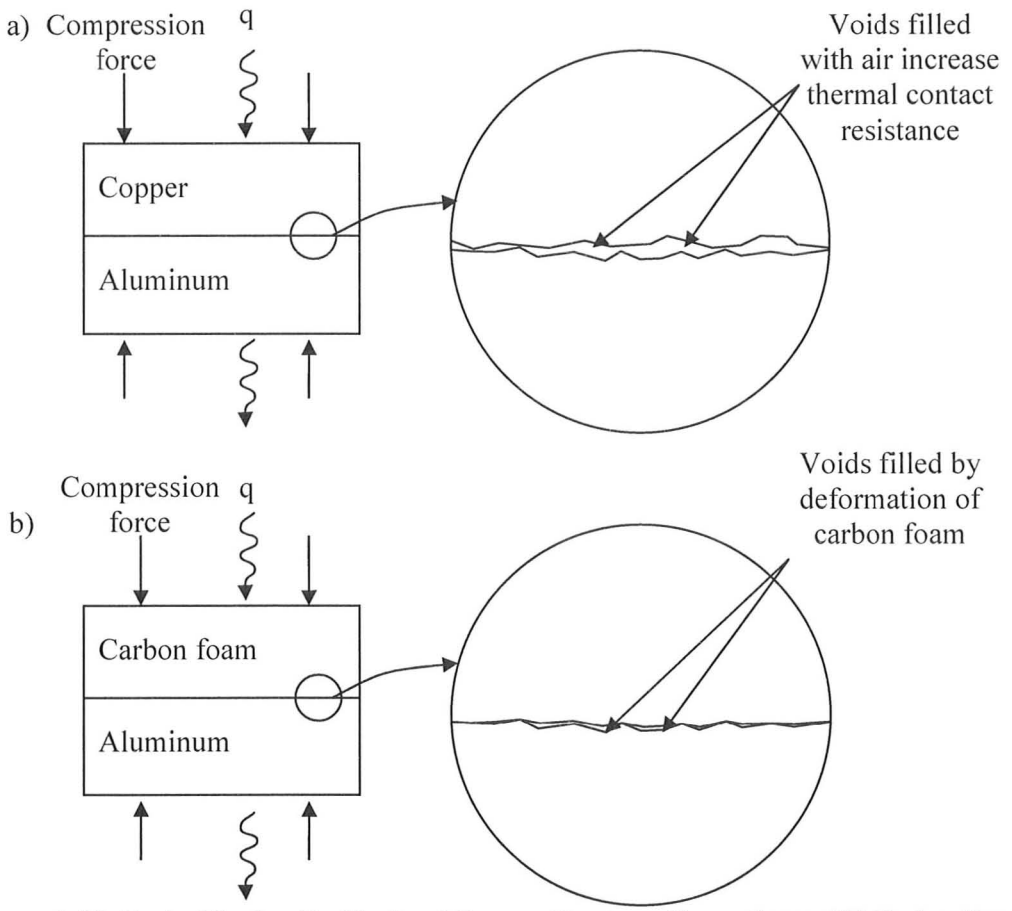

Figure A-16: Contact Surface Profiles for a) Copper-Aluminum Connection and b) Carbon Foam-Aluminum Connection

Table A-3: Thermal Conductivity of Carbon Foam and Copper Calculated from Temperature Drop for Alternate Orientation

Material	ΔT (K)	Thermal Conductivity (W/mK)
Carbon TC1813	5.5	31
Copper	0.4	382

An attractive feature of carbon foam for weight sensitive applications is its low density in the range 0.4-0.65 g/cc. When comparing the variation of thermal conductivity with density a general trend can be seen of k increasing with density (Figure A-17).

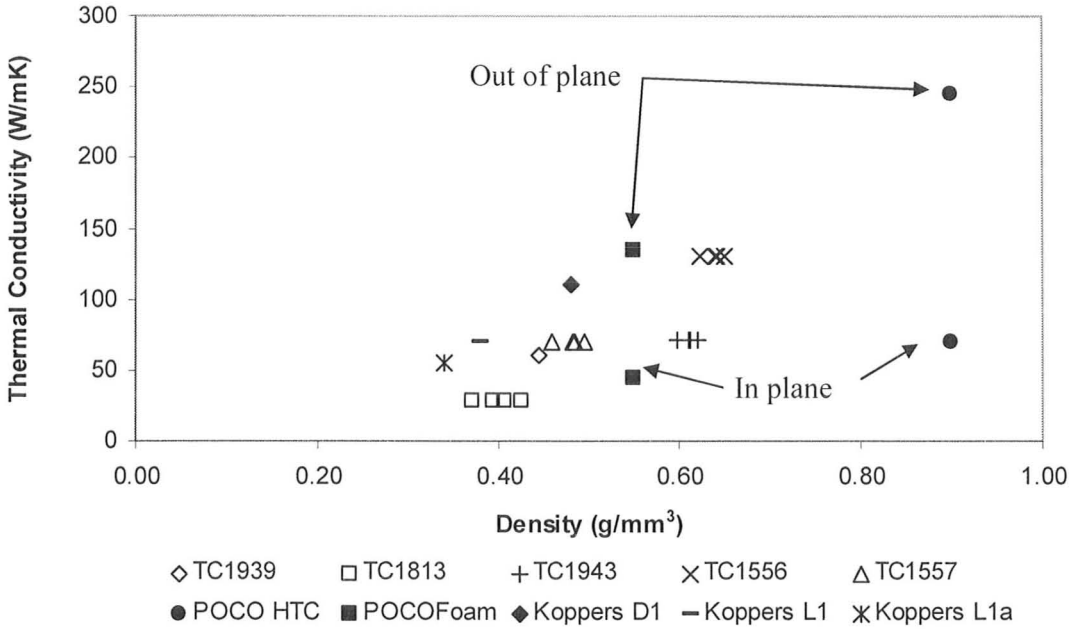

Figure A-17: Thermal Conductivity vs. Density for all Carbon Foams Tested

Due to the imprecise nature of backing out thermal conductivity values from the test facility that was used, additional samples of carbon foam were sent to a high-accuracy thermal interface material tester (Kempers et al., 2008). Details of the analysis performed are presented in Appendix B and the calculated thermal conductivity is shown in Table A-4. The conductivity found for TC1813 was 28.2 W/mK and corresponds within the range of accuracy of the calculated value from the alternate orientation calculated in the controlled heat flux test facility. A key problem with the results is that due to the geometry of carbon available for testing only one direction could be tested and anisotropic properties remain hidden. For carbon TC1939, testing in the controlled heat flux test facility suggests a thermal conductivity of 118 W/mK and the thermal conductivity found from the high-accuracy thermal interface material tester is 59.9

W/mK. This discrepancy is striking. However TC1813 presents the situation where the thermal conductivity from the high accuracy tester is twice that of the original test, it is

Table A-4: Thermal Conductivity of Carbon Foam Calculated using a High-Accuracy Thermal Interface Material Tester (Kempers, 2008)

Material	Thermal Conductivity (W/mK)
TC1939	59.9
TC1813	28.2
TC1943	71.1
TC1556	130.9
TC1557	70

however explained by considering TC1813 has anisotropic properties. Anisotropic properties of TC1813 were confirmed by testing in a different orientation where the conductivity was found to be 61 W/mK which is the same as was found at the high accuracy tester.

An explanation for this low conductivity can be found when examining images of the carbon foam structure from a scanning electron microscope (SEM). An SEM image of sample TC1557 is included in Appendix A and shows cracking of the carbon structure which could occur due to thermal contracting while cooling. The presence of these cracks would cause the graphitic structures to be non-continuous and a thermal contact resistance at the cracks decreases effective thermal conductivity of the material.

The initial goal when carbon foam investigation began was to use carbon foam to replace the heat pipe unit in the system to conduct heat directly from the processor and *northbridge* to the fin plate. Testing on three samples in-situ revealed poor conductivity which was confirmed by testing in a controlled heat flux test facility. Testing of one of the samples, TC1813, in an alternate orientation confirmed that the foam has anisotropic

thermal conductivity which varied by a factor of two. Additional types of carbon were then obtained and tested in a high-accuracy thermal material tester which revealed the highest thermal conductivity of a tested sample to be 130.9 W/mK, well below the thermal conductivity that was expected. Through the testing, composition TC1939 was found to also have anisotropic thermal conductivity which varied by a factor of two. The orientation of testing with respect to the maximum thermal conductivity was not known for any of the samples. Since the conductivity has been demonstrated to change with orientation, the thermal conductivity of all samples tested could increase or decrease by a factor of two when measured in different directions. Assuming the material with the highest measured thermal conductivity, TC1556, was tested in the direction in which it has lower conductivity, in a different orientation, its conductivity could conceivably be 260.2 W/mK. This however is still far below the initially estimated values which would make a direct conduction solution feasible for use in a computer system.

A positive characteristic of carbon foam is its reduced contact resistance compared with copper for applications without thermal paste. Another good property of carbon foam is its low specific thermal conductivity which is defined as the thermal conductivity divided by the specific gravity with reference to water at 4°C. Composition TC1556, with a thermal conductivity of 130.9 W/mK, has a specific thermal conductivity of 205 W/mK/SG compared with aluminum which has a specific thermal conductivity of 74 W/mK/SG and copper with a value of 45 W/mK/SG. If weight were a primary concern in a system, than carbon foam has a distinct advantage over metals.

The required thermal conductivity for a solid conduction medium to be feasible for the current geometry will be explored in the following chapter, System Model. Alternately, a geometry which would work with the currently available thermal conductivity will also be explored.

Appendix B High Accuracy Thermal Material Test Facility

Carbon foam samples were also tested off site in a high accuracy thermal conductivity test facility (Kempers et al, 2008). The test apparatus works by measuring the heat flow through the sample held between two meter bars (Figure B-1). The meter bars are carefully instrumented with four thermistors spaced evenly along the length to measure the linear temperature profile to allow for extrapolation of the surface temperature where the sample is sitting. The data acquisition system connected to the test apparatus automatically output all the required variables during testing. The variables included the temperature from each thermistor mounted in the meter bars, the ambient temperature, the electrical power applied to the heaters, the measured sample thickness, the force applied to compress the sample, the water temperature at the bottom of the lower meter bar, the extrapolated meter bar surface temperatures and the difference between them, heat transfer rates through the meter bars, the specific thermal resistance and the applied pressure.

Five types of carbon foam were tested, TC1939, TC1813, TC1943, TC1556 and TC1557. Carbon TC1939 and TC1813, multiple samples with different heights were available while for the other three types of carbon only one height was available (Table B-1).

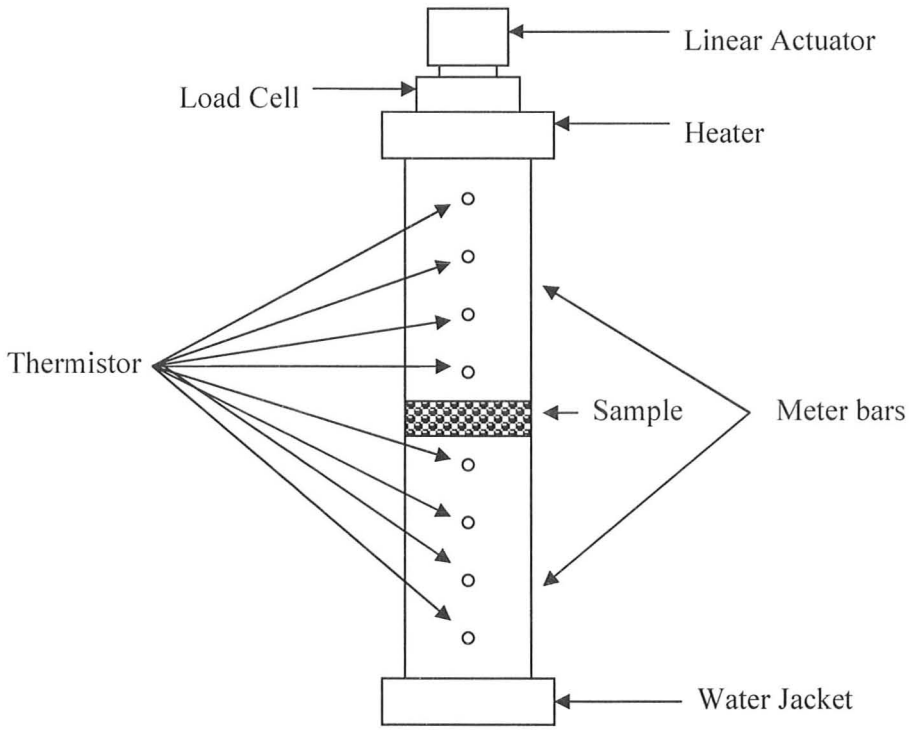

Figure B-1: High-Accuracy Thermal Interface Material Tester

Table B-1: List of Carbon Foam Samples Tested in High-Accuracy Thermal Interface Material Tester

Material	Samples	Area (mm x mm)	Thickness (mm)
TC1939	3	40.32 x 39.6 40.08 x 39.7 40.2 x 40.0	4.55 11.97 16.38
TC1813	3	39.67 x 38.0 38.99 x 38.53 39.08 x 38.41	11.99 4.7 15.84
TC1943	1	40.13 x 40.34	13.74
TC1556	1	40.24 x 40.33	17.43
TC1557	1	40.22 x 40.07	19.73

Data from the thermal conductivity test apparatus was recorded per step change in pressure. For each test the samples were cyclically loaded over 31 pressure steps as indicated in figure with the peak pressure being reached three times (Figure B-2). Of interest for analysis are the sample thickness and the specific thermal resistance (bulk resistivity). The bulk resistivity includes the contact resistance and the thermal resistance through the sample being measured. To find the thermal conductivity, the sample resistance had to be found by removing the contact resistance from the bulk resistance.

When more than one height of a sample is available, the contact resistance can be determined by assuming that the contact resistance is the same for each sample and only the sample resistance changes with changing height; this will be referred to as the "Intercept Method". Plotting the RA (bulk resistance) value vs. the thickness from the TC1813 composition for each of three different heights, contact resistance was found by finding the intercept of a linear trend line with the y axis (Figure B-3). A possible source of error can be seen by finding the intercept from a trend line drawn between any two points as seen in Table B-2. The contact resistance using the intercept method was found for each pressure step and is plotted vs. pressure in Figure B-4. By placing a 2nd order polynomial trend line on to the curve of contact resistance vs. pressure, an equation for contact resistance as a function of pressure was found (Figure B-4).

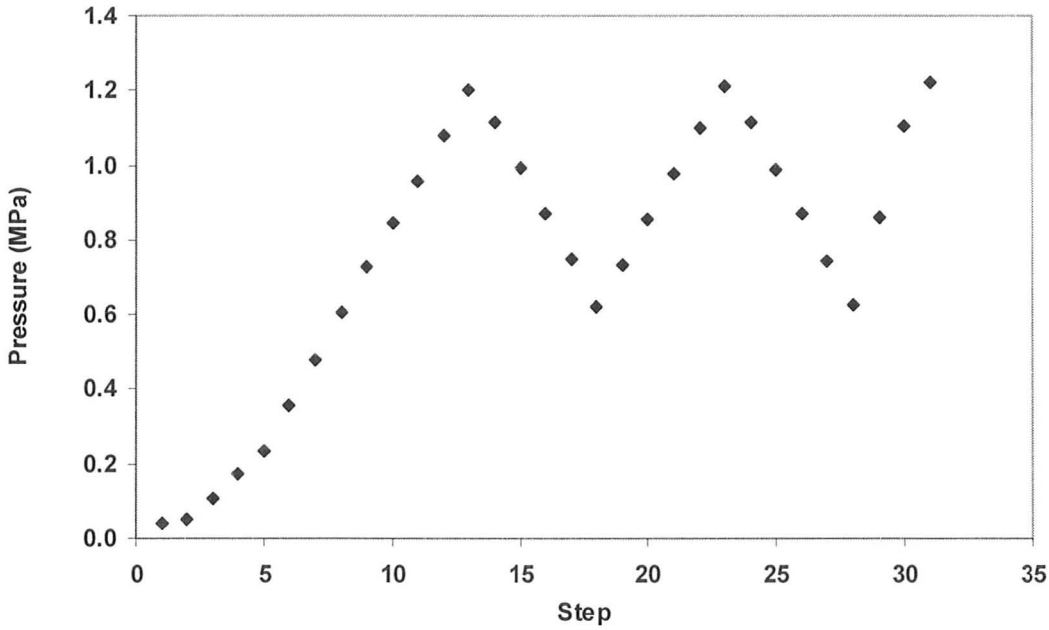

Figure B-2: Plot of Pressure vs. Step for High Accuracy Test Facility

Table B-2: Variation of Intercept (Contact Resistance) Based on Heights Used

Heights (m)	Intercept (m^2K/W)
0.00474, 0.0120, 0.0158	1.124×10^{-4}
0.00474, 0.0120	1.188×10^{-4}
0.00474, 0.0158	1.135×10^{-4}
0.0120, 0.0158	8.001×10^{-5}

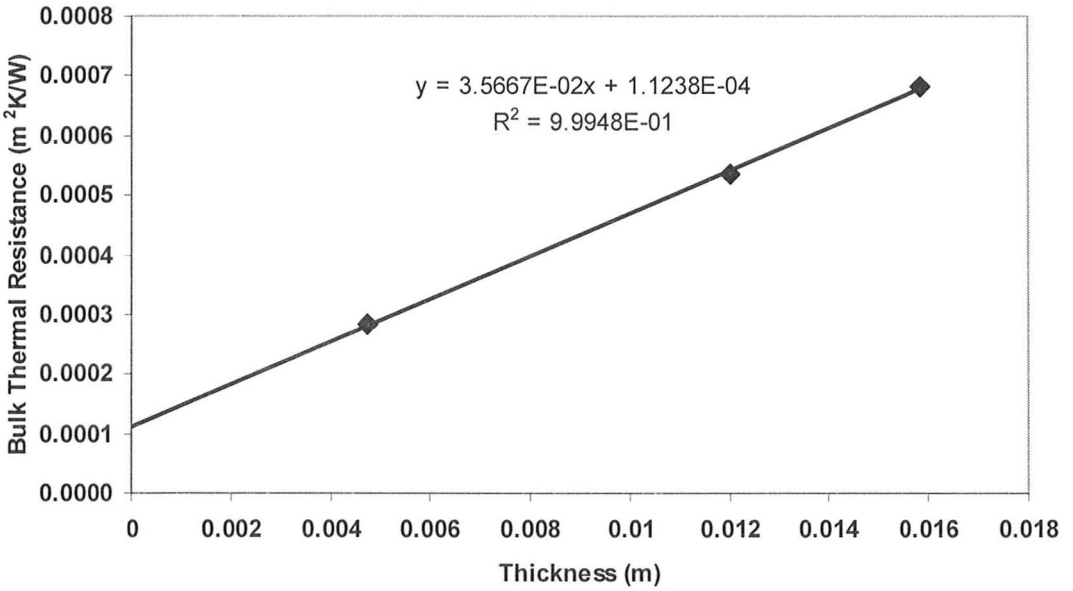

Figure B-3: Plot of RA vs. Thickness Showing the Intercept (Contact Resistance)

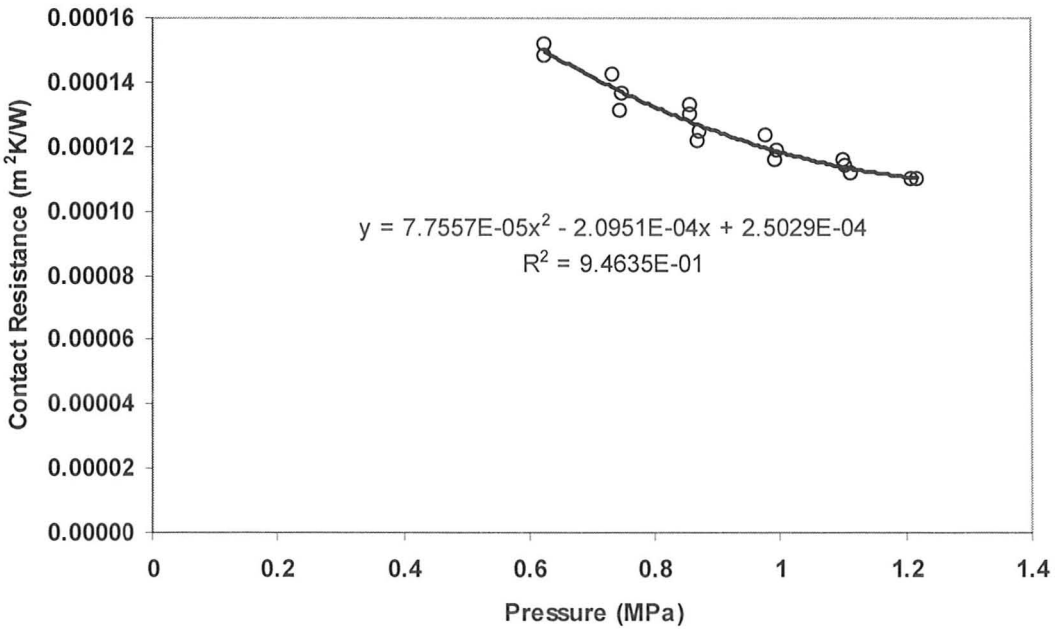

Figure B-4: Plot of Contact Resistance vs. Pressure for TC1813 Carbon Foam

When considering the thermal resistance of the sample including both the contact resistance and the bulk resistance of the sample, only the contact resistance should change with pressure. It is assumed that the bulk thermal conductivity does not change with pressure for this analysis.

Each of the three carbon compositions that have only one height were analysed by applying a polynomial equation for contact resistance as a function of pressure and using an iterative solver to find the coefficients. The values for the coefficients of the polynomial from TC1813 were used as a starting point to find optimal values for each single sample, using an iterating solver. The criteria for iteration was to achieve the minimum difference between maximum and minimum thermal conductivity values, set the average contact resistance to the average resistance from the TC1813 sample, and each of the coefficients were only allowed to vary over a small range so that local maximums and minimums were found. For the analysis, values were used starting at the first pressure peak (step 13), because before this point the contact resistance fluctuates widely. This wide fluctuation is thought to be due to small surface irregularities that are crushed when the maximum pressure is first reached. Applying this method to each sample yielded the thermal conductivity (Table B-3).

Although TC1939 has two heights, the iterative method was applied to see if it gave the same result as the intercept method. With the TC1939 composition only two samples were tested after the lowest height (4.55mm) was crushed in the test facility. This is a possible source of error in the intercept method for TC1939, since using only the two larger heights produced more error in the TC1813 analysis and a similar result could

occur in TC1939. For TC1939, the conductivities found for both heights were the same. The planar alignment is not known for any of the samples since they were cut from pieces with unknown planar alignment.

An interesting observation is made when comparing the conductivities for the TC1813 composition from the different tests as seen in Table B-4. This indicates that the foam has anisotropic thermal conduction properties and the thin orientation corresponds to the orientation tested in the high precision test facility.

Additional graphs are presented from the analysis conducted on the highly accurate thermal conduction test facility. Graphs are presented showing pressure and k plotted vs. step, Pressure and Contact Resistance plotted vs. step, Contact Resistance plotted vs. Pressure, and k plotted vs. Pressure. Graphs are shown for TC1943, TC1556, TC1557, and TC1939.

Table B-3: Thermal Conductivity for all Carbon Foams Tested in the High-Accuracy Thermal Interface Material Tester

Material	Thermal Conductivity (W/mK)	Figures
TC1943	71.1	Figures B-5, B-6, B-7, B-8
TC1939	59.9	Figures B-9, B-10, B-11, B-12
TC1813	28.2	Figures B-13, B-14, B-15, B-16
TC1556	130.9	Figures B-17, B-18, B-19, B-20
TC1557	70	Figures B-21, B-22, B-23, B-24

Table B-4: Thermal Conductivity for TC1813 Carbon Foam from Different Tests

Test	Thermal Conductivity (W/mK)
Controlled Heat Flux Test Facility – Normal orientation	51-71
Controlled Heat Flux Test Facility – Alternate orientation	30.5-32.2
High-Accuracy Thermal Interface Material Tester	28.2

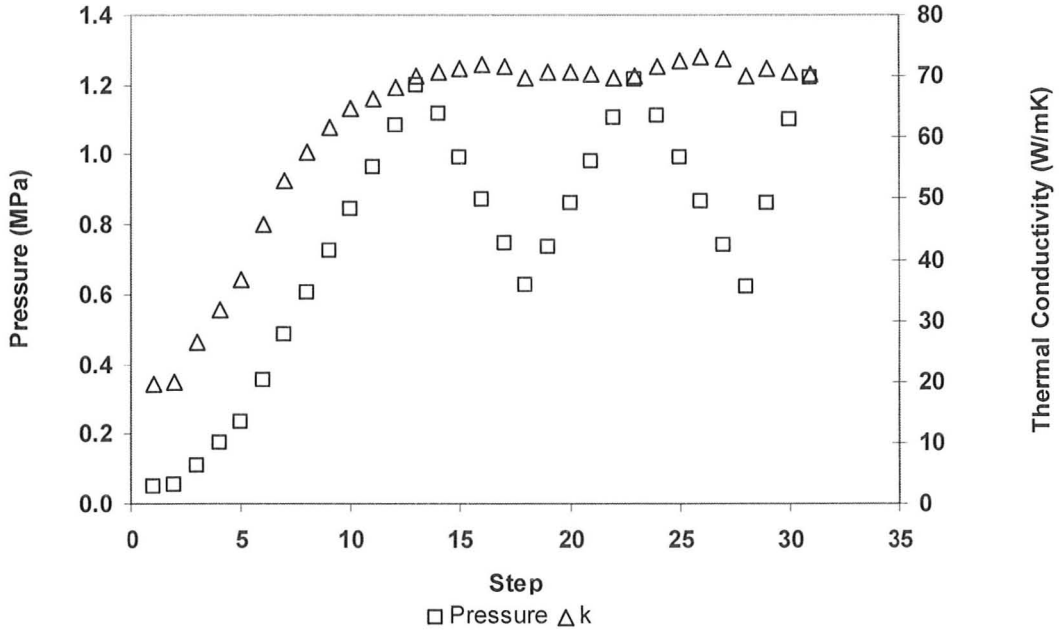

Figure B-5: Pressure Thermal Conductivity vs. Step for TC1943

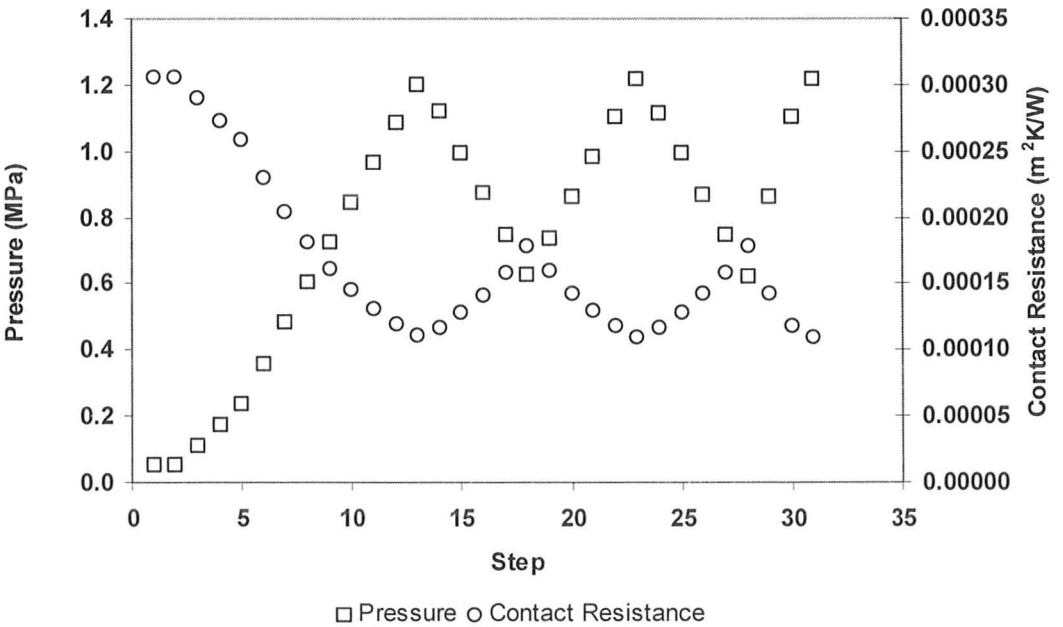

Figure B-6: Pressure and Contact Resistance vs. Step for TC1943

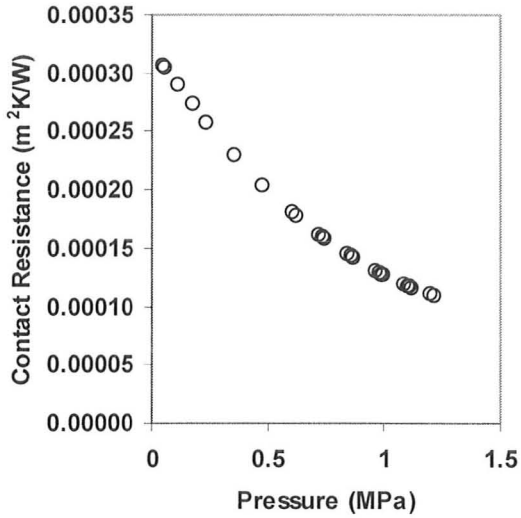

Figure B-7: Contact Resistance vs. Pressure for TC1943

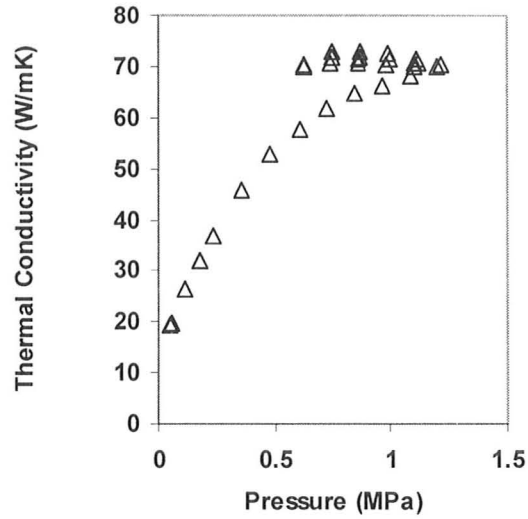

Figure B-8: Thermal Conductivity vs. Pressure for TC1943

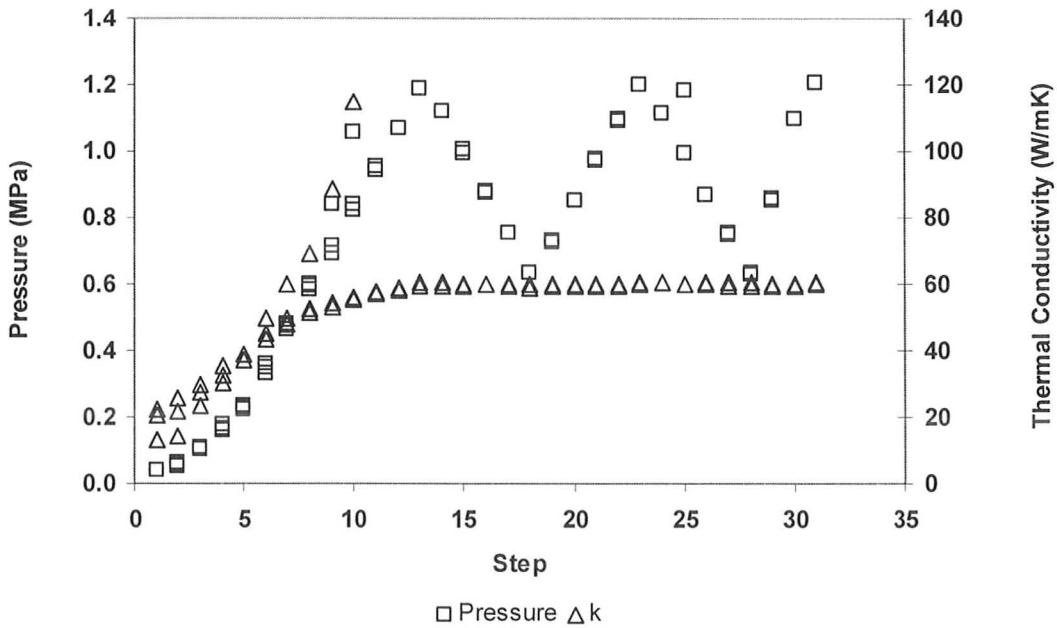

Figure B-9: Pressure and Thermal Conductivity vs. Step for TC1939

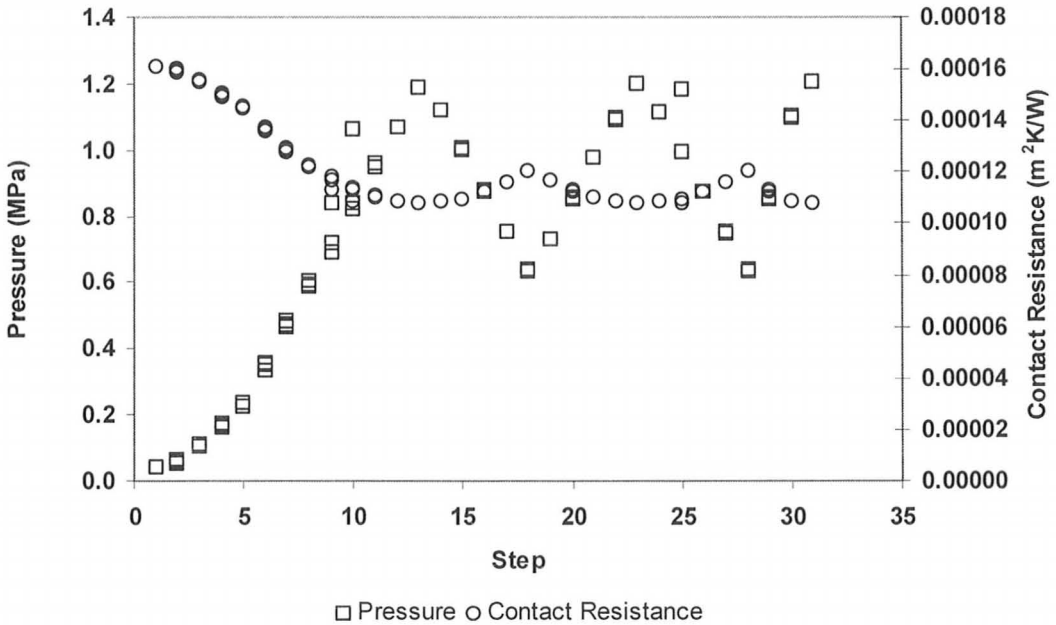

Figure B-10: Pressure and Contact Resistance vs. Step for TC1939

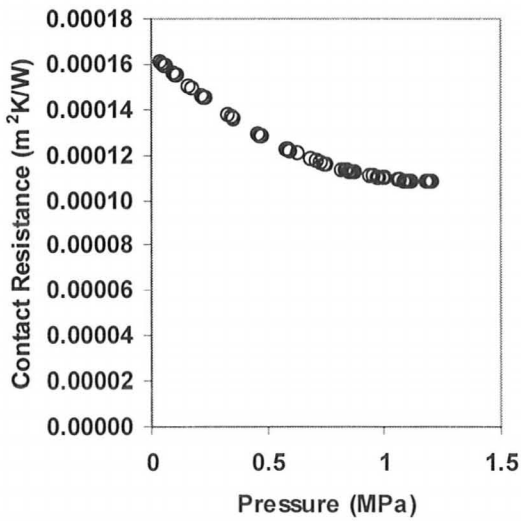

Figure B-11: Contact Resistance vs. Pressure for TC1939

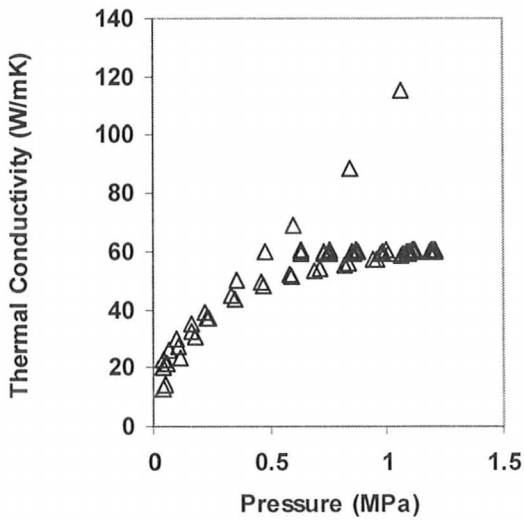

Figure B-12: Thermal Conductivity vs. Pressure for TC1939

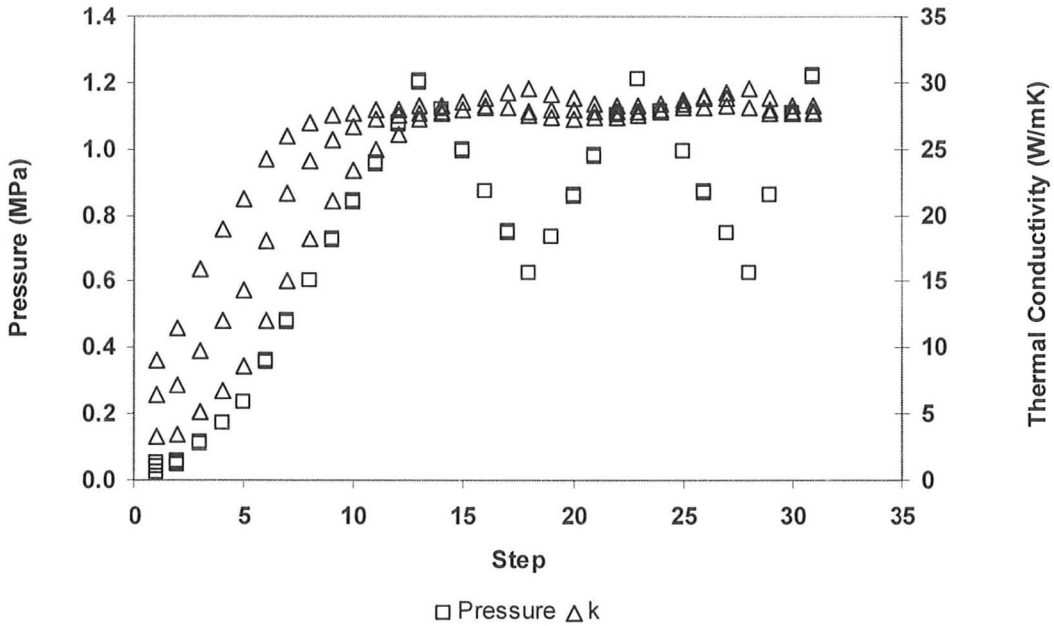

Figure B-13: Pressure and Thermal Conductivity vs. Step for TC1813

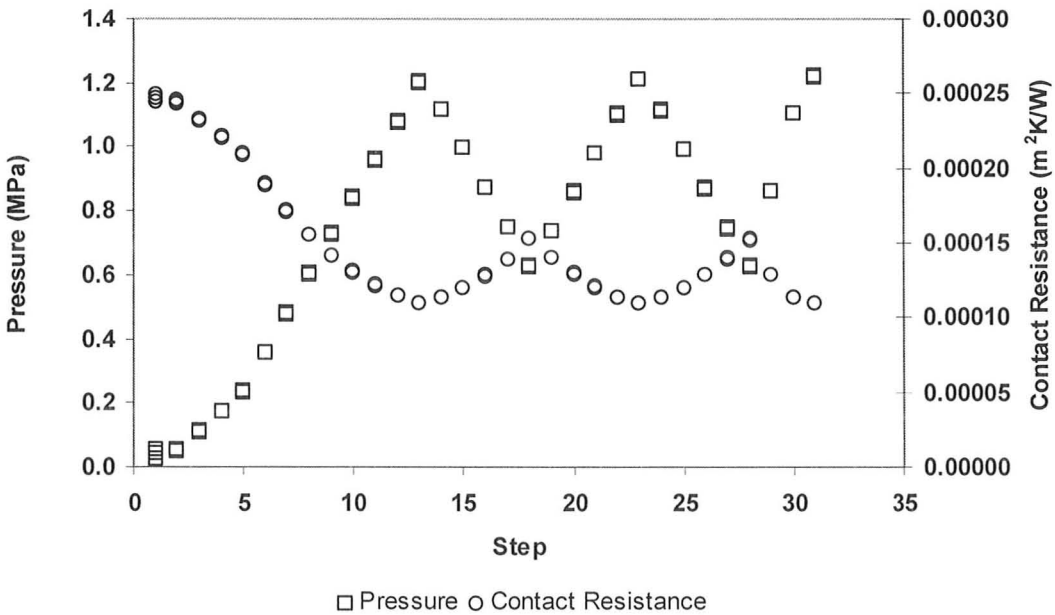

Figure B-14: Pressure and Contact Resistance vs. Step for TC1813

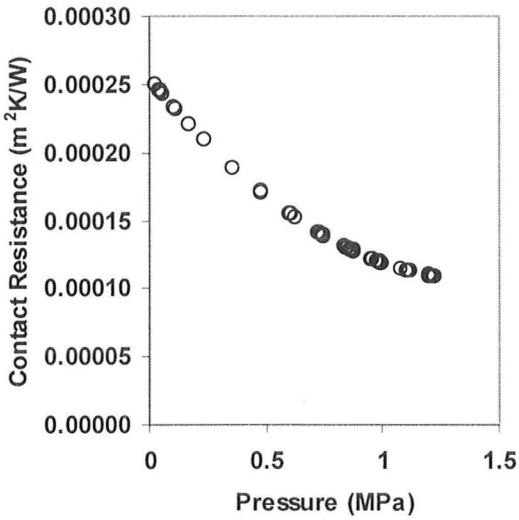

Figure B-15: Contact Resistance vs. Pressure for TC1813

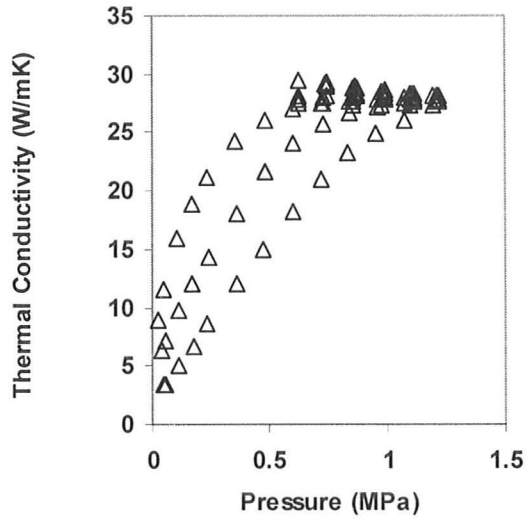

Figure B-16: Thermal Conductivity vs. Pressure for TC1813

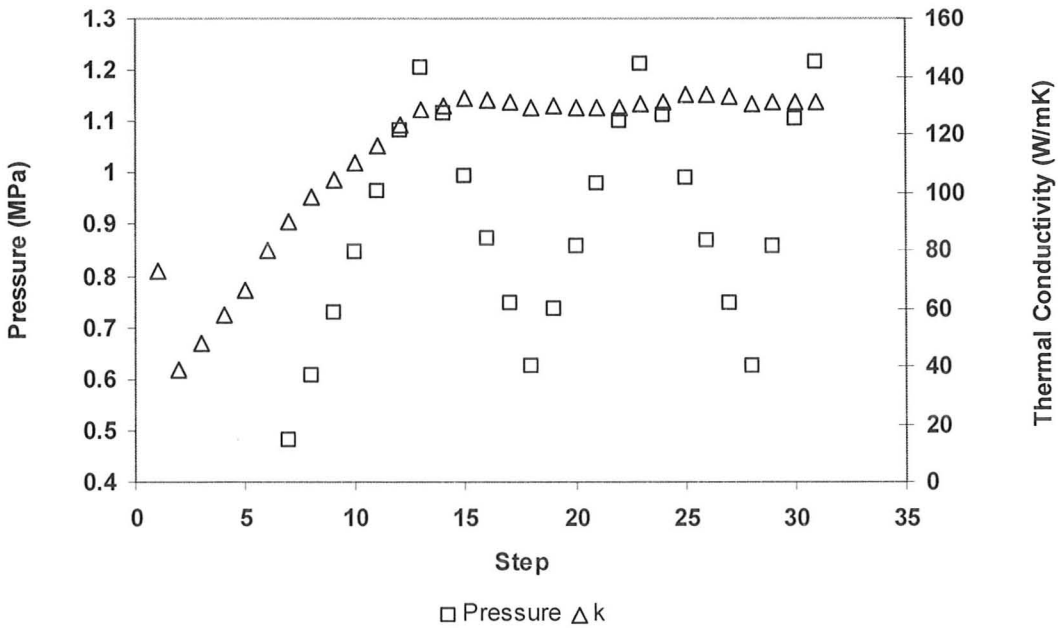

Figure B-17: Pressure and Thermal Conductivity vs. Step for TC1556

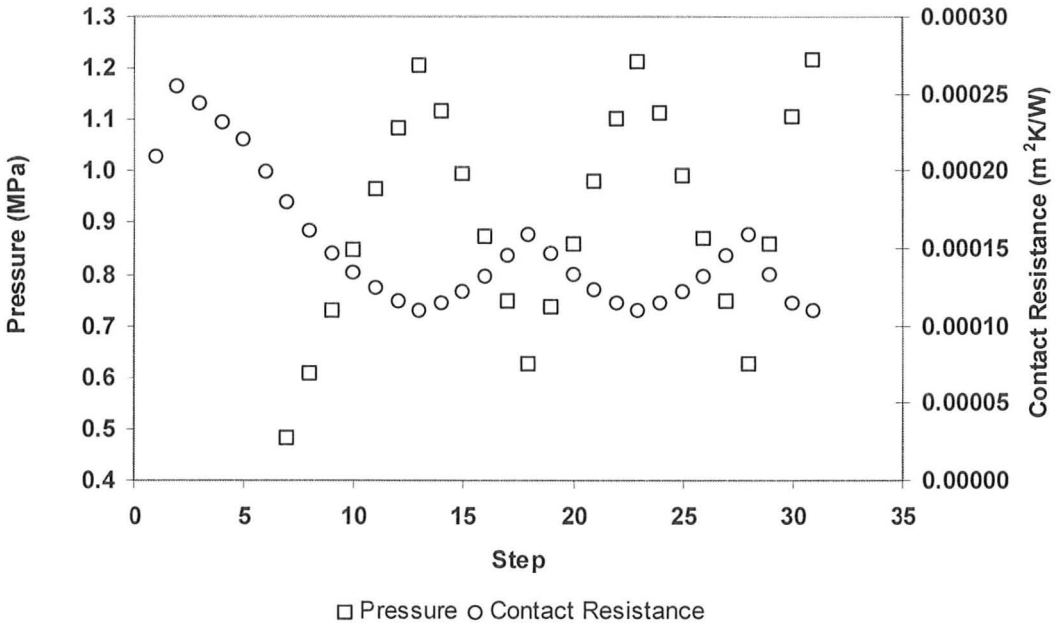

Figure B-18: Pressure and Contact Resistance vs. Step for TC1556

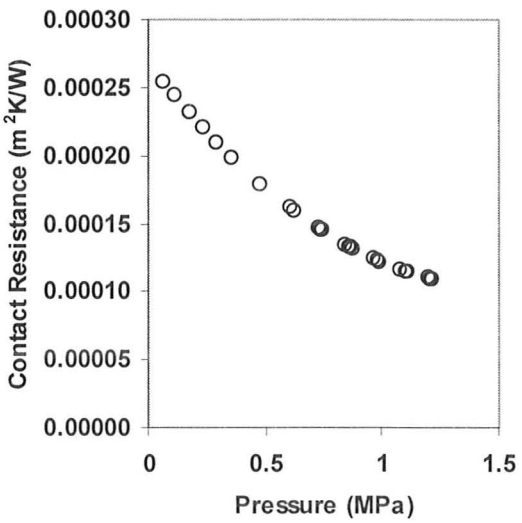

Figure B-19: Contact Resistance vs. Pressure for TC1556

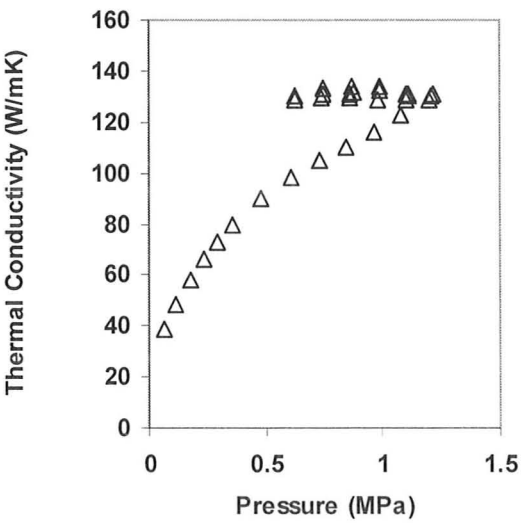

Figure B-20: Thermal Conductivity vs. Pressure for TC1556

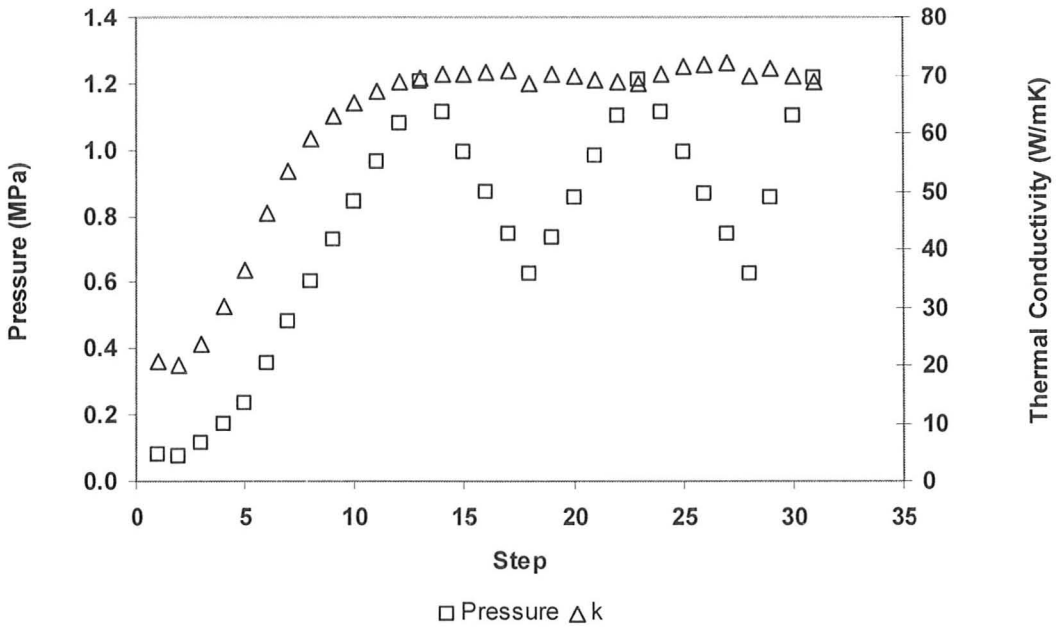

Figure B-21: Pressure and Thermal Conductivity vs. Step for TC1557

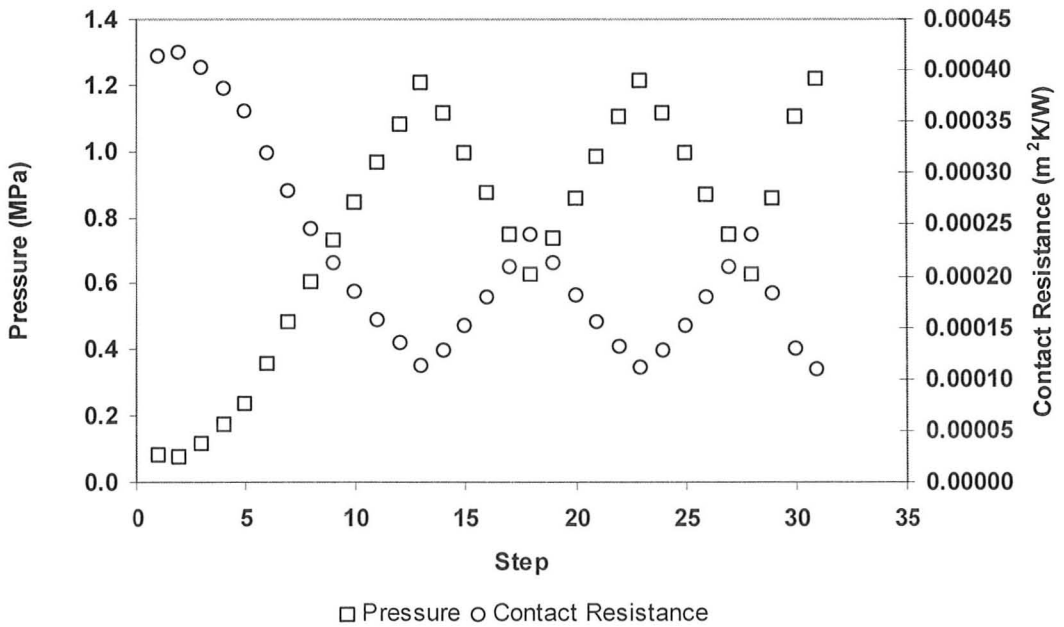

Figure B-22: Pressure and Contact Resistance vs. Step for TC1557

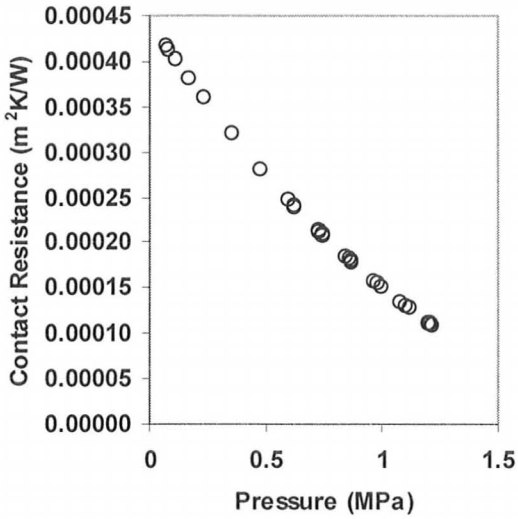

Figure B-23: Contact Resistance vs. Pressure for TC1557

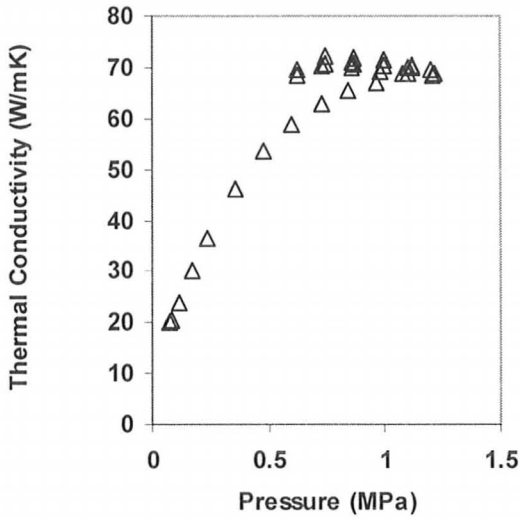

Figure B-24: Thermal Conductivity vs. Pressure for TC1557

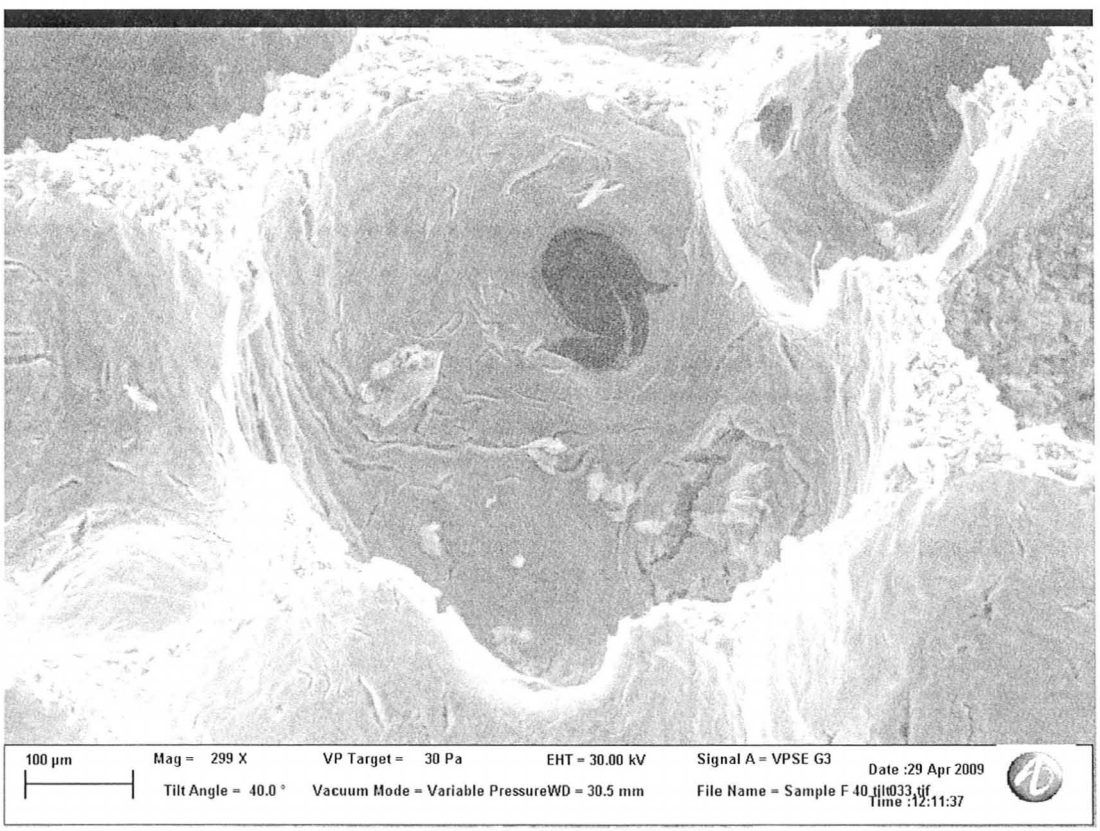

Figure B-25: SEM Image of TC1557 Showing Cracking of Carbon Structure

REFERENCES

ANSYS Inc., 2007, "ANSYS CFX, Release 11.0 Help File".

Aung, W., Kessler, T. J. and Beitin, K. L., 1973, "Free convection cooling of electronic systems", IEEE Trans. Parts, Hybrids Packag., vol. PHP-9, no. 2, pp. 75-86.

Bar-Cohen, A. and Rohsenow, W., 1983, "Thermally Optimum Arrays of Cards and Fins in Natural Convection", IEEE Trans. CHMT-6 No 2, pp. 154-158.

Bar-Cohen, A. and Rohsenow, W., 1984, "Thermally Optimum Spacing of Vertical, Natural Convection Cooled, Parallel Plates", ASME J. Heat Transfer, 106, pp. 116–122.

Betchen, L. J., Straatman, A. G. and Thompson, B. E., 2006, "A non-equilibrium finite-volume model for conjugate fluid/porous/solid domains", Numerical Heat Transfer, Part A, 49, pp. 543-565.

Bodoia, J. R. and Osterle, J. F., 1964, "The development of free convection between heated vertical plates", ASME J. Heat Transfer, vol. 84, pp. 40-44.

Cess, R. D., 1973, "Free-convection Boundary-layer Heat Transfer", Ch. 6, in Handbook of Heat Transfer, Eds. Rohsenow, W. M. and Hartnett, J. P., McGraw-Hill, New York USA.

Chu, R. C., Simons, R. E., Ellsworth, M. J., Schmidt, R. R. and Cozzolino, V., 2004, "Review of Cooling Technologies for Computer Products", IEEE Trans. Device Mater. Reliab., vol. 4, no. 4, pp. 568–585.

Culham, J. R. and Muzychka, Y. S., 2001, "Optimization of plate fin heat sinks using entropy generation minimization", IEEE Trans. Compon. Packag. Technol., vol. 24, no. 2, pp. 159-165.

Dube, V., Akbarzadeh, A. and Andrews, J., 2004, "The effects of non-condensable gases on the performance of loop thermosyphon heat exchangers", Applied Thermal Engineering 24, pp. 2439-2451.

Dunn , P. and Reay, D. A., 1982, Heat Pipes, 3rd Ed., Pergamon Press, Oxford, UK.

Elenbaas, W., 1942, "Heat Dissipation of Parallel Plates by Free Convection", Physica (Utrecht), 9(1), pp. 665–671.

Extech Corp, 2001, "Model 382860 True RMS Power MultiMeter – Instruction Manual", Version 1.6.

Faghri, A., 1995, Heat Pipe Science and Technology, Taylor & Francis, Washington, DC.

Fried, E., 1969, "Thermal Conduction Contribution to Heat Transfer at Contacts", Thermal Conductivity, Tye, R. P., ed., vol. 2, Academic Press, London.

Gaies, D. and Faber, K.T., 2002, "Thermal properties of pitch-derived graphite foam", Carbon, 40, pp. 1131-1150.

Gallego, N.C. and Klett, J., 2003, "Carbon foams for thermal management", Carbon 41, pp. 1461-1466.

Gao, M. and Cao, Y., 2003, "Flat and U-Shaped Heat Spreaders for High-Power Electronics", Heat Transfer Engineering, 24:3, pp. 57 – 65.

Grujicic, M., Zhao, C.L. and Dusel, E.C., 2004, "The effect of thermal contact resistance on heat management in the electronic packaging", Applied Surface Science, vol. 246, iss. 1-3, pp. 290-302.

Holahan, M., 2005, "Fins, Fans, and Form: Volumetric Limits to Air-Side Heatsink Performance", IEEE Trans. Compon. Packag. Technol., vol. 28, no. 2, pp. 255-262.

Intel Corporation, 2007, "Mobile Intel 945GME Express Chipset Graphics and Memory Controller Hub (GMCH) for Embedded Applications", Intel Document Number 308623-002.

Intel Corporation, 2008, "Intel Core 2 Duo Processor and Intel Core 2 Extreme Processor on 45-nm Process for Platforms Based on Mobile Intel 965 Express Chipset Family – Datasheet", Intel Document Number 318914-001.

Intel Corporation, 2009a, "Intel Core 2 Extreme Quad-Core Mobile Processor and Intel Core 2 Quad Mobile Processor on 45-nm Process – Datasheet", Intel Document Number: 320390-002. http://download.intel.com/design/processor/datashts/320390.pdf

Intel Corporation, 2009b, "Intel Core i7 Processor Extreme Edition and Intel Core i7 Processor – Datasheet, Volume 1", Intel Document Number: 320834-002. http://download.intel.com/design/processor/datashts/320834.pdf

Intel Corporation, 2009c, "Mobile Intel 4 Series Express Chipset Family – Datasheet", Intel Document Number: 320122-006. http://www.intel.com/Assets/PDF/datasheet/320122.pdf

Kandlikar, S. G. and Grande, W. J., 2004, "Evaluation of Single Phase Flow in microchannels for High Heat Flux Chip Cooling—Thermohydraulic Performance

Enhancement and Fabrication Technology", Heat Transfer Engineering, vol. 25, no. 8, pp. 5 - 16

Karagiozis, A., Raithby, G. D. and Hollands, K. G. T., 1994, "Natural Convection Heat Transfer from Arrays of Isothermal Triangular Fins in Air", ASME J. Heat Transfer, 116, pp. 105–111.

Kempers, R., Kolodner, P., Lyons, A. and Robinson, A. J., 2008, "Development of a high-accuracy thermal interface material tester", in Proc. 11th Intersociety Conf. Thermal and Thermomechanical Phenomena in Electronics Systems (ITHERM), pp. 221-226.

Khan, W. A., Culham, J. R. and Yovanovich, M. M., 2006, "The Role of Fin Geometry in Heat Sink Performance", ASME J. of Electron. Packag., vol. 128, December, 2006, pp. 324 - 330.

Klett, J., 1999, "High thermal conductivity, mesophase pitch-derived graphitic foams", Composites Manufacturing, vol. 15, iss. 4, pp. 1–5.

Klett, J., Hardy, R., Romine, E., Walls, C. and Burchell, T., 2000, "High-thermal-conductivity, mesophase-pitch-derived carbon foams: effect of precursor on structure and properties", Carbon 38, pp. 953-973.

Klett, J. W., McMillan, A. D., Gallego, N. C., Burchell, T. D. and Walls, C. A., 2004, "Effects of heat treatment conditions on the thermal properties of mesophase pitch-derived graphitic foams", Carbon 42, pp. 1849-1852.

Kobayashi, T., Ogushi, T., Sumi, N. and Fujii, M., 2000, "Thermal Design of an Ultraslim Notebook Computer", IEEE Trans. Compon. Packag. Technol., vol. 23, no. 1, pp. 6-13.

Koppers Inc., 2006, "Technical Data Sheet – KFOAM Grade L1a", Pittsburgh, PA, USA.

Kreith, F. and Bohn, M., 2001, Principles of Heat Transfer, 6th Ed., Brooks/Cole, Pacific Grove, CA.

Leong, K.C., Liu, C.Y. and Lu, G.Q., 1997, "Characterization of Sintered Copper Wicks Used in Heat Pipes", J. of Porous Materials, vol. 4, iss. 4, pp. 303-308.

Measurement Computing, 2006, "PCI-DAS-TC – Specifications", Version 1.1.

Min , G., Zengmin, S., Weidong, C. and Hui, L., 2007, "Anisotropy of mesophase pitch-derived carbon foams", Carbon 45, pp. 141-145.

Nabi, A., Rodgers, P. and Bar-Cohen, A., 2006, "Prediction of Thermal Performance Degradation of Air-Cooled Fine-Pitch Fin Array Heat Sinks due to Fouling", in Proc. 22nd IEEE Semiconductor Thermal Measurement and Management Symp. (SEMI-THERM XXII), pp. 2-9.

Nakayama, W., 2000, "Thermal Issues in Microsystem Packaging", IEEE Trans. Adv. Packag., vol. 23, no. 4, pp. 602-607.

Omega Inc., 2005, "Revised Thermocouple Reference Tables – Type T", Omega Document z207.

Peterson, G. P., 1994, "An Introduction to Heat Pipes: Modelling, Testing, and Applications", New York, NY, USA. John Wiley & Sons.

Poco Graphite Inc., 2002, "Poco HTC Product Datasheet", Decatur, Texas, USA.

Prasher, R. S., 2003, "A Simplified Conduction Based Modeling Scheme for Design Sensitivity Study of Thermal Solution Utilizing Heat Pipe and Vapor Chamber Technology", J. Electron. Packag. vol. 125, pp. 378-385.

Rohsenow, W. M. and Hartnett, J. P., 1973, "Basic Concepts of Heat Transfer", Section 1 in Handbook of Heat Transfer, Eds. Rohsenow, W. M. and Hartnett, J. P., McGraw-Hill Inc., New York, USA.

Roknaldin, F. and Sahan, R. A., 2003, "Cooling solution for next generation high-power processor boards in 1U computer servers", Adv. Electron. Packag., vol. 2, pp. 629–634.

Russel, M. K., Young, C., Cotton, J. S. and Ching, C.Y., 2010, "The effect of orientation on the thermal performance of a sintered and grooved U-shaped heat pipe", ITHERM 2010, Las Vegas.

Saini, M. and Webb, R. L., 2003, "Heat Rejection Limits of Air Cooled Plane Fin Heat Sinks for Computer Cooling", IEEE Trans. Compon. Packag. Technol., vol. 26, no. 1, pp. 71-79.

Sauciuc, I., Chrysler, G., Mahajan, R. and Prasher, R., 2002, "Spreading in the Heat Sink Base: Phase Change Systems or Solid Metals??", IEEE Trans. Compon. Packag. Technol., vol. 25, no. 4, pp. 621 - 628.

Schmidt, R., 2004, "Challenges in Electronic Cooling - Opportunities for Enhanced Thermal Management Techniques - Microprocessor Liquid Cooled Minichannel Heat Sink", Heat Transfer Engineering, vol. 25, no. 3, pp. 3 – 12.

Shah, R.K. and Bhatti, M.S., 1987, "Laminar Convective Heat Transfer in Ducts", in Handbook of Single-Phase Convective Heat Transfer, Eds., S. Kakac, R. K. Shah and W. Aung, New York, NY. Wiley.

Sparrow, E. M. and Bahrami, P. A., "Experiments on natural convection from vertical parallel plates with either open or closed edges", ASME J. Heat Trans., vol. 102, pp. 221-227, 1980.

Starner, K. E. and McManus, H. N., 1963, "An Experimental Investigation of Free Convection Heat Transfer From Rectangular Fin Arrays", ASME J. of Heat Trans., vol. 85, pp. 273-278.

Straatman, A. Gallego, N., Thompson, B. E. and Hangan, H., 2006a, "Thermal Characterization of Porous Carbon Foam – Convection in Parallel Flow", Int. J. Heat Mass Trans., 49, pp. 1991-1998.

Straatman, A. G., Gallego, N. C., Yu, Q. and Thompson, B. E., 2006b, "Characterization of porous carbon foam as a material for compact recuperators", Proc. IGTI ASME Turbo Expo 2006, GT2006-90598.

Straatman, A.G., Gallego, N.C., Yu, Q., Betchen, L. and Thompson, B.E., 2007 "Forced Convection Heat Transfer and Hydraulic Losses in Graphitic Foam", ASME J. Heat Trans. 129, pp. 1237-1245.

Tuckerman, D. B. and Pease, R. F., 1981, "High performance heat sinking for VLSI", IEEE Electron. Device Lett., vol. EDL-2, no. 5, pp. 126–129, May 1981.

Webb, R. L., 2005, "Next Generation Devices for Electronic Cooling With Heat Rejection to Air", J. Heat Trans. vol. 127, pp. 2-10.

Welling, J. R. and Wooldridge, C. B., 1965, "Free Convection Heat Transfer Coefficients From Rectangular Vertical Fins", ASME J. of Heat Trans., vol. 87, pp. 439-444.

Wuttijumnong, V., Nguyen, T., Mochizuki, M., Mashiko, K., Saito, Y. and Nguyen, T., 2004, "Overview Latest Technologies Using Heat Pipe And Vapor Chamber for Cooling of High Heat Generation Notebook Computer", in Proc. 20th IEEE Semiconductor Thermal Measurement and Management Symp. (SEMI-THERM XX), pp.221-224.

Xie, H., Ali, A. and Bhatia, R., 1998, "The use of heat pipes in personal computers", in Proc. 6th Intersociety Conf. Thermal and Thermomechanical Phenomena in Electronics Systems (ITHERM), pp. 442–455.